A national laboratory of the U.S. Department of Energy
Office of Energy Efficiency & Renewable Energy

National Renewable Energy Laboratory

Innovation for Our Energy Future

Subcontract Report
NREL/SR-520-38681
October 2005

Trajectory-Oriented and Fault-Tolerant-Based Intelligent Process Control for Flexible CIGS PV Module Manufacturing

Final Technical Report
13 May 2002–30 May 2005

L. Simpson, J. Britt, R. Birkmire, and T. Vincent
ITN Energy Systems, Inc.
Littleton, Colorado

NREL is operated by Midwest Research Institute Battelle Contract No. DE-AC36-99-GO10337

Subcontract Report
NREL/SR-520-38681
October 2005

Trajectory-Oriented and Fault-Tolerant-Based Intelligent Process Control for Flexible CIGS PV Module Manufacturing

Final Technical Report
13 May 2002–30 May 2005

L. Simpson, J. Britt, R. Birkmire, and T. Vincent
ITN Energy Systems, Inc.
Littleton, Colorado

NREL Technical Monitor: R.L. Mitchell

Prepared under Subcontract No. ZDO-2-30628-07

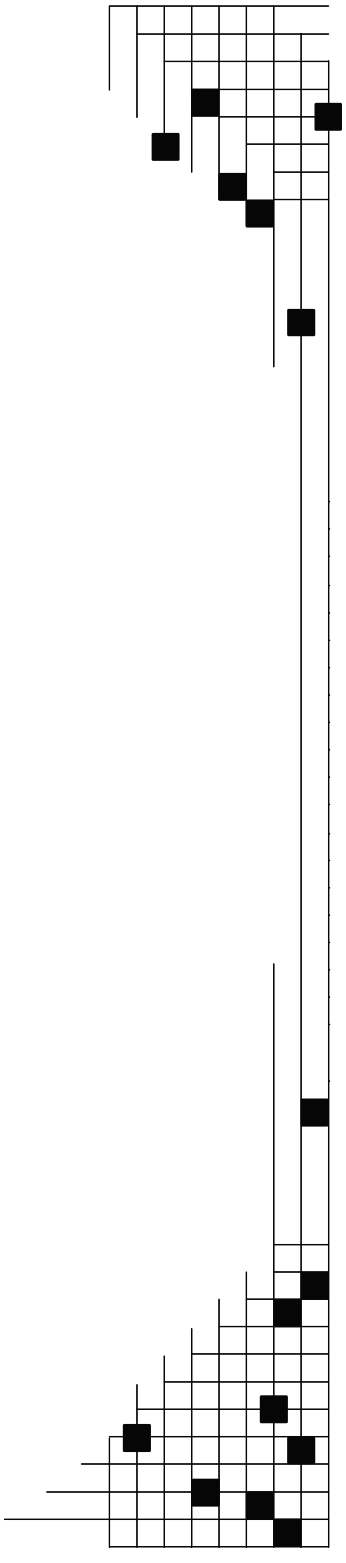

National Renewable Energy Laboratory
1617 Cole Boulevard, Golden, Colorado 80401-3393
303-275-3000 • www.nrel.gov

Operated for the U.S. Department of Energy
Office of Energy Efficiency and Renewable Energy
by Midwest Research Institute • Battelle

Contract No. DE-AC36-99-GO10337

Executive Summary

ITN Energy Systems, Inc., and Global Solar Energy, Inc., with the assistance of NREL's PV Manufacturing R&D program have continued the advancement of CIGS production technology through the development of trajectory oriented predictive/control models, fault tolerance control, control platform development, in-situ sensors, and process improvements. Modeling activities included the development of physics-based and empirical models for CIGS and sputter deposition processing, implementation of model-based control, and application of predictive models to the construction of new evaporation sources and for control. Model-based control is enabled through implementation of reduced or empirical models into a control platform. Reliability improvement activities include implementation of preventive maintenance schedules; detection of failed sensors/equipment and reconfiguration to continue processing; and systematic development of fault prevention and reconfiguration strategies for the full range of CIGS PV production deposition processes. In-situ sensor development activities have resulted in improved control and indicated the potential for enhanced process status monitoring and control of the deposition processes. Substantial process improvements have been made, including significant improvement in CIGS uniformity, thickness control, efficiency, yield, and throughput. In large measure, these gains have been driven by process optimization, which in turn have been enabled by control and reliability improvements due to this PV Manufacturing R&D program. This has resulted in substantial improvements of flexible CIGS PV module performance and efficiency. This program has also resulted in implementation of fully functional process control software with accompanying graphical user interfaces to enable implementation of model-based control and reconfiguration capabilities and in-situ sensor based real-time control. Finally, the program has been leveraged to develop improved processing systems both at the component and configuration levels.

Table of Contents

1. Background

Interest in thin film photovoltaics (PV) has expanded dramatically, but wide-scale commercial use remains limited by performance and cost. These factors are often interrelated and negatively impacted by the lack of reliable and accurate process control. ITN Energy Systems, Inc. (ITN) and Global Solar Energy, Inc. (GSE) are using a comprehensive and systematic program to integrate intelligent process control into the manufacture of flexible, lightweight copper indium gallium diselenide (CIGS) based PV modules. Process control has been a priority since the outset of this endeavor, enabling the development of a fully integrated CIGS module manufacturing facility. GSE's production facility (Figure 1) is fully equipped to manufacture up to 5 MW per year of flexible, lightweight CIGS PV products. Key CIGS manufacturing facilities includes: molybdenum back contact, large-area CIGS absorber layer, cadmium sulfide, and transparent conductive oxide deposition systems; module lamination, and PV product finishing equipment. Each production deposition system is capable of processing 12-in. wide, 1000-ft. long polymer or stainless steel in a low-cost, automated fashion. GSE's substantial thin-film photovoltaic module process/product achievements were instrumental in receiving a R&D 100 2004 award by R&D Magazine for being one of the year's 100 most significant technological innovations. Today, the CIGS PV modules produced at GSE are the only truly flexible PV commercially available with over 10% efficiency (Figure 2) that can be folded/rolled for compact storage and transported/deployed extremely quickly, breakage-free. This innovative technology is being incorporated in a number of products for military and commercial applications (Figure 4).

Figure 1. Example Production CIGS PV Module Manufacturing Deposition Facilities at GSE (right).

To capitalize on the potential cost reductions that thin film processing methods can provide for polycrystalline PV modules, every manufacturing step must be controlled at a level where quality and yield are maximized. Depending on the complexity and extent of fundamental scientific understanding of each process, the transition to large-scale manufacturing can be more difficult and costly than anticipated. A critical requirement is the development and implementation of diagnostic tools and associated predictive models that can quantitatively assess the relationship of processing conditions to product properties. The PV Manufacturing R&D effort enabled GSE/ITN to complete a fully integrated process control development program with models, control platform, and diagnostic tools (sensors) for intelligent processing of PV modules, with the ultimate goal of improving CIGS module performance, process throughput, and yield

In general, diagnostic capabilities for manufacturing thin films are rudimentary, and manufacturers can only assess their product after module completion. Inadequate diagnostics and predictive models result in sub-optimal control and correspondingly lower quality and yield. For system failures, the most common strategy consists of sophisticated interlocking and alarm mechanisms to stop the process when a fault is detected. Process models/simulators are required for unanticipated process upsets, reactor variability/drift, and operation in unstable processing regimes where repeatability can be achieved only through dynamic feedback/feed-forward control. Similarly, in-situ, real-time process diagnostics development, in the form of sensors, is also required since their use has been proven to improve process yield/quality and reduce module costs.

The essence of our PV Manufacturing R&D effort was to develop trajectory oriented and fault tolerance based intelligent process control using predictive physics-based process models and strategic process/film property sensors to significantly improve yield, throughput, and performance of flexible CIGS PV modules. Implementation of trajectory-oriented control consisted of four tasks, specifically, development of

mathematical relationships (models) between control variables and final product properties (system identification), reduction of models into computationally efficient form(s), establishment of optimum trajectories for film properties during deposition and implementation into a control platform. Fault tolerance activities included detection, location, and isolation of faults, and implementation of appropriate corrective actions that minimize faults from becoming critical failures. Diagnostic tool activities involved integration of existing and alternative sensors to increase reliability and/or provide process information. All effective model/sensor features were incorporated into a robust control platform that enabled autonomous and continuous manufacturing, with automatic data storage and presentation for operator monitoring. For reference, a brief overview of the program efforts by phase is provided below, while this report is comprehensive and provides all details organized by topic. Specifically, while interrelated, this report is organized into five main subjects that include development and implementation of: physics-based models, fault tolerance, a control platform, diagnostic tools (sensors), and process/equipment advancements based on control development/models.

	Total Area	Aperture Area	
	Cell	P3	SlimLine[(1)]
V_{max} [V]	0.455	27.00	42.11
I_{max} [A]	1.992	1.61	1.69
P_{max} [W]	0.906	43.38	71.21
V_{oc} [V]	0.607	35.01	57.47
I_{sc} [A]	2.347	1.90	2.01
FF [%]	63.67	65.28	61.50
η [%]	13.17	11.13	10.10
Area [cm^2]	68.80	3898	7085

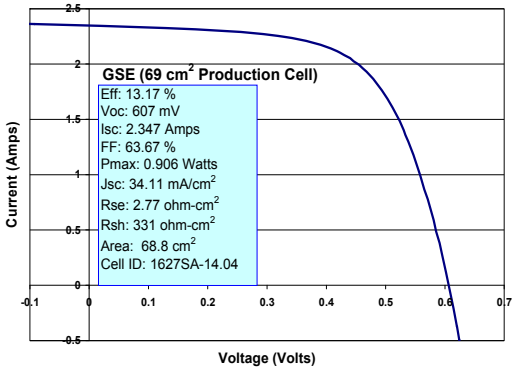

Figure 2. Production cell and module I-V characteristics. [(1)] NREL verified measurement demonstrate that during the PV Manufacturing R&D program, substantial improvements in performance were achieved.

The Phase I research efforts included:

- the development of trajectory-oriented models for control of the Mo and CIGS production deposition systems;
- the detection and location of potential faults in production Mo and CIGS deposition systems;
- the development of a software package that enables hardware interfacing, model implementation and simple graphical user interface; and
- the investigation of the feasibility and utility of implementing new and/or existing diagnostic tools in the Mo, CIGS, CdS, and ITO deposition systems on CIGS production systems.

The Phase II research efforts included:

- the design and implementation of trajectory oriented control models on both the Mo and CIGS deposition systems; the development of control models/algorithms for ITO deposition system;
- the evaluation of the performance of the fault tolerance strategy on a research system;
- the implementation of reduced models, control algorithms, and new sensors into the production system; and
- the implementation of the sensors developed in Phase I for the Mo, CIGS, and ITO deposition systems to enhance process control.

The Phase III research efforts included:

- the demonstration of fault tolerance control for Mo, CIGS, and ITO deposition processes;
- the implementation of the model-based control on the ITO system;
- the integration of fault tolerance into the control platform of production deposition systems;

- the implementation of pre-process data flow for the production system control platform; and
- an investigation of the implications of diagnostic results and the process control experiences on the Mo, CIGS, and ITO deposition systems in Phase II on equipment design.

Figure 4. Representative portable products that use GSE's CIGS PV Modules.

2. Summary of Results

During the PV Manufacturing R&D program, outstanding improvements in processing and increased yields of large-area cells occurred with average efficiencies increasing more than 300% (>150% maximum efficiency increases, Figure 3) to where ~13% material (~70 cm^2) is frequently manufactured (Figure 5). Since this program was primarily directed at increasing average efficiency, the fact that average efficiency (normalized) has increased by more than a factor of two compared to the maximum efficiency is an indication of the benefits obtained from this PV Manufacturing R&D program. Cell yields have also improved dramatically during the project (Figure 6). An increase of greater than four fold to >90% yields occurred during the program and a significant amount of that increase can also be directly attributed to PV

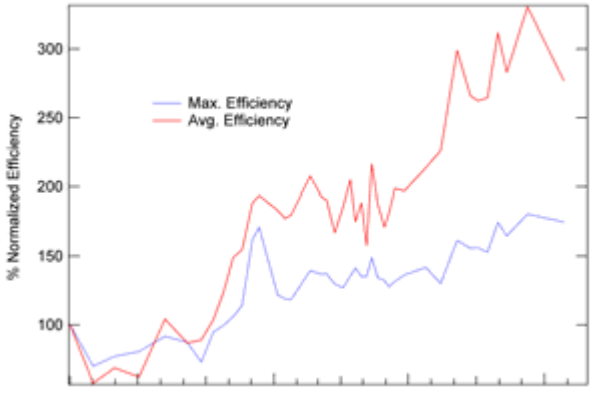

Figure 3. Normalized increase in efficiencies of production PV during ITN/GSE's PV Manufacturing R&D Program.

Manufacturing R&D activities. Improved process control (Figure 7 and Figure 8) and fault tolerance along with preventive maintenance schedules lowered fault events (Figure 9) and provided well-controlled deposition of individual CIGS elements.

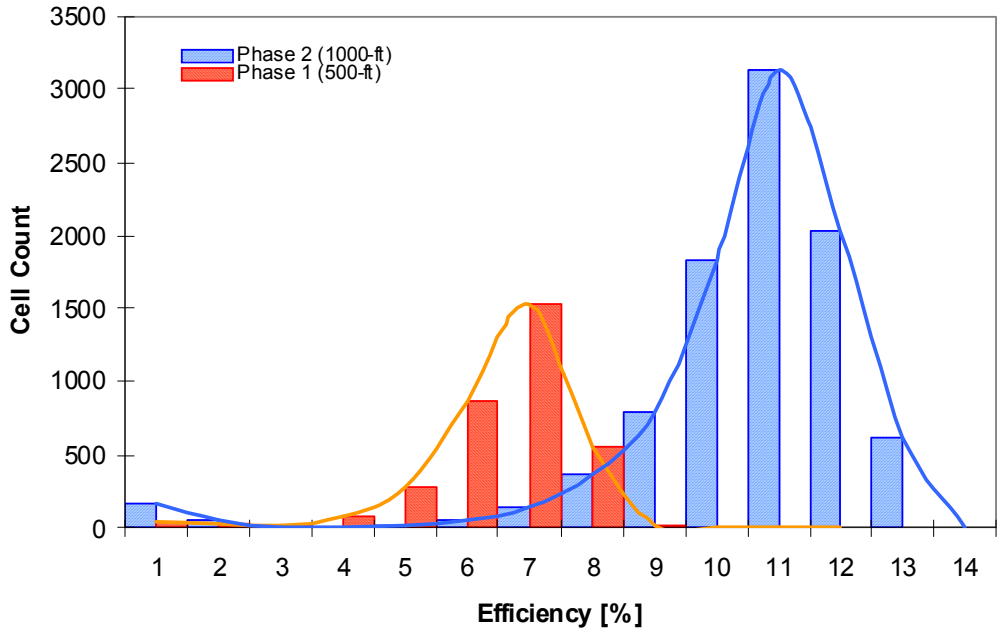

Figure 5. Comparison of cell efficiency and count for individual runs in Phase 1 and Phase 3

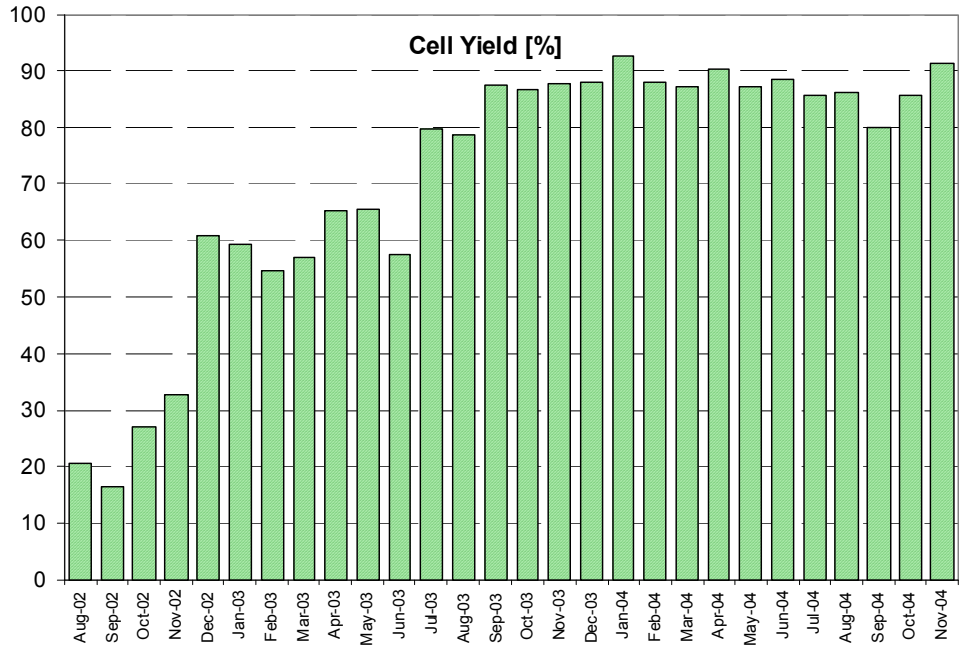

Figure 6. Time line of cells yielded for CIGS production during the PV Manufacturing R&D program.

Models were used to provide both revolutionary new evaporation sources and substantial process control improvements. In addition, fault prevention and tolerance activities increased reliability and identified several areas where reconfiguration/recovery methodologies were applied. Finally, several sensors were identified and implemented to provide real-time measurements for improved process control. The main

benefits from the different activities of the program resulted in substantially improved control/yields providing improved systematic evaluation through "design of experiments" that enabled process parameters to be more quickly identified and reproducibly obtained in production. These identified, improved processing parameters along with the improved control (Figure 7 and Figure 8) and decrease in faults (Figure 9) led to substantially improved performance and yields. Furthermore, the improved control and subsequent process parameter identification enabled a 100% increase in throughput of CIGS film processing without sacrificing performance or yields (Figure 10). Thus, in general, the expectations for CIGS PV performance improvements at the outset of this PV Manufacturing R&D program were far exceeded, enabling the future viability of thin-film flexible CIGS based photovoltaic manufacturing.

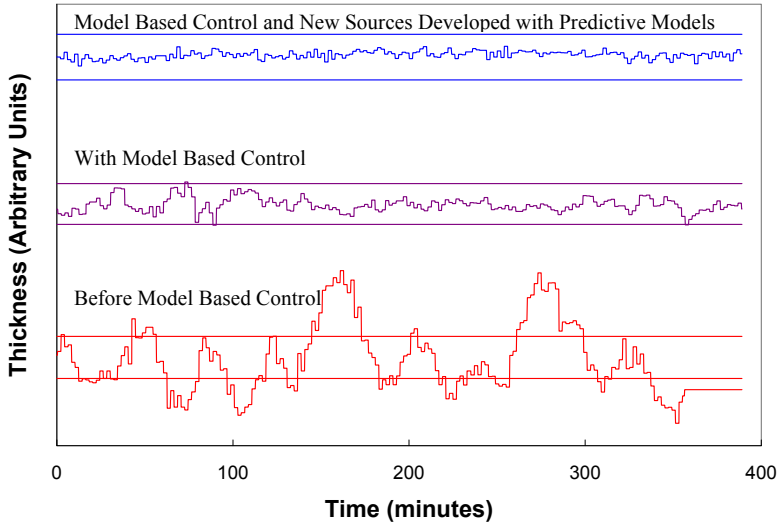

Figure 7. Comparison of thickness variability improvements with improved model development; the solid lines indicate +/- 5% from the average

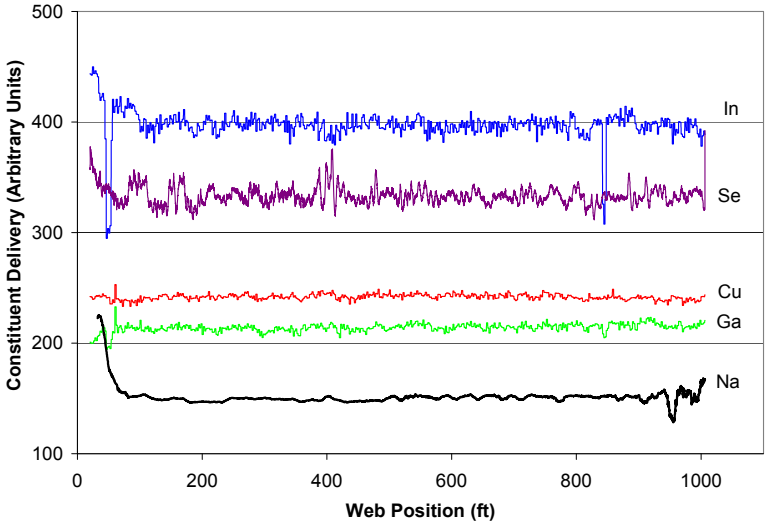

Figure 8. Real-time composition and flux signals monitored by in-situ sensors during a 1000 ft. CIGS deposition on stainless steel with active process control over a continuous 17 hour deposition period

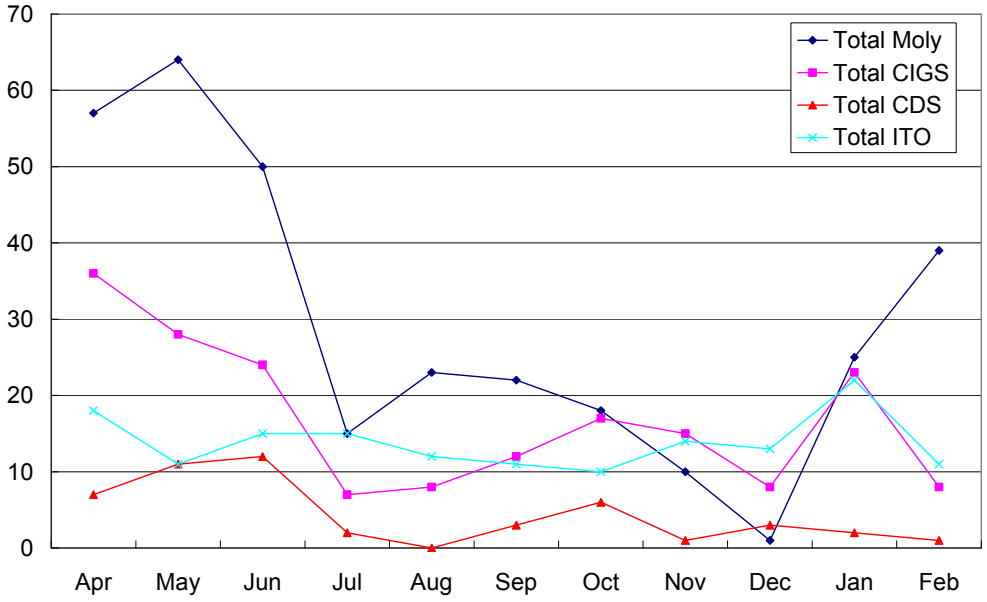

Figure 9. Frequency of anomalies or unplanned deviations (incidents) per 1000 ft. for different deposition processes demonstrates the significant gains made during the PV Manufacturing R&D program.

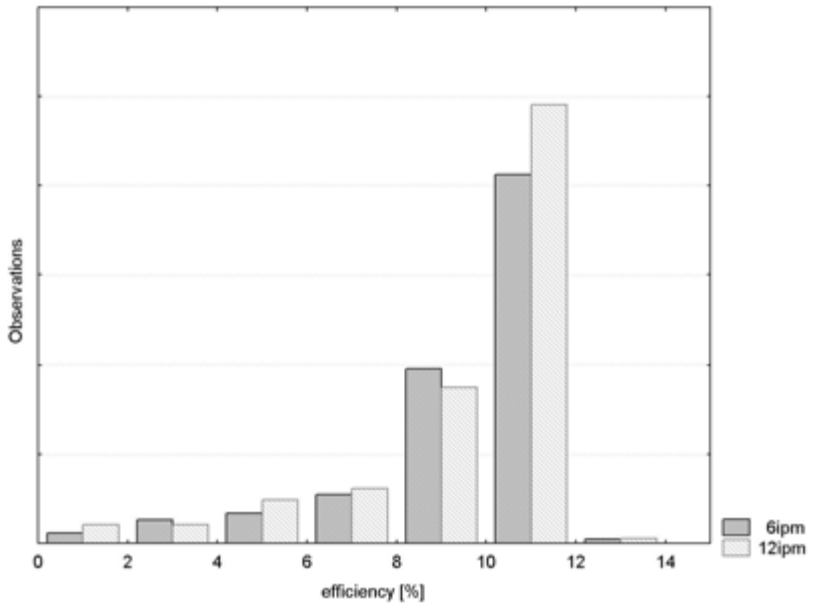

Figure 10. Representative cell efficiencies, showing a two-fold (100%) increase in absorber formation rate with no significant impact on cell yield, distribution or average efficiency.

3. Trajectory Oriented Model Development and Implementation for Production System IP Control

Physics-based models are key for better understanding of the process and as an important component for improved process control. Information learned on droplet nucleation and plume uniformity has directly led to design changes of the thermal evaporation sources. Furthermore, models identify fast transient dynamics for feedback control as well as slower dynamic effects that require gradual set point adjustments. Thus, model development was an important area of focus during the PV Manufacturing R&D program. As discussed above, the models enabled improved processes and hardware (e.g. evaporation sources), more robust dynamic control, and fault detection and recovery. In addition to model development, critical process variables were identified for improved control, and correlations were established between film growth parameters and film properties to enable improved performance and model development. The following sections describe the role of models for CIGS PV deposition systems.

3.1. Physics-Based Model Development and Implementation

In addition to model development for evaporation and sputtering, this effort also performed the required model validation and reduction necessary for utilization in efficient real-time process control. This involved tuning parameters to a particular reactor by perturbing process inputs and recording the response with available process sensors. A related process occurs for model reduction, where the reduced model structure is a generic low order differential equation or response surface, rather than specific physical laws. These models are then used to determine input trajectories and to determine internal states given sensor measurements. In addition, the source models provided temperature relationships between the melt and source outlet, predicted outlet dynamics including condensation, and predicted system time constants for transient input conditions. Therefore, the source models were used to predict quantifiable differences in source design changes to identify/validate improvements. Source design improvements resulted in significantly enhanced side-to-side uniformity and considerable reduction in the potential for recondensation in the effusion source outlet. Source redesign efforts have eliminated several undesirable operating characteristics and have substantially improved stability of the flux delivery, thus minimizing thickness variation, as shown in Figure 8. Detailed model development and implementation efforts for the program are provided below.

3.1.1. CIGS

The models developed and integrated for CIGS film production deposition systems focused on three major areas – mass sources, mass transfer, and deposition (Figure 11). Specific models developed included:

- *Finite Element (FE) Thermal* – A physics-based finite element thermal model of the effusion cells, with 2606 nodes, was developed in ABAQUS.[i]
- *Melt Convection* – A reservoir flow model was developed with the heat transfer model to determine the vapor flow in the source above the melt and to determine the conditions at the source outlets. From this vapor flow model, the conditions at specific points within the source was determined (pressure, velocity, and mass flow rates).

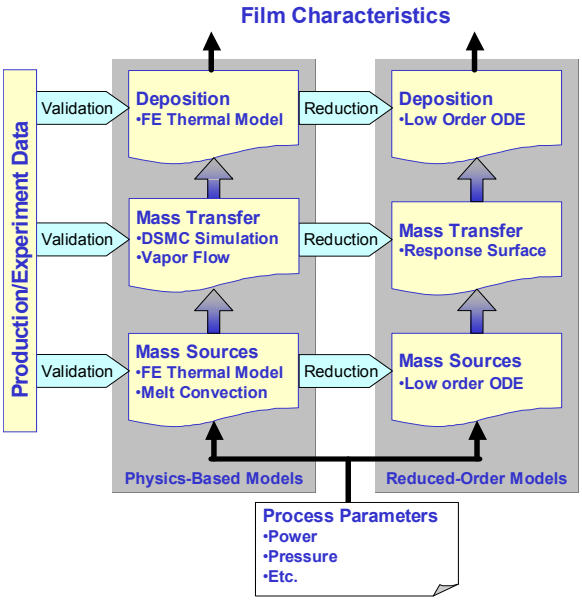

Figure 11. Outline of the individual modules combined to provide an overall model of CIGS processing.

- *Boundary-layer Flow* – The vapor flow model results are then put into a source outlet boundary-layer flow model, based on one of the codes in the CHEMKIN suite.[ii] This model was used to determine the nucleation behavior of droplets forming in the source outlet.
- *Plume Interaction* – The vapor flow results are also used as inputs to a Direct Simulation Monte Carlo (DSMC)[iii] module of the effusion source plumes. This enables investigation of plume interaction effects (including back-pressure at the source), and provides predictive plume shape capabilities to improve thin film thickness uniformity across the substrate.
- *Deposition* – Modeling efforts of the heat transfer to the web included effusion source surroundings, reactor geometries, and web/heater assembly configurations. This model was created and analyzed using ABAQUS; results from the effusion source models were simplified and applied as boundary conditions. Model results provided insight to web heating changes with source outlet geometry changes, as well as an effective heater model to predict thermal gradients throughout the web.[iv]

Mass Source Model - Finite Element (FE) Thermal

A physics-based finite element thermal model of the effusion cells, with 2606 nodes, was developed in ABAQUS (Figure 12, ABAQUS is a commercial software modeling package). The FE thermal model was originally developed to address poor cross web uniformity and nucleation/growth of particulates ("spitting") that were deposited on the substrate (Figure 13).

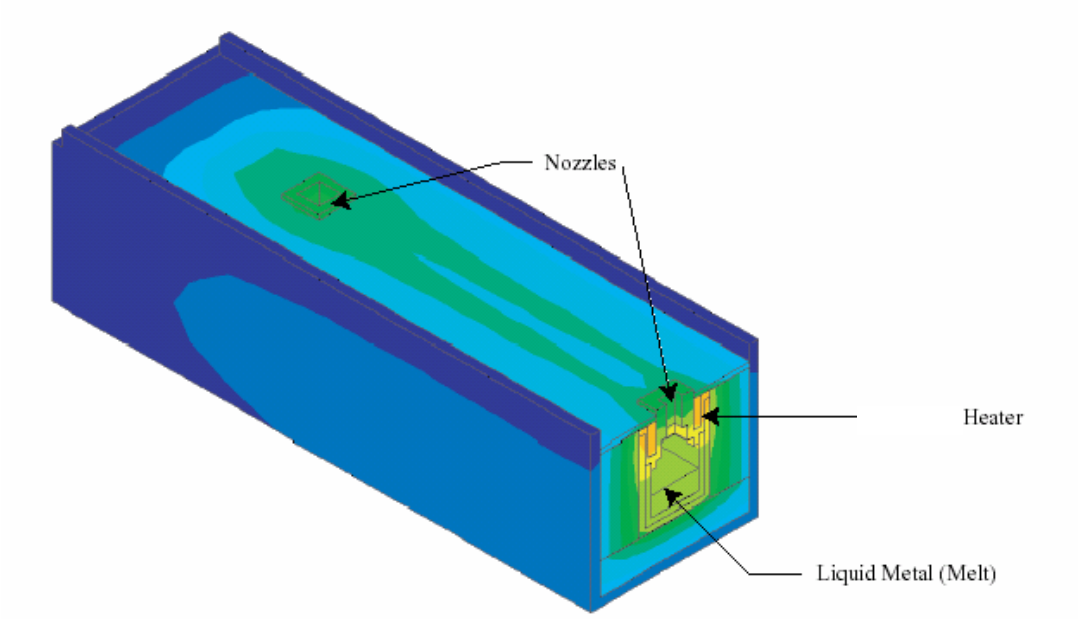

Figure 12. Finite Element ABAQUS Thermal Model of a thermal evaporation source provides detailed information about temperatures and transient behavior in the sources.

Based on information from this model a new metals evaporation source design was created and implemented. The new source design was so successful that source behaviors that posed major problems at the outset of the PV Manufacturing R&D program were entirely alleviated. Additional efforts increased the accuracy and adaptability of the ABAQUS model, improving the transient response predictability of the model. Figure 14 depicts thermocouple test data and the ABAQUS results for the equivalent power settings at various important locations. Note the solid line is ABAQUS data and the dashed is experimental. The data demonstrate the ability of the models to accurately represent internal source temperatures.

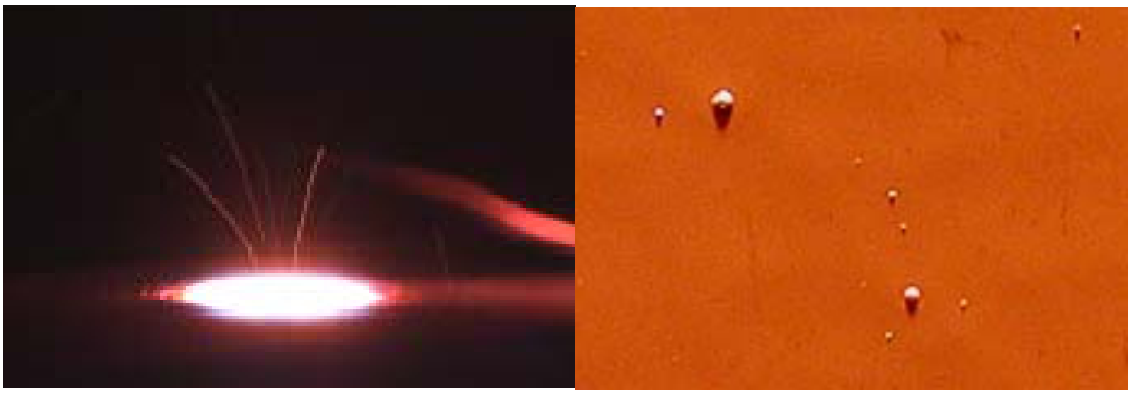

Figure 13. "Spitting" from the source nozzle (Left) causes particulates to form on the substrate (right). Courtesy of The Institute for Energy Conversion.

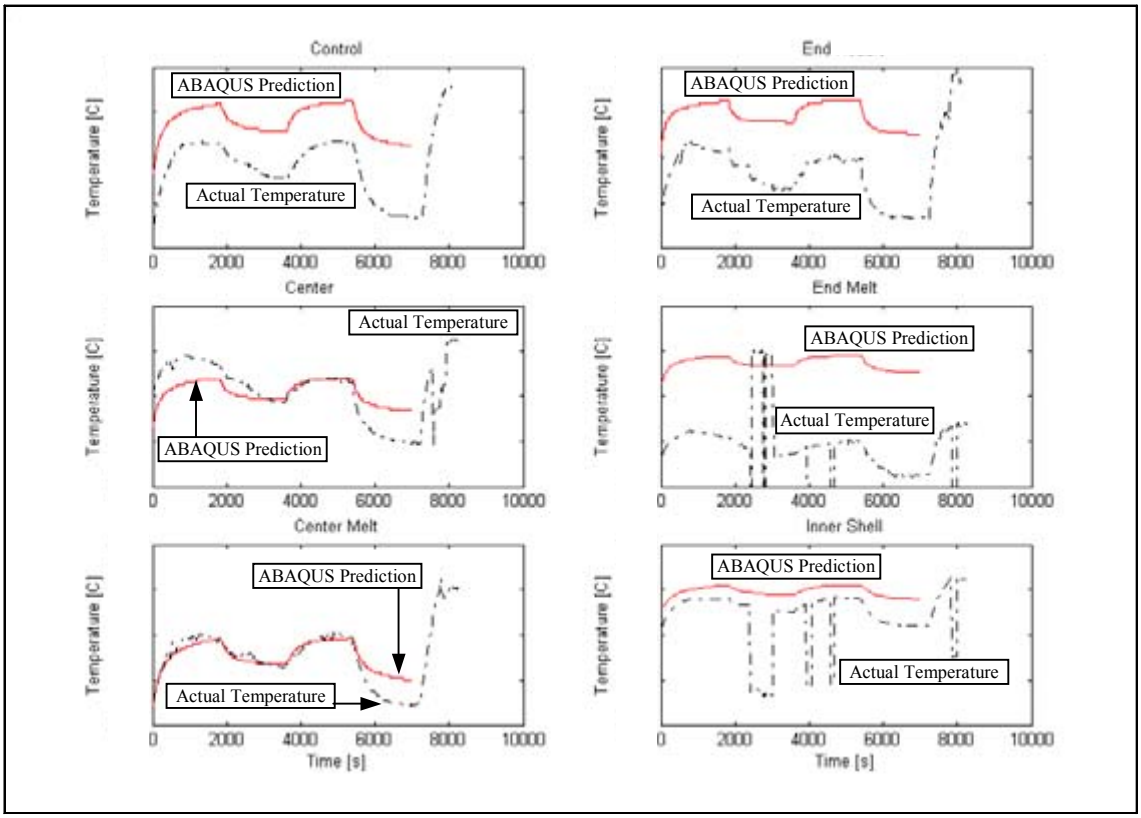

Figure 14. Comparison of Actual and ABAQUS Predictions of Source Temperature Responses. Note that the actual temperature responses have "drop outs" related to signal error, not actual changes.

To be useful for real-time process control, the validated FE thermal models are expressed using ordinary differential equations. Extension of previous source and chamber modeling work was done to produce more accurate reduced models that could be implemented for real-time processing. The reduction process was used to find the state space models of the system. For example, the ABAQUS effusion model was configured in nine different ways since there are three different metals and three different melt heights (10%, 50%, and 90%) to represent different periods during the deposition process. Reduced state models were determined for each combination, and they compared well with the ABAQUS models (Figure 15).

shows the system response of both a reduced model and the ABAQUS model for a 50% full copper source to a series of step inputs.

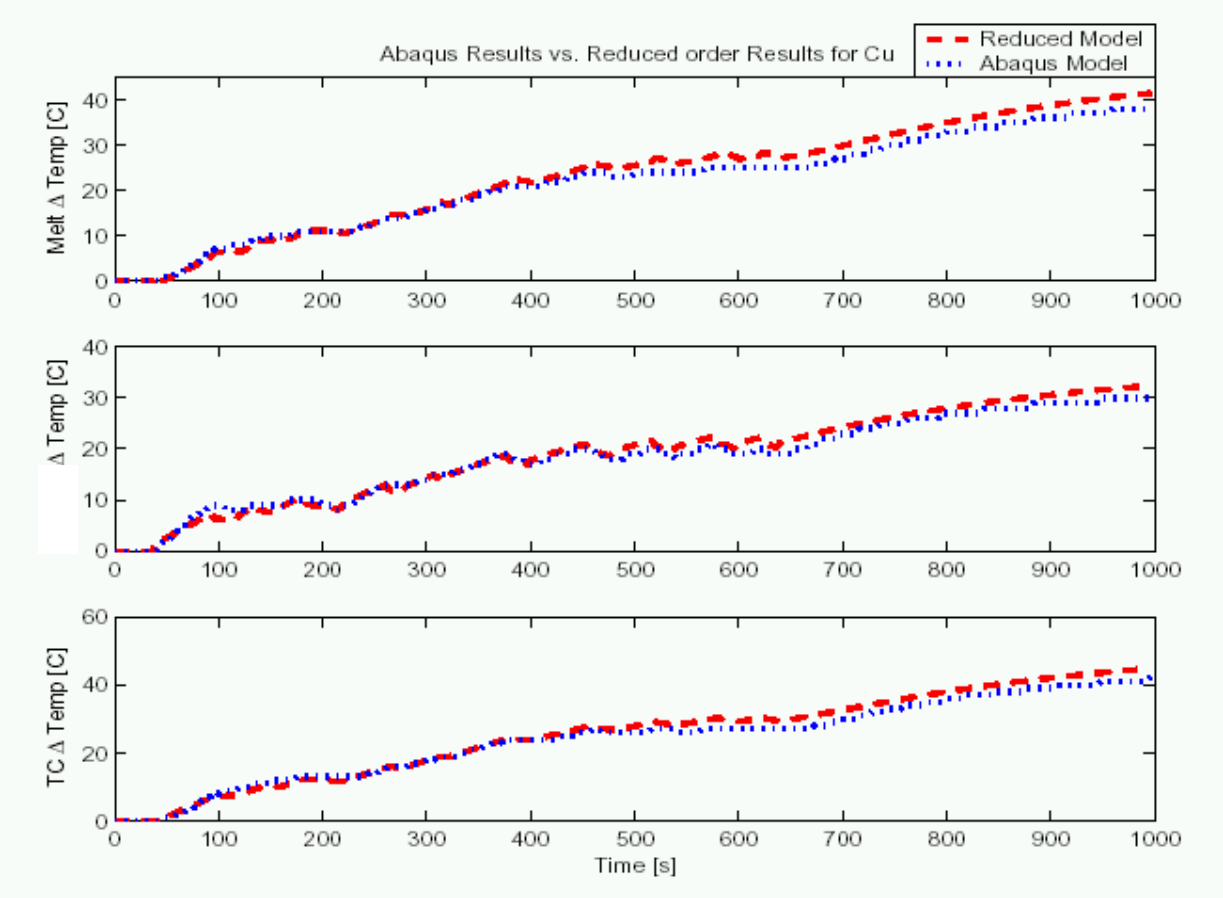

Figure 15. Comparison of ABAQUS and Reduced Models for different locations of a 50% Filled Cu Source.

Mass Transfer Model – Direct Simulation Monte Carlo

The Direct Simulation Monte Carlo (DSMC)[iii] model enables investigation of plume interaction effects, (including backpressure at the source), and provides predictive plume shape capabilities to improve thin film thickness uniformity across the substrate. Results of the DSMC model simulated vertical velocity field, temperature, ratio of critical diameter to hard sphere diameter, nucleation rate, and collision frequency. Representative plots of nucleation and growth rate are shown in Figure 16 with the cross section of the source outlet at the lower left corner. From these contour plots, it is evident that the gas rapidly expands to the near vacuum region at which the vapor flow accelerates and drops significantly in temperature. Regions of interest are the inner effusion source region and the bubble above the effusion source of colder temperature.

From the plot of nucleation rate (Figure 16), it is apparent that the bubble above the effusion source exit is the area of maximum nucleation due to the cold temperatures in this region. This area is even more important in that the ratio of critical diameter to hard sphere atom diameter is less than one. This means that nucleation in this region is collision controlled.[v]

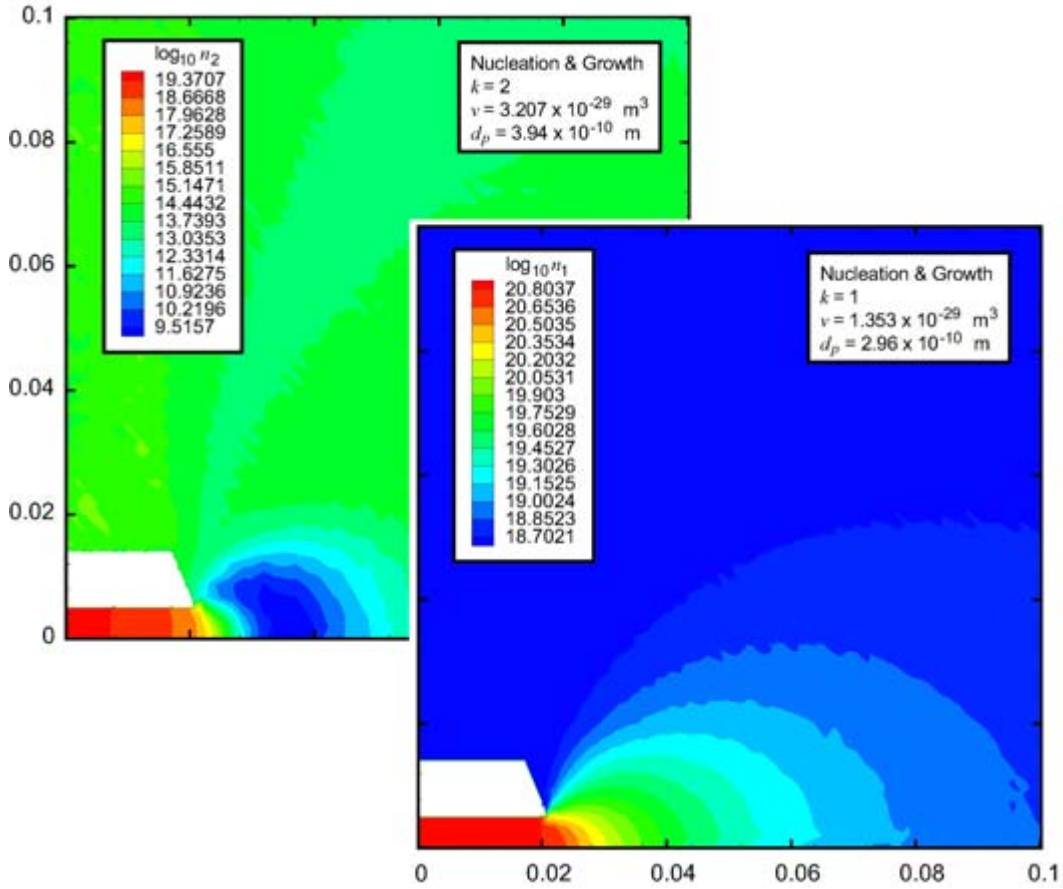

Figure 16-Contours of the size distribution function considering nucleation and growth by evaporation or condensation.

Modeling has shown regions where the nucleation rate is very high, but the kinetic-theory collision frequency is quite small. Since the flow is moving at sonic (or greater) velocities in the source exterior where the nucleation rate is high, the residence time is very small. For substantial droplets to grow, there must be sufficient time for atom-atom collisions, and subsequently, time for a metal cluster to grow. Additional research created a model that explained the process of droplet nucleation, including number of droplets and cluster size. Ultimately, understanding of droplet formation enabled source designs that eliminated this type of event, thus increasing yield and efficiency since droplets usually result in shorts.

The plume model (Figure 17 and Figure 18) was used in addition to the DSMC model and considers the effect of Se scattering in predicting plume shape and deposition uniformity for different rates. The data indicate that the model works very well and provides an accurate representation of the effused flux from the source outlets. This information was successfully used to develop source outlet geometries that enabled uniform deposition over the width of the webs.

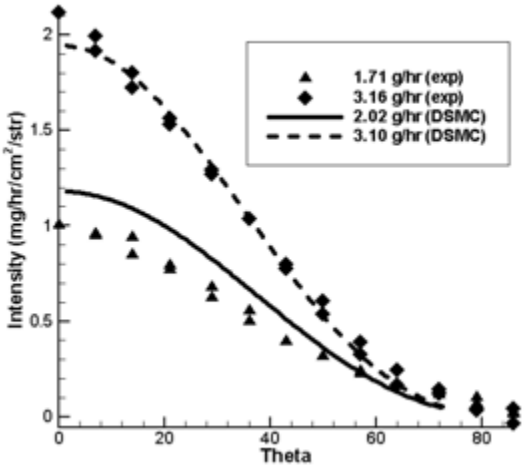

Figure 17. Comparison of ITN experimental and DSMC results at two mass flow rates.

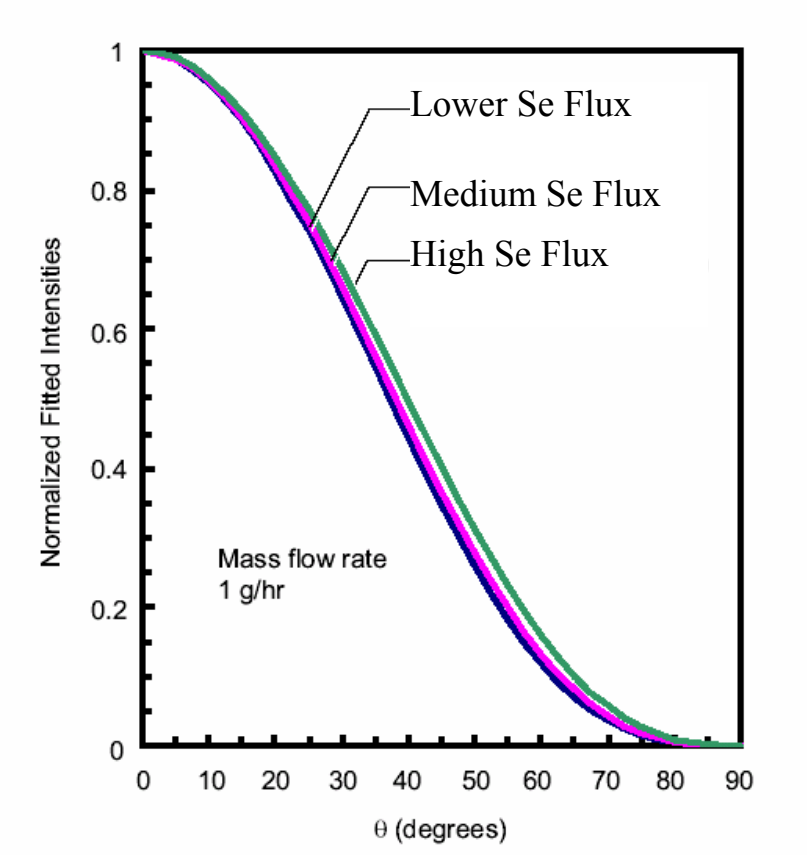

Figure 18. Normalized copper flux distributions for various selenium fluxes as predicted by DSMC modeling.

Deposition Model

Whereas the FE thermal model focused just on the effusion source, the deposition model (Figure 19) included the source, substrate heater, and the chamber walls. It evaluated the heat transfer to the web, including effusion source surroundings, reactor geometries, and web/heater assembly configurations

(Figure 20). This model was created and analyzed using ABAQUS; results from the source models (FE thermal for Cu, Ga, and In) were simplified and applied as boundary conditions. Model results provided insight to web heating changes with source outlet geometry changes, as well as an effective heater model to predict thermal gradients throughout the web.

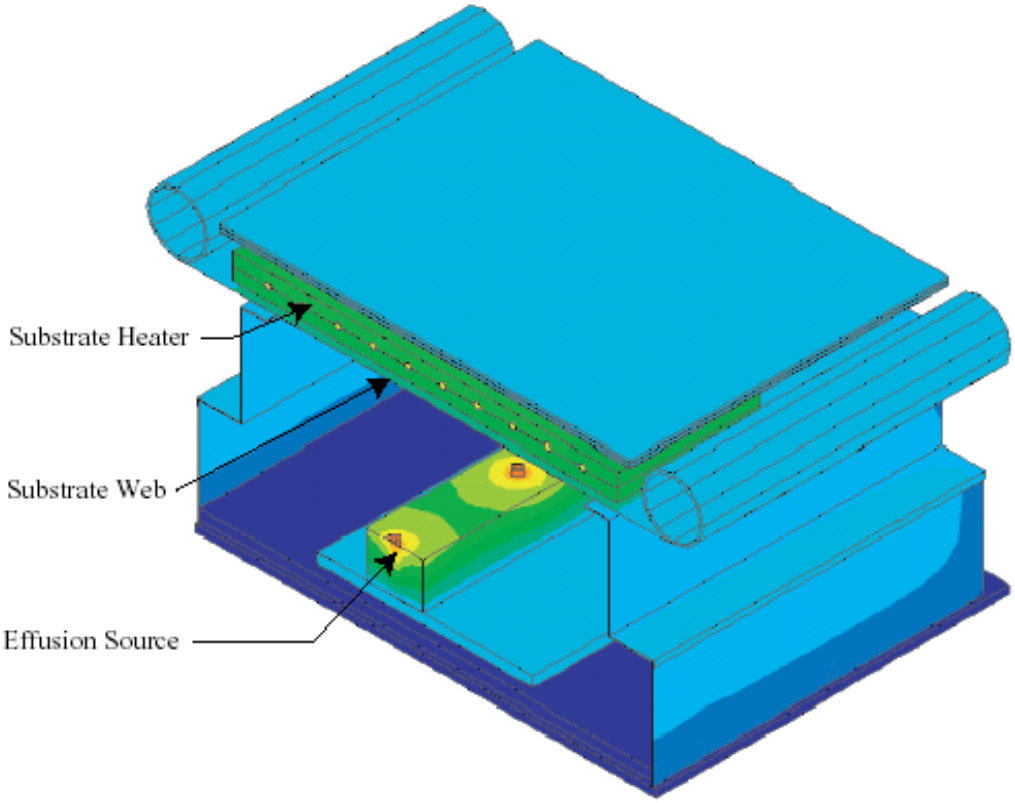

Figure 19. Schematic of Chamber Component used for the Deposition Model

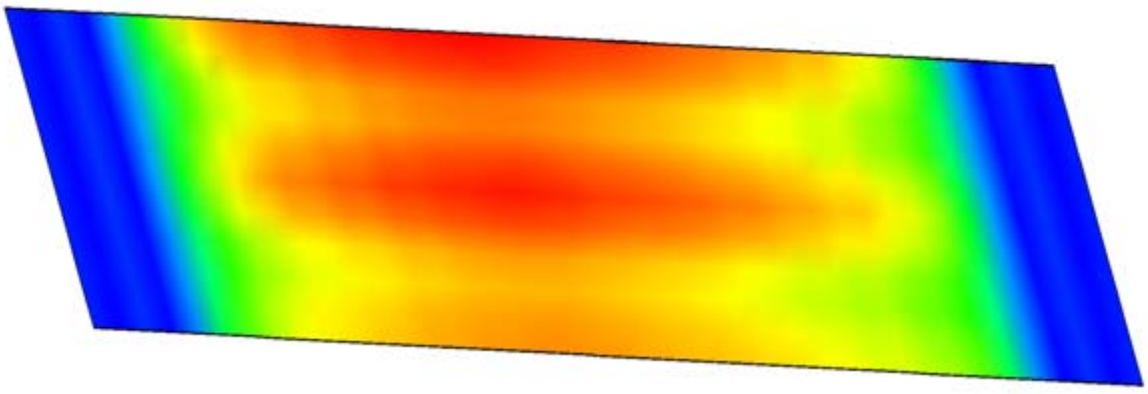

Figure 20. Qualitative temperature contour plot showing underside of web.

When work started on the deposition model, it was found that the chamber was strongly affecting the source during start-up. To evaluate this, the reduced source model was first simulated with previous start-up production data (Figure 21).

The next step estimated the model between real power and the chamber output signal. Finally, to get the correct estimate of temperature during startup, the outputs from both the effusion source and the chamber

source were added together (Figure 22). This combination produced a good estimate of the effusion source temperatures for start-up (Figure 23).

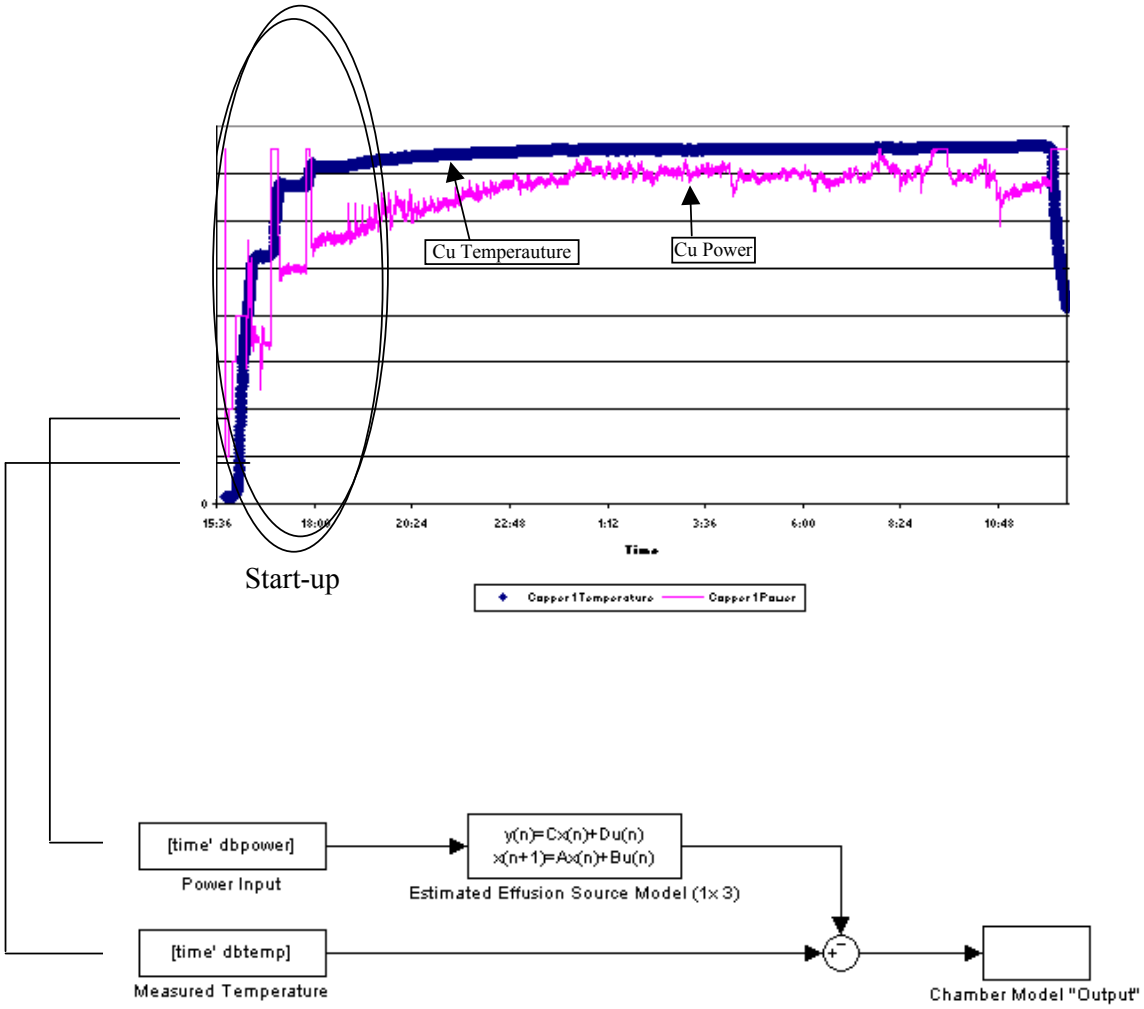

Figure 21. Schematic of Model Process used to Simulate Actual Deposition Chamber Output

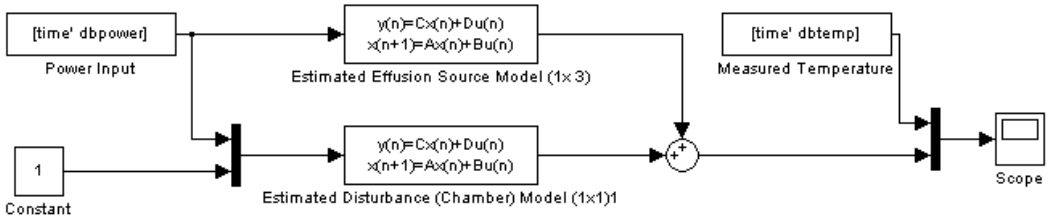

Figure 22. Schematic of model assimilation process

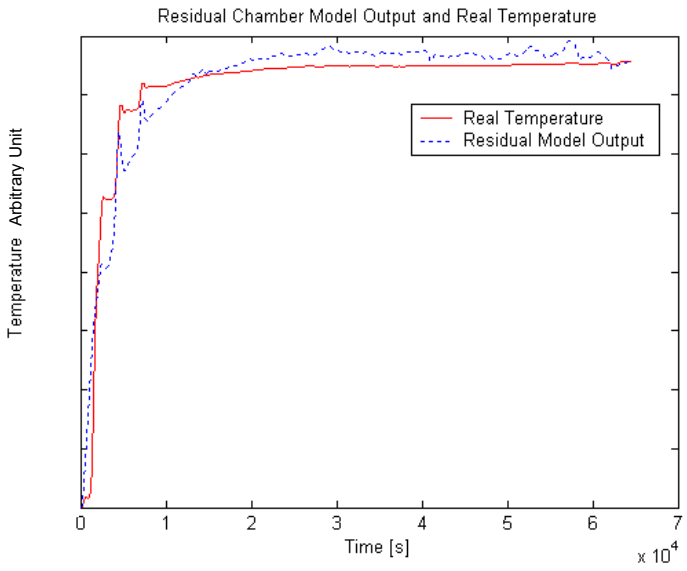

Figure 23. Comparison of predicted temperature and actual temperature

The steady-state temperature data from CIGS production runs were used to help fine tune inputs to the full ABAQUS deposition model. The model was validated with the results in Table 1, which are consistent with measured temperatures.

Table 1 – Comparison of predicted and actual temperatures.

TC Number	Description	Temperature Difference (Predicted - Measured Temperature)
1	Chill Plate (NOP side)	-16°C
2	Chill Plate (OP side)	6°C
3	Source Plate (NOP side)	1°C
4	Source Plate (OP side)	-8°C
5	Upper Cover, Take-up end	6°C, 1°C
6	Upper Cover, Pay-out end	2°C, -3°C
7	Source Plate	-10°C, -9°C
8	Upper Cover, NOP end	54°C, 27°C, 45°C
9	Upper Cover, OP end	-7°C, -2°C, 33°C
10	Se Source, top wall	Not in model
11	Se Source, inside Se melt	Not in model
12	Between Web and Substrate heater, Beginning of dep zone	44°C
13	Between Web and Substrate heater, Center of dep zone	0°C
14	Between Web and Substrate heater, End of dep zone	38°C

The model provided important information about the temperature gradients on the web. The web is about 200°C hotter above the source than when it enters the deposition zone (Figure 24). Across the web, there is an approximately 50°C change (Figure 25). Thus, this model enables improved uniformity, ability to determine CIGS processing temperatures, and dynamic control during warm-up or from large changes in processing. This was used to positively impact overall performance and yield.

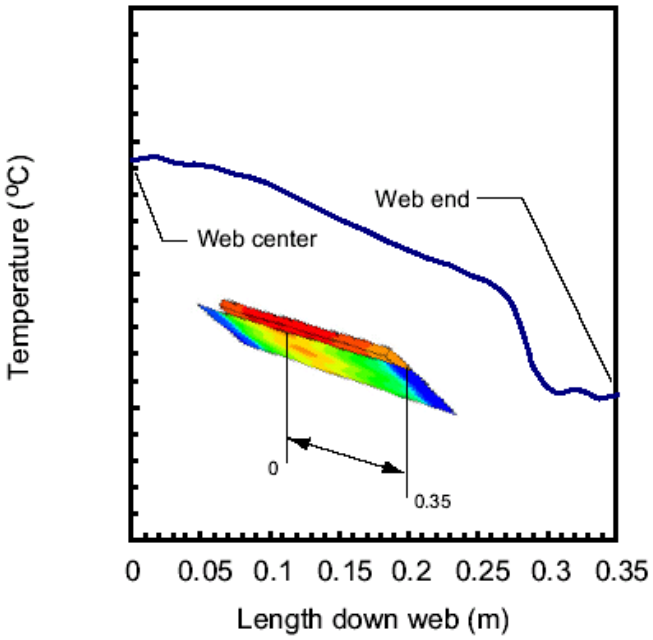

Figure 24. Variation of temperature along the length of the web at the web centerline

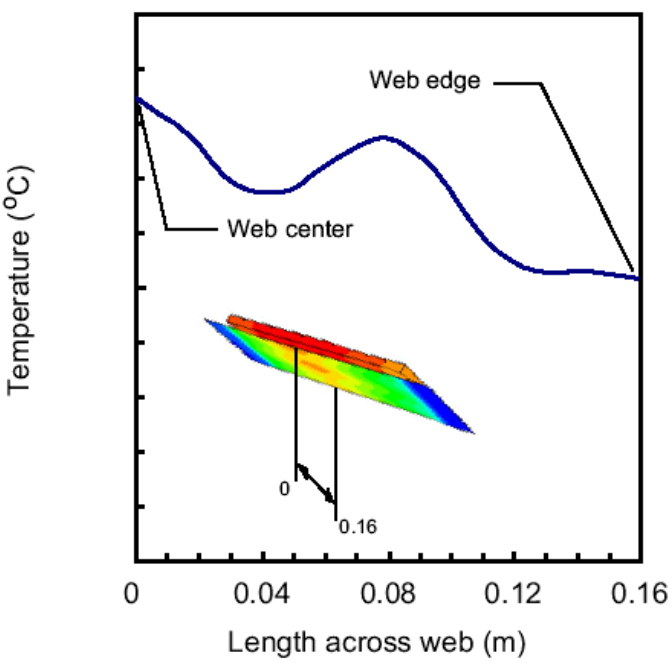

Figure 25. Variation of temperature along the width of the web from the centerline to the outer edge

Multiple Effusion Source Rate Estimate

The physics-based models developed for this program were used in a number of ways, including improved or enabling process control. For example, contributions from multiple effusion sources are determined from a process that renders the deposited film useless for PV. Thus, this procedure is used minimally and real-time contributions are unknown. Because of the nonlinear dependence of effusion rate on temperature, there is the possibility of obtaining information about the absolute effusion rate using only the change of effusion rate with temperature. If implemented, the procedure could increase yield by not taking the compositions out of bounds and could improve down-web uniformity to enhance efficiency. To evaluate how the contribution estimation will work, a simulation was performed using MATLAB. Based on these simulations, perturbations were designed and used to determine the contributions from multiple effusion sources.

The MATLAB simulation was developed along with several corresponding reduced gallium and indium models. These reduced models were incorporated into a simulation system with existing gallium and indium temperature controllers and set point estimators. A schematic of the methodology for developing reduced models is shown in Figure 26.

Running this simulation required an estimate of effusion rate from melt temperature. This is stated functionally as:

$$R_{Effusion} = Ke^{pT}$$

The goal of the simulations was to estimate ***K*** and ***p*** from measured thickness data, so ***K*** and ***p*** were selected and compared with the simulation estimates. Model outputs for both gallium and indium are shown in Figure 27 and **Figure 28** and compared with the experimentally obtained system response from the CIGS deposition chamber where the perturbations were applied. The data in the figures demonstrate the ability of the models to provide accurate dynamic response predications, thus enabling unique measurement capabilities to determine the effusion rate from each source in a multiple source configuration. The goal is to be able to apply a short series of small temperature perturbations to the effusion sources to accurately calculate the contribution from each in a multiple source system. In addition, the models also provide predictions of the anticipated accuracies of the measurements based on the number and size of the perturbations and the noise in the deposition systems (**Figure 28**).

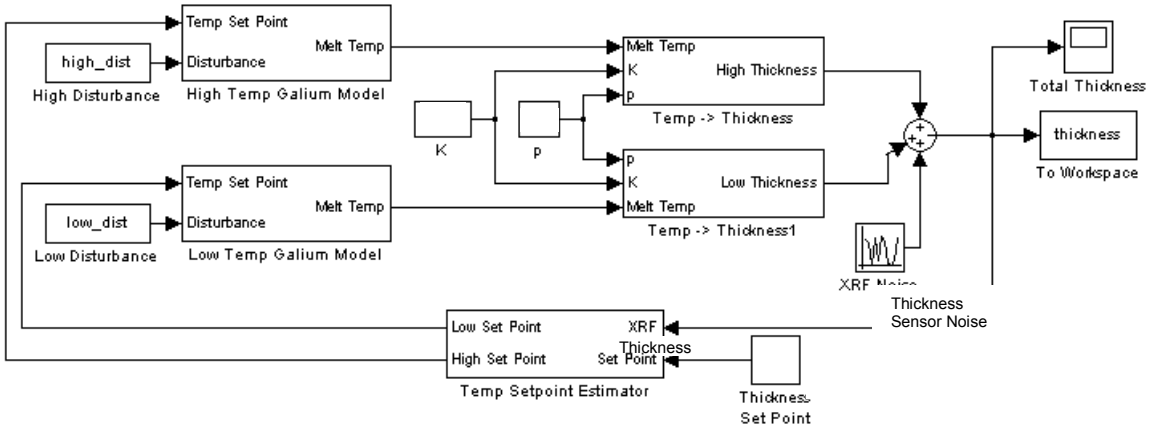

Figure 26. Schematic of MATLAB simulation for gallium rate estimation.

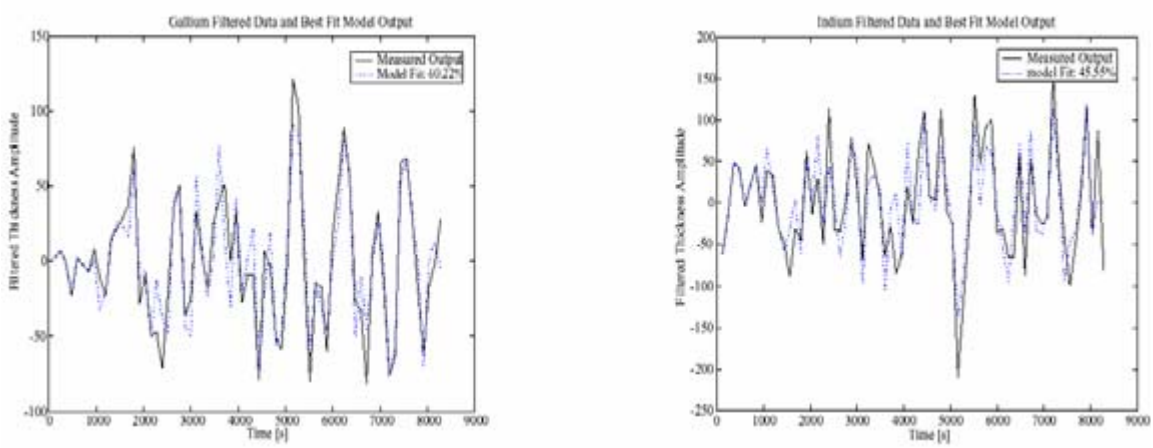

Figure 27. Filtered Gallium (left) and Indium (right) Data and Model Output

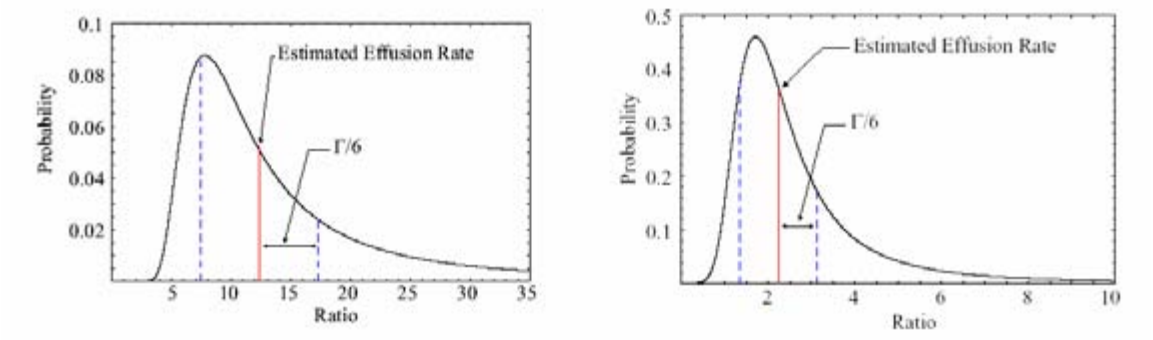

Figure 28. Ratio Probability Distribution for Gallium (left) and Indium (right) experiments indicate that the accuracy of the measurement will probably need to be improved to provide information for enhanced process control.

In addition to providing predictive information about each component in the process, models were utilized to provide improved control of individual element deposition from each CIGS source. Model-based control was implemented for all the CIGS deposition sources (NaF, In, Ga, Cu, and Se) based on sensor input and non-linear dynamic models. Compared to simple PID control, model-based control is advantageous for decreased thickness variation of individual constituents, as shown in Figure 7, corresponding to better control of film properties including Cu/(In+Ga) and Ga/(In+Ga) ratios. Process modifications resulting from model-based control combined with improved source design improved overall yields and performance. Production data was used for validation; however, the physics-based models are too complex to be used directly for process control. For this purpose, the physics-based models were simplified into reduced-order models, which were also validated by production data and operate approximately 2000 times faster than the full physics-based models.

3.1.2. Sputter Deposition Modeling

A commercial software package, PvPro, incorporates physics-based models based on Monte Carlo simulation to provide predictive sputtering deposition processing. The software incorporates operating conditions (e.g. process temperature, power/voltage/current levels, and gas pressure) and calculates deposition rates and distribution. This provides accurate deposition information of one of the cathodes in the chambers, so each cathode's deposition rate can be calculated/predicted for improved hardware design and enhanced process control. This set of physics-based model tools was applied to both the Cr/Mo and ZnO/ITO deposition systems. Models have been incorporated as real-time sputter control algorithms to

compensate for time variations in the deposition rates associated with target wear. This strategy considers several parameters, including time and power history, to determine the wear of a target, and this, in turn, is used to actively adjust the power set point to maintain a specified film thickness. The compensation algorithms that provide power set points to each target power supply at any given time are given by:

$$PowerSP_{next} = PowerSP_{start} + k \times KWH_{total}$$

where $PowerSP_{start}$ is the power set point when the target is new, k is the set point stepping value, and KWH_{total} is the total energy consumed by the target since it was installed. $PowerSP_{start}$ and k values were validated against production data. It has been found that k = 2.6877 for ITO and 2.3253 for Mo systems. This technique works very well, enabling desired Mo and ITO film thickness to be produced during manufacturing.

Indium Tin Oxide (ITO)

In addition to physics-based models used to provide flux and distribution information, models were also developed to provide ITO film property optimization for PV modules. The most important issue for ITO processing is a trade between conductivity and transparency, which are inversely related. To better understand the issues, physics-based models were developed to associate power/efficiency losses related to the transparent conducting oxide (TCO) layer (in this case ITO). However, as part of the trade, aperture losses due to grid fingers, joule heating, dark distributed diode losses and shadowing must also be included to perform proper optimization. Basic models for each loss mechanism along with transmission and conductivity models for the ITO layer were combined and validated against data from production material (Figure 29). This model is used to provide appropriate processing targets for optimum ITO performance and is being continually compared to production-made ITO for evaluation purposes. Proper ITO optimization may provide 0.5 to 1% absolute efficiency improvement in PV device performance, while loss of proper control may significantly degrade overall performance.

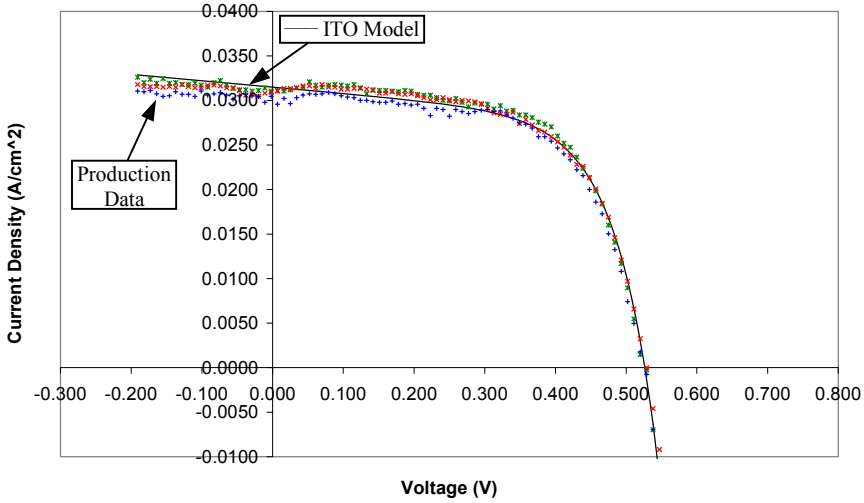

Figure 29. Small-area device J-V data along with a shunted ideal solar cell equation fit to the data.

3.2. Production CIGS PV Testing

As part of our production PV process evaluation, a systematic series of tests and analyses were performed comparing the different processed layers of production CIGS cells with base line, research-based processed layers. The main goal was to determine any performance differences and potential improvements associated with the large area production CdS, ITO, and grid array processing along with the specific causes. In addition to standard I-V, QE, and spectral absorption analysis, samples are analyzed with XRD

and spectroscopic ellipsometry. Typical testing involved completed CIGS PV cells (68.8 cm^2) cut into four equal sections (quarter cells) that were sufficiently small to fit into the characterization equipment. Direct comparison of performance was made with material that was pulled from the production processing before CdS and/or ITO deposition, along with completed material where one, two or three of the top layers were removed. All cells were finished with the research-based processing and compared with the production material.

After thorough testing and analysis of the three layers on top of the CIGS absorber, the production step that was found most different between production and research-based processing was the top current collection grid. The production system used a silver paste as the top current collector where the research system used a Ni/Al evaporated current collector. Measurements of the production grids showed hysteresis and unstable behavior in the dark and light JV characteristics when subjected to a reverse bias of more than –0.1 V (Figure 31). The behavior was evident when efficiencies were 8% or higher.

JV tests were performed on production material by sweeping from reverse to forward to reverse (RFR) forward to reverse to forward (FRF) for comparison. Large differences were observed depending on pre-test biasing conditions that were varied from –0.2V to -0.5V. Repeatability, stability and sweep dependence of the measurements were all issues. In general, FRF sweeps gave fill factors (FF) that were up to 10 to 15 percent lower, while Voc and Jsc were not significantly affected. In some cases FRF sweeps resulted in very unstable JV characteristics that recovered to a certain degree after forward bias light soaking (Figure 31). Also, cell efficiencies improved more than 15% when the current collector was changed from the silver-paste (production) to the evaporated Ni/Al grid (research). While the specific mechanism for the significant difference is still being determined, the research clearly identifies a potential area for improved performance and also indicates that the other production processes are performing adequately. The most significant loss mechanism, excluding current collector grids, of the production-completed devices was in the series resistance, lowering the fill factor, due to ZnO/ITO layers. Other than that devices completed with the research reactors were no different than the devices from the production reactors. This latter data instigated a reoptimization of the ZnO/ITO processing which in turn resulted in improved performance of production modules.

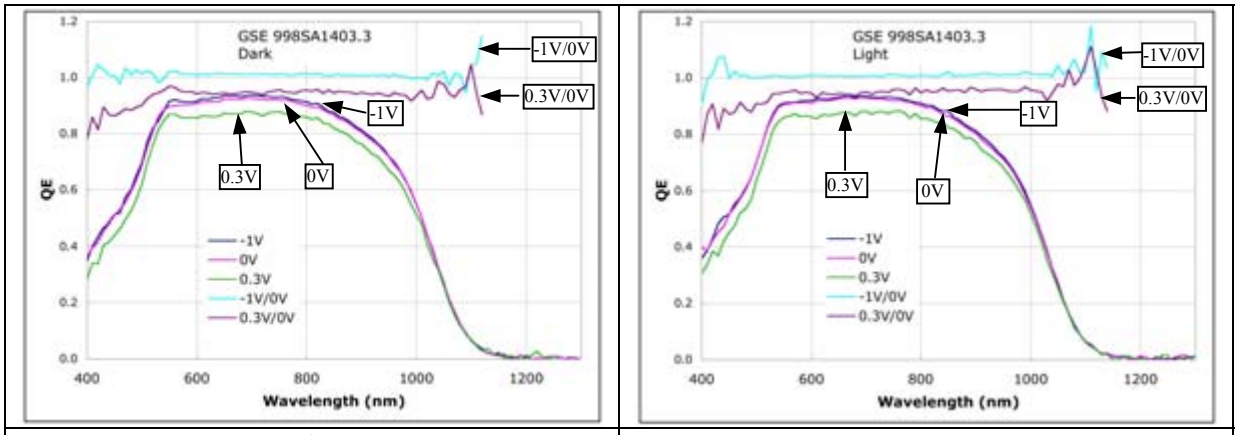

A **B**

Figure 30. QE data of a quarter cell at different voltage bias; (A) in the dark, (B) under 10mW/cm^2 ELH illumination.

CIGS PV Cell Characterization

Variable Angle Spectral Ellipsometric (VASE) analysis was performed to provide additional information about the different material layers in the production PV cells. The multi-layer film structures that gave the best fit to data did not match the qualitatively different Ga profiles. That is, for some of the samples the model showed a Ga rich surface layer, while for others Ga content decreased monotonically from the Mo interface to the free surface. The fitting algorithm assumes knowledge of optical properties as a function of Ga content. For $CuInGaSe_2$ the reference sample had a Cu/(Ga+In) ratio of 0.9. If there were variances in this ratio from one edge to the other, they might affect the "best fit" obtained from the fitting software. Data were obtained for the numbered coupons labeled in Figure 32. Figure 33 shows representative VASE data

along with corresponding model fits that are used to determine the structure (e.g. thicknesses) of the component films. To obtain appropriate fits to the data and keep the fitting computation time reasonable, the following assumptions were used in the models:

- Surface roughness and intermix layer are of the same thickness, except for $CuInGaSe_2$/CdS which was assumed to be 50% higher,
- Intermix layers are modeled as an equal mixture of materials in contact,
- Ga content in the $CuInGaSe_2$ film decreases from the Mo interface into the film, goes through a minimum then increases at the surface.

The major conclusion from the spectroscopic ellipsometry analysis of the numbered sections is that coupon 5-3 had a significantly thicker oxide layer thickness, compared to the other coupons. This is a little unexpected since substantial color difference are observed and are probably due to CdS thickness variations. Repeated data analysis using different CdS reference data provided no major differences in the results.

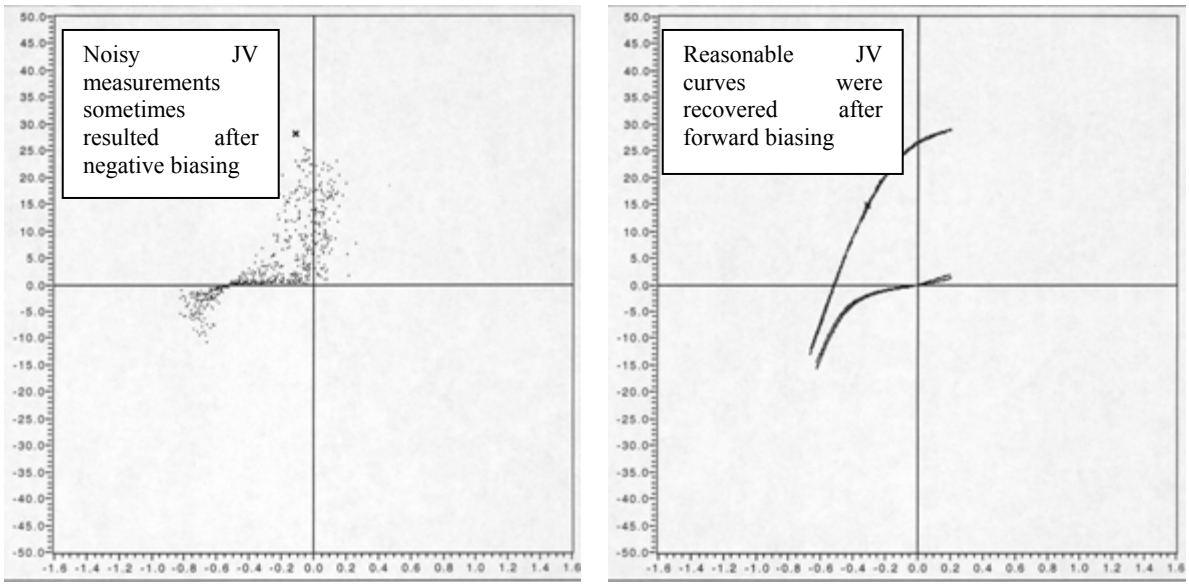

Figure 31. JV test results of forward, reverse, and forward sweeps of production CIGS cells. After reverse biasing, some of the cells resulted in very noisy JV curves (Left). However, some of the samples were recovered and produced good JV curves (Right) after 30 minutes light soaking at +0.6V (FRF sweep).

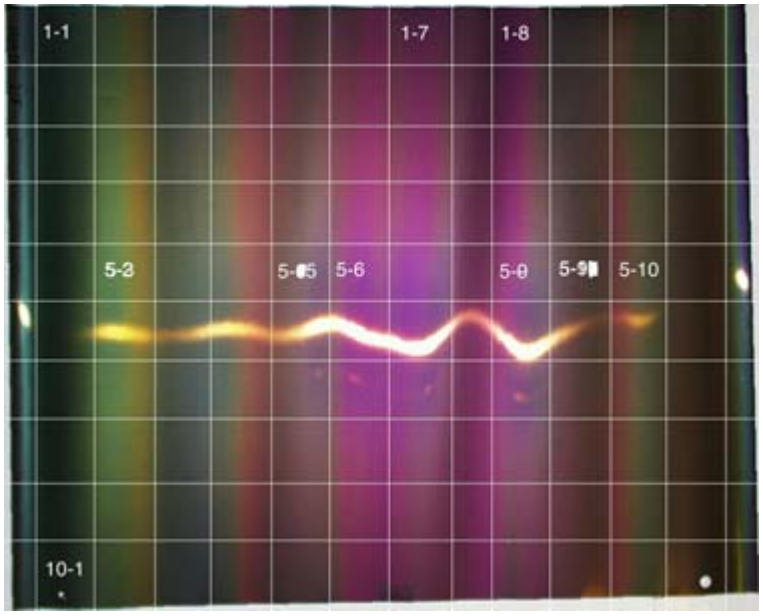

Figure 32 Photograph of representative production CIGS PV cell material demonstrating the easily observed color variations through the sample. The cell is divided into 1" X 1" sections for comparative analysis. Specific numbered sections were analyzed with spectroscopic ellipsometry.

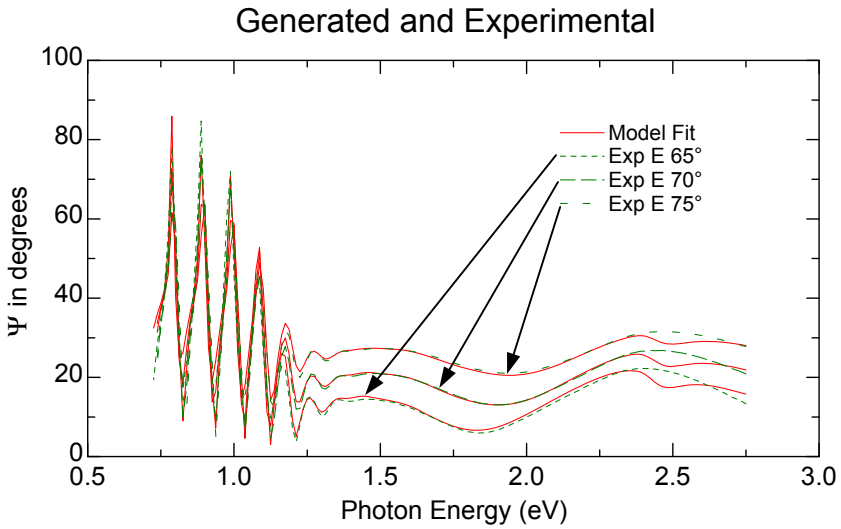

Figure 33. Representative comparison of experimentally measured VASE data and calculated model fits.

4. Fault Tolerance Development and Implementation

In general, fault tolerance describes a set of systematics by which components and systems that fail are detected and recovery strategies implemented to allow continued operation even at a reduced level. This enables throughput to be maintained since the system does not have to be shut down for every failure and it enables high quality material to continue to be produced to maintain performance and yields. For this program ITN and team developed, implemented and demonstrated models to detect and locate potential faults, intelligent decision-making approaches to identify options to resolve problems that are identified, and recovery strategies that enable operation even when components fail.

Diagnosis is the process of identifying malfunctioning system components. Ideal attributes include:

- Detecting and diagnosing faults as early as possible
- Discriminating between different failures with good resolution. A diagnosis is said to be *correct* if all fault-free components are identified as not faulty. Otherwise a diagnosis is said to be *incorrect*. A diagnosis is said to be *complete* if all faulty components have been identified. Otherwise, it is considered to be *incomplete*. A correct and complete diagnosis is desirable, but an incorrect and complete diagnosis is acceptable.
- Being robust to noise and uncertainties.
- Identifying multiple faults.
- Adapting to changes in environment, such as a process change.

Depending on the form of information required and the way it is used, diagnostic techniques are broadly classified as either redundancy-based or process history-based. Adequacy of these methods were evaluated for each of the subsystems/components.

Redundancy can be provided either in the form of hardware redundancy or functional redundancy. Since it may not be possible to incorporate hardware redundancy because of cost and physical constraints, model-based diagnosis, which is based on functional redundancy, has been selected. In functional redundancy, relationships exist between measured variables.

Process history-based methods make use of large amounts of process data and numerous techniques, such as statistical, neural nets, rule-based, and qualitative trend analysis. Techniques that were considered under model-based include observers, parity-space, and bond graphs, while the process history techniques include statistical and quantitative trend analysis.

Model-based diagnosis consists of interaction of observations and predictions. Observations indicate what a system is actually doing while the model of the system predicts what the system is supposed to do. Discrepancy between these two is used to detect and locate faults. The goal of model-based diagnosis is to perform correct and complete diagnosis, isolate the faults, reconfigure and restore the system to its normal operation with respect to input-output relationship by replacing the faulty components, or changing the appropriate parameters to force the system to return to the acceptable range of operation, or move the system to a safe mode of operation.

The basic assumption in model-based diagnosis is that the model is correct and all the discrepancies are due to faulty components in the system. Many times this assumption may not be true. The discrepancies may be due to error in modeling, noise, or drifts in the physical system. A mechanism is needed to correct these problems. Discrepancies will be analyzed by a fault set generator to produce the possible fault set. This set could be used to refine the model. Continuous monitoring will help to refine the fault set untill the predictions due to the fault set are consistent with the observed values. Considering the fact that qualitative and quantitative schemes have their limitations, the models used a hybrid scheme incorporating both the techniques. The model described the system behavior under fault-free and faulty conditions and accounted for dynamic behavior of the system.

4.1. Systems and Implementation

Identification of fault prevention/tolerance strategies for all levels of the CIGS PV production deposition systems was performed. In addition, specific subsystems were identified where implementation of fault tolerance methodologies could be beneficial. These fault tolerance issues included:

- Source thermocouple accuracy and failures
- Sodium fluoride sensor reliability
- Substrate heater failures
- Line voltage regulation
- Source power and current

- Se flux over range state monitoring and response, and
- Sputtering source arc detection.

Furthermore, to enhance system reliability, a systematic evaluation of equipment failures was performed and a preventive maintenance schedule developed (Table 2). In addition, redundant operator input was implemented to decrease the relatively high incidence of system faults induced by input error. The main reconfiguration strategies included redundant components, unstable state detection and reconfiguring and alternative sensor control. Several examples of fault tolerance/reconfiguration strategies are provided below to illustrate the complexity and unique approaches needed to provide robust operation.

Table 2 - Initial Maintenance Schedule

Maintenance Task	Period
Mechanical Pump - Check Oil	Every 2 weeks
Mechanical Pump - Change Oil –	Annually
HiVac - Check Oil –	Monthly
HiVac - Change Oil and clean	Annually
Bell Jar - Clean	Monthly
Substrate Heater - Replace TC	Every third week.
Substrate Heater – Replace	Every sixth week
Se Heater – Replace	Every other week
Metals Effusion Sources – TC	Check daily

4.1.1. Fault Tolerance on CIGS Deposition Systems

Thermocouples

Decision-making algorithms were designed as part of the fault-tolerant strategies for various controllers. Results generated by the fault-detection algorithms determine when faults have occurred. However, for example, an abrupt change in the temperature measurement is not necessarily a faulty thermocouple (Figure 34). Thus when a fault is detected, a comparison is made with a second measurement to ensure that the thermocouple is actually faulty. When a thermocouple is deemed to have failed, control is switched to a second (redundant fault tolerance) thermocouple or, for indium and gallium, control is switched to source input power.

For the copper effusion source the control is more complex. In this case two controllers are designed to control the effusion rate of copper. In the primary controller, thermocouple and XRF measurements are used in the feedback loop. In the secondary controller, input source power set points are controlled by XRF measurements. Figure 35 is a block diagram of the control loop with the thermal model directly replacing the source thermocouple. This is the simplest implementation and use of the thermal model. Every time the power is sampled, the thermal model calculates a new temperature. This temperature is compared to the estimator temperature, and the controller adjusts the power appropriately. Implementation of redundant source thermocouple, fault detection and fault recovery for CIGS source control has improved yield and throughput by preventing system upsets due to faulty sensors and system shutdown once the sensor is identified as defective.

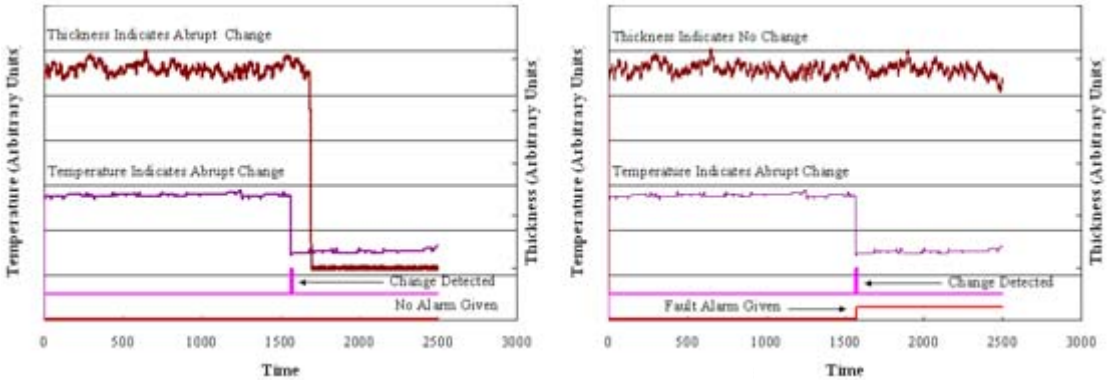

Figure 34. Example of fault detection process – An abrupt change in temperature measurement is not a thermocouple fault (left) and (2) is a thermocouple fault (right)

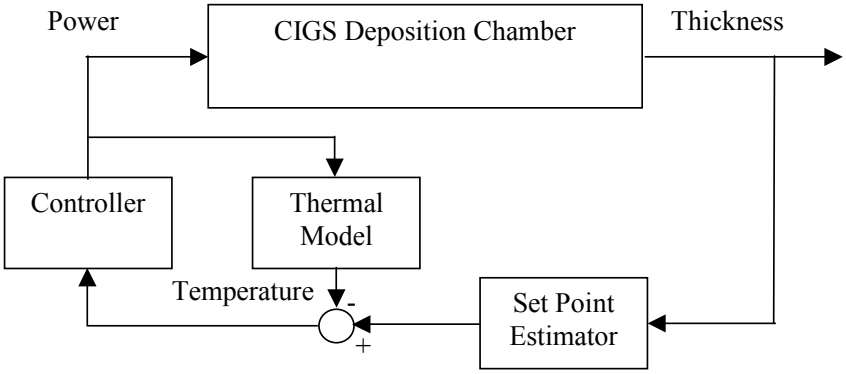

Figure 35. Example of fault recovery control loop using reduced thermal models

NaF

Control of NaF delivery and thickness is important for adhesion and efficiency. Since direct thickness control is presently not available, delivery control based on flux measurements has been determined to provide superior control compared to that of source temperature. However, flux sensor failure occurs fairly frequently and unpredictably. Thus, a decision-making algorithm was developed to compare measured flux sensor noise with predictive models for the sensor response based on source temperature measurements. Once the flux monitor becomes too noisy (Figure 36), sodium fluoride control is switched from flux based to thermocouple control. Since the NaF measurement sometimes returns to a normal state after a faulty event, the fault tolerant algorithm continually checks to determine if the NaF sensor is deemed normal and then re-engages the flux based supervisory control loop. Results indicate that this fault tolerant strategy is operating as designed: to eliminate process upsets, due to faulty flux sensors and yet enable superior module performance through better control of NaF thickness, thus improving yields.

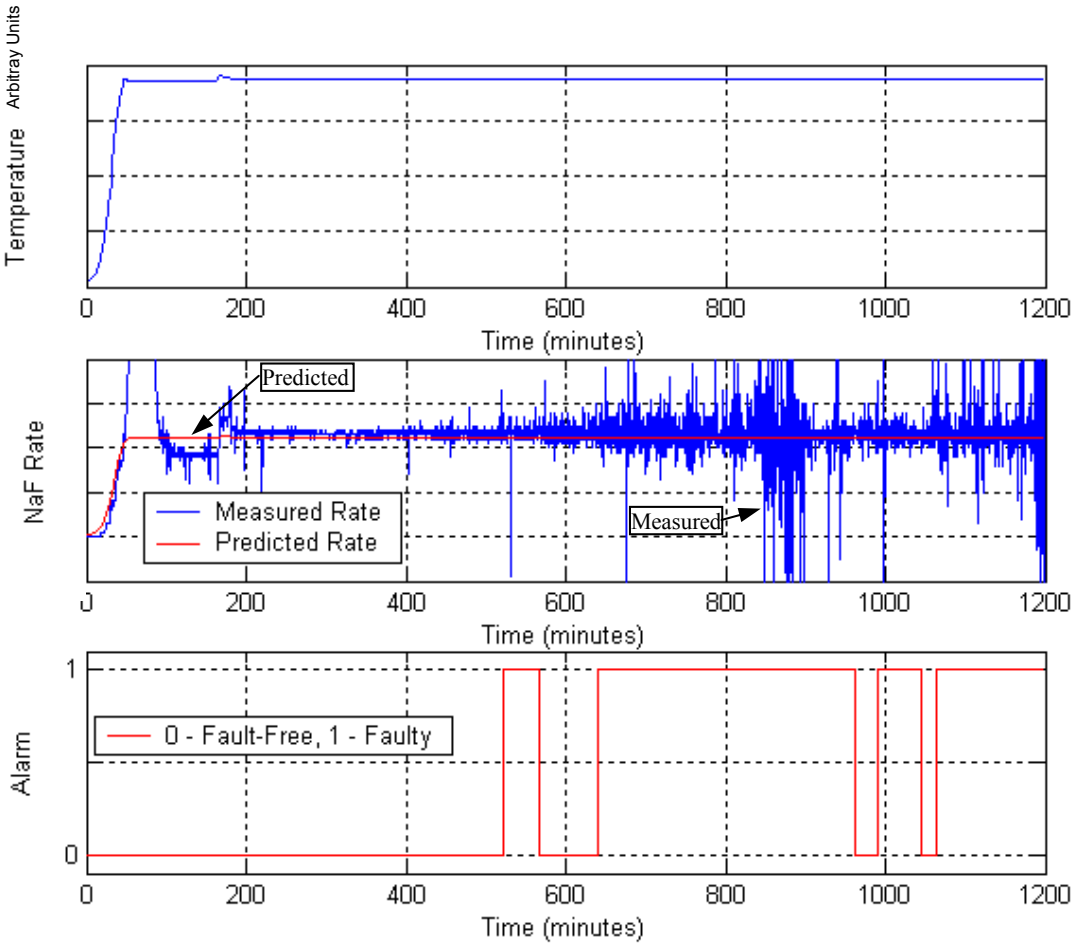

Figure 36. Comparison between measured NaF flux and a predictive model is used to determine when the sensor is faulty. Based on a prescribed set of conditions, when the sensor is determined to be faulty, an alarm is enabled and the supervisor control switches to a fault recovery strategy using NaF source temperature for control.

Se

The fault tolerance strategy for Se is similar to that of NaF. Again, control based on Se flux has been demonstrated to be far superior to that of source temperature/power. However, unanticipated process upsets occur where the flux sensor goes out of range, thus not providing useful measurements for control. A fault-detection algorithm was developed to identify these large spikes in signal, leading to an alarm. A decision-making algorithm causes the sensor to turn off and temporarily switches to constant source power control to eliminate out-of-bounds Se delivery and thus preserve CIGS yield and performance. The Se sensor is then probed at set intervals to determine if it has recovered. Se flux sensor control is reinstated when it is recovered (Figure 37) to provide optimum CIGS module performance. Since more than one Se flux monitor is used in a given processing chamber, capabilities for independent isolation and fault recovery strategies were implemented to maximize process control even with one sensor being disabled.

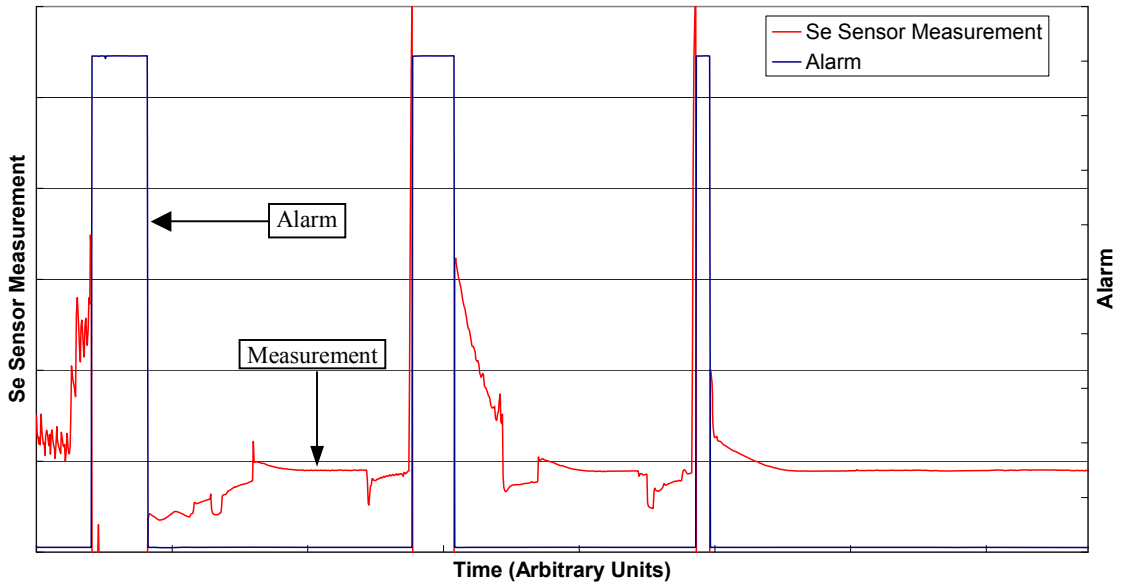

Figure 37. Se fault tolerance showing large spikes leading to an alarm and constant power control. Once the sensor is recovered, Se sensor control is reinstated.

CIGS Early Fault Detection

The CIGS deposition process requires a methodical, well-controlled warm-up. It generally takes three hours for the process to go from ambient temperature and pressure to standard deposition conditions. Frequently component failures occur during this time, typically in resistively heated components. Upon failure, the system warm-up will be stopped, cooled and then vented. The closer the system is to production deposition conditions, the longer it takes to cool down. This can be upwards of two to three hours. Thus, to maximize throughput, yield, and performance, immediate detection of failed components and autonomous shut down is essential. Autonomous capabilities are needed since operators are typically busy performing other tasks and only monitor start up progress a few times per hour. Thus, detection algorithms were developed to continuously monitor heaters and other components during warm-up to detect faults. The embedded software autonomously compares sensor/power measurements with expected/normal values and autonomously shuts down the system when a critical process component failure is detected and recovery is not possible, to minimize the cool down period.

4.1.2. Fault Tolerance for Sputter Deposition

Several thin film layers in the device stack (e.g., Mo, ZnO and ITO) are deposited using a sputter process. To coat 1000-ft rolls of material, the sputter process must operate reliably and continuously, using multiple cathode-target assemblies for up to 16 hours. Failure to operate reliably in production can result in aborted deposition runs and/or variability in the properties of the thin-film coatings. Figure 38 shows the relative ranking of incident categories where inadvertent process interrupts occurred during Cr/Mo deposition. The data indicate that arcing is the predominant cause of cycle interruptions. Occasional arc formation during processing is a common characteristic of sputter deposition in general that can result in poor film qualities/reduced product yield and, when severe, damage to equipment.

The process control platform on each of the sputter chambers was configured to detect arcouts (defined as a deviation in measured cathode power greater than a pre-defined threshold value) and respond by disabling the problem cathode and sounding an alarm to alert operators of the event. Previously, an operator was required to successfully restart the cathode or the deposition cycle automatically halted. To eliminate the dependence on human intervention for recovery, an automated, more intelligent approach for handling target arc events was designed and implemented within the control platform software. Upon detection of an arcout condition on any target, the control software attempts to restart the target up to three times. If the

restart attempts are unsuccessful, the problem target is disabled and a spare target, if available, is automatically turned on. If no corresponding spare target is available, deposition is halted.

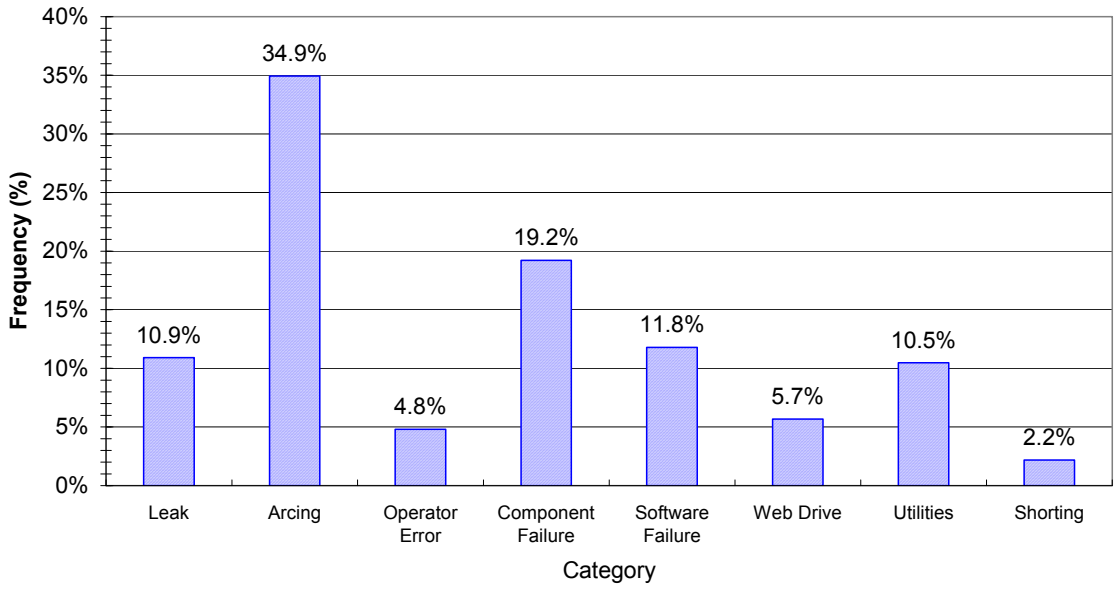

Figure 38. Breakdown of Sputter Process Interruptions by Cause.

As shown in Figure 39, successive integration of the arc fault detection and recovery responses resulted in an increasing number of arcout events being handled automatically by the software algorithms. The corresponding decreases in the fraction of arcout events ultimately leading to process interrupts dramatically demonstrates the benefit of employing fault tolerance/recovery in manufacturing. Because arc-related cycle interrupts necessitate venting of the vacuum chamber to correct the problem, the initiation of another pump down sequence (an additional 8-10 hours of equipment non-utilization), and approximately 10 feet of material (1%) being wasted, the resulting cost savings is significant.

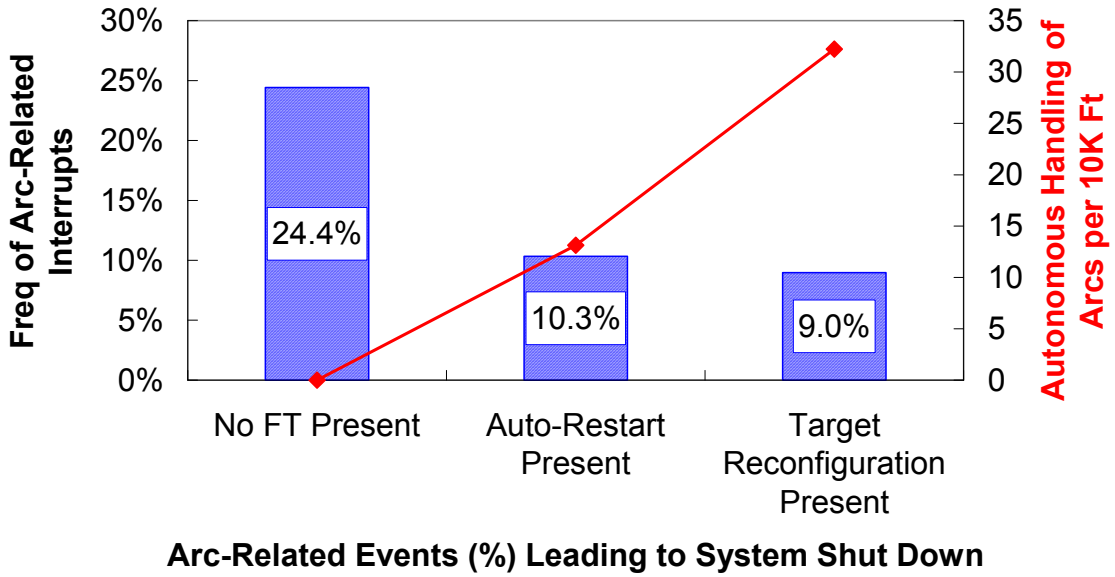

Figure 39. Effect of Fault Tolerance Algorithms on Arc-Related Interrupts.

5. Intelligent Process Control Platform

In order to implement trajectory-oriented control, control platforms were developed and integrated on production deposition systems with extensive flexibility and extensibility. The control platform allows model-based control/fault tolerance implementation, data input/output (IO), hardware interfacing, and a graphical user interface (GUI) for rapid dissemination of information. In addition to developing a robust and stable operating system, this effort also developed the communications, protocols and interfaces for all hardware systems including reliable data transmission and signal processing/interpretation for each sensor. Initial activities for this effort included a systematic evaluation of several commercial and custom control platforms and operating systems. Based on capabilities, requirements, and technical support issues, different control platforms were selected for different manufacturing processes. For CIGS model-based process control, a commercially available control platform was selected for the production manufacturing systems. Provided below is a general overview of the types of issues that were addressed by the control platform for transferring data and integrating physics based models and controllers. This is followed by representative examples of how specific control platform components were development and integrated together. Specifically, details are provided for the integration into the control platform of:

- An optical sensor and the corresponding controllers/autonomous data analysis capabilities;
- The automatic data handling capabilities for tabulating and displaying process parameters from sputter processing;
- Custom software designed and integrated to operate an XRF CIGS film inspection system.

5.1. Data Input/Output

A personal computer (PC) is used as a control platform base for CIGS manufacturing. To perform the required tasks, the PC must communicate with sensors and controllers attached to the manufacturing process. Communications are limited by the capabilities of the PC, including serial and parallel ports, peripheral component interconnect (PCI) slots, universal serial bus (USB) and network interfaces. Another limitation is the operating system. Not all interfaces are supported by all operating systems. For example Windows NT does not support USB.

The CIGS process uses a large variety of sensors and controllers, including: Keithley GPIB multimeter; XTC/2 quartz crystal monitor (QCM) Opto22 digital and analog input and output; Eurotherm controllers and an in-situ thickness sensor. The control platform is responsible for coordinating input and output from sensors and controllers. Each sensor and/or controller/model communicates with the control platform via a standard interface. The data bus is the component over which the data is transferred. Software supports the protocols used to decipher the information on the data bus. The following section describes the details of data collection and the control platform.

5.1.1. Data Collection

Data collection is accomplished through commercial packages that are highly configurable with appropriate communication drivers. The key issues in choosing most control platforms include reliability and support.

5.1.2. Protocols in Use

RS-485

The RS-485 standard allows for half-duplex, differential, multi-drop (32 nodes) attached to one pair, (2-wires) on a length of wire no greater then 4000ft.

IEEE 488

The IEEE 488 bus was developed to connect and control programmable instruments and to provide a standard interface for communication between instruments from different companies. The interface is also known as General Purpose Interface Bus (GPIB).

OPC

Object linking and embedding (OLE) for Process Control (OPC) is based on a Microsoft© specified protocol, namely, OLE. OPC lies on top of OLE to standardize the interface between an individual/group of sensors to an OLE client. The client is usually the control platform and an intermediate software module is the server. The server contains sensor specific code to "talk" to the sensor. Because the client-server interface is a standard, any OPC server should be able to forward data to any OPC client. OPC is TCP/IP Network aware, and data from remote PCs that are part of the same network is available to an OPC client. This does somewhat reduce the hardware limitations of an individual PC as the control platform host. One disadvantage to OPC is its reliance on an operating system vendor proprietary specification.

Dynamic Data Exchange

Dynamic Data Exchange (DDE) is a feature that enables Windows based programs to link together and communicate data via the Windows operating system. While the DDE method is considered rather old technology it is still a solid, reliable and tested interface that is well understood and easy to use.

5.1.3. Sensors

PID Controllers

Programmable process controllers are used for CIGS manufacturing. These controllers provide setpoint programming, PID and value position control. The controllers are connected to the control platform via RS-485.

Multimeter

Digital multimeters are used for PV manufacturing to measure the electrical properties of the photovoltaic material during the production process. This multimeter connects to the control platform via IEEE 488.

Digital and Analog I/O

PV manufacturing uses SNAP Controllers. The control platform communicates with the Controller via Ethernet. The SNAP Controller communicates to distributed I/O via RS-485 serial link. Desired data are downloaded from the SNAP Controller.

Quartz Crystal Monitor (QCM)

Thin Film Deposition Controllers use QCMs to measure deposition rates. The QCMs are connected to the control platform via IEEE488.

In-situ Composition Sensor

In-situ composition sensors measure the composition of material deposited in the manufacturing environment. The in-situ composition sensors communicate with the control platform via Dynamic Data Exchange.

Future Growth

The ability to add new sensors to the control platform is somewhat hardware limited by the amount of open space on the PC data bus. It is important to move towards a hardware and software solution to meet this need. RS-485 and IEEE-488 both allow for daisy chaining. Also network-enabled sensors diminish the individual PC hardware limitations. Equally important is to add a second layer to allow existing and future products to communicate with these devices. OPC is an option, as a default hardware communication standard.

5.2. Models and Controllers

The control platforms used for the project were designed to be flexible and easily extendable for use in controlling the production processes with a modular design. All of the devices, models and controllers are separated into modular components that can be added or removed while leaving the remaining project fully functional. This is achieved through the use of tag (variable) databases that are accessible to all modules but are also separate modules in themselves.

5.2.1. CIGS Auto Recovery of Out-of-Range Selenium Flux

As a fail-safe protection mechanism, the Se sensors trip themselves off when the selenium flux goes over range. When this occurs it is desirable to have the chamber recover from the over-range situation automatically. The control software that handles the restart of the Se sensors was developed and has been in place for sometime. However, for improved control the automatic recovery routines were expanded to include an automatic suspension and subsequent restart of the XRF control in response to an over-range event. The main issue involves an overcompensation of by the XRF-based controller due to the Se thickness being out of specification compared to the other metal sources. Thus, in addition to the Se control being temporarily suspended, the XRF-based control also was suspended and synchronized to reengage 20 minutes after the Se sensor is restarted. Subsequent modifications only disengages the XRF control for the specific metal sources affected by the Se sensor faults, rather than the XRF-based control for the entire process. This enables improved thickness/composition control, even in the presence of a faulty Se sensor. All these features were integrated on the production deposition systems.

5.2.2. CIGS Web Break Run-On

Previous control software used the detection of a web break as the trigger to stop the web drive and shut off power to the heaters. This results in the last ten feet of web resting directly over the heated sources and burning the material. This final ten feet of web was discarded when removed from the chamber, resulting in a 1% loss in the total 1000 feet of processed web. Thus the control software was modified to continue the web drive to remove the additional ten feet after a web break so that the remainder of the web is wrapped at the take-up mandrel. This function was implemented into the control platform with the addition of a timed delay after the web break detection that allows the web to run-on for several seconds before shutting the drive down. This simple modification has directly resulted in an average saving per web of approximately four feet.

5.3. Reflectometry for in-Situ, Real-Time CIGS Properties

Real-time sensors capable of measuring critical film properties enable process variability minimization and product yield and efficiency maximization. This is especially true in a roll-to-roll based process, where extended times and volumes of material accrue between opportunities to measure material quality with post-process characterization. For the CIGS layer, the optical behavior in the visible to near infrared (NIR) range is strongly dependent on several important optoelectronic material properties. Thus, optical reflectance in the region of 700 nm to 1700 nm potentially makes available important CIGS parameters, such as thickness, optical absorption and real index of refraction. In the CIGS ternary alloy system, throughout the range of compositional interest, the material generally becomes opaque at wavelengths shorter than 700 nm, and weakly absorbing and featureless at wavelengths longer than 1700 nm. Within

this range, however, the optical properties expressed in the complex dielectric function can be correlated to material properties of composition and defect density. The complex dielectric function, in addition to important properties such as thickness and surface roughness then determine the reflectance that is registered at the CIGS surface.

Appropriate forms for the complex dielectric function for CIGS (Figure 40), indium-gallium diselenide (IGS, Figure 41) and molybdenum (Figure 42) were selected from literature sources, along with tabulated values of the real and imaginary components as a function of wavelength for selected compositions, including CIS and CGS. Optical data was collected in the form of transmission and reflection of CIGS and IGS films made on quartz substrates over the wavelengths of interest and used in achieving a best fit of the expressions for the complex dielectric functions to actual polycrystalline material in thin film form. Likewise, the parameters of dielectric function for molybdenum were found using numeric least squares approaches to build a best fit to the actual reflectance of molybdenum coated substrate used at GSE.

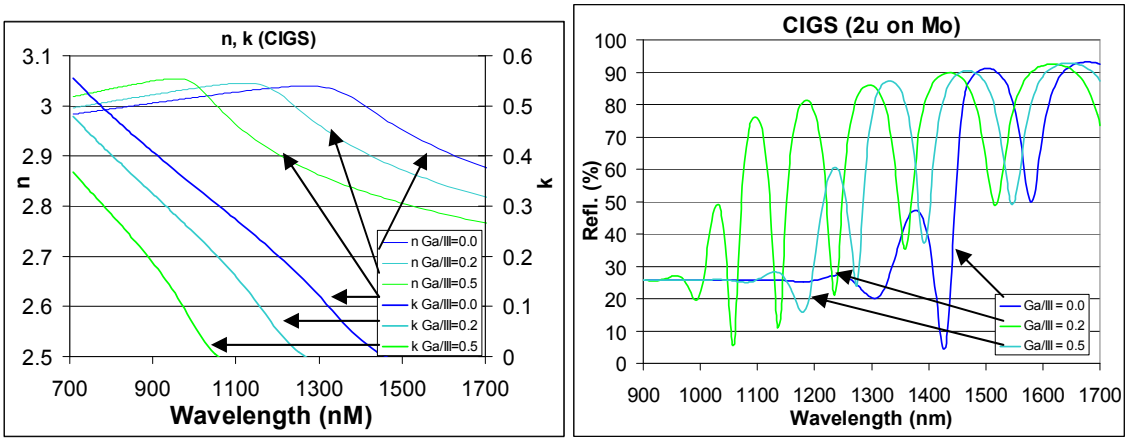

Figure 40. Left: The modeled dielectric function for various compositions of CIGS. The optical transparency at short wavelengths increases with increasing Ga content for this ternary alloy. Right: The calculated reflectance for a CIGS layer 2 microns thick having various compositions. The optical transparency at short wavelengths increases with increasing Ga content, causing increased amplitude of reflectance at those wavelengths.

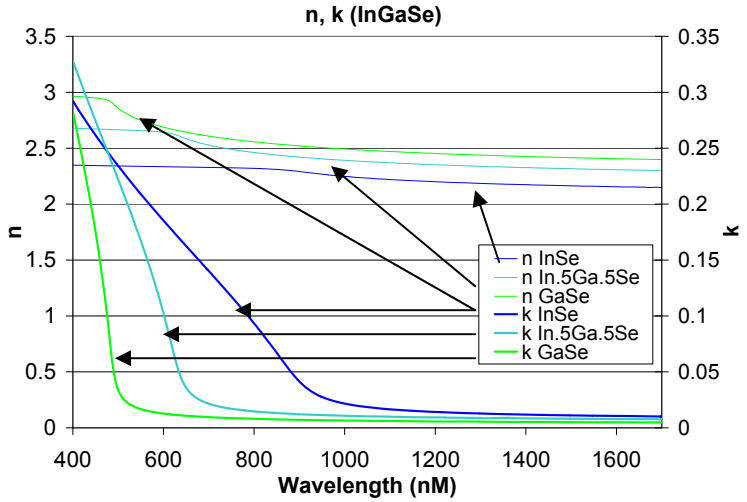

Figure 41. The modeled dielectric function for various compositions of InGaSe. The optical transparency at short wavelengths increases with increasing Ga content for this binary compound.

Using standard optical equations for interfering reflection at normal incidence through a thin film, and the modeled properties of the CIGS or InGaSe semiconductor, on a molybdenum substrate with an upper interface in vacuum (or air), reflectance could be calculated. The reflectance spectrum was sensitive to film thickness and composition (Figure 40). Based on the modeled relationships, in-situ reflectance spectra obtained from growing InGaSe and CIGS films on moving stainless webs were translated, in real-time by numerical routines, to provide several important film properties including: film thickness, Ga/(In+Ga) ratio, and a number indicative of a density of defect states.

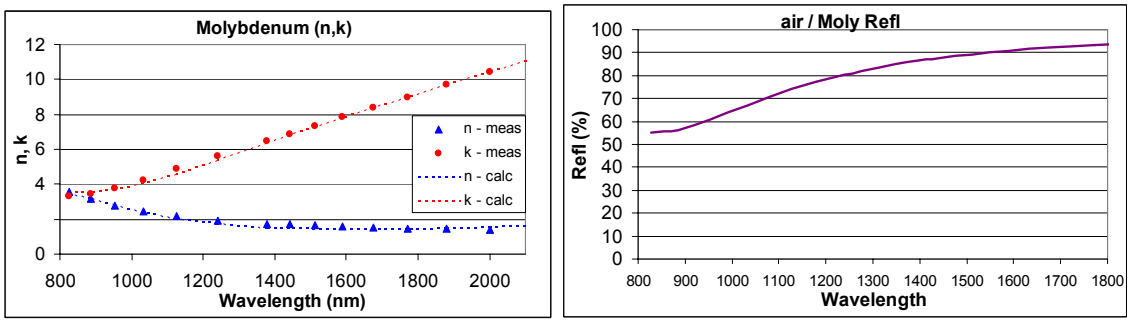

Figure 42. Left: The calculated and measured n and k for the thin film molybdenum substrate. Right: The calculated reflectance (in air) for the thin film molybdenum substrate.

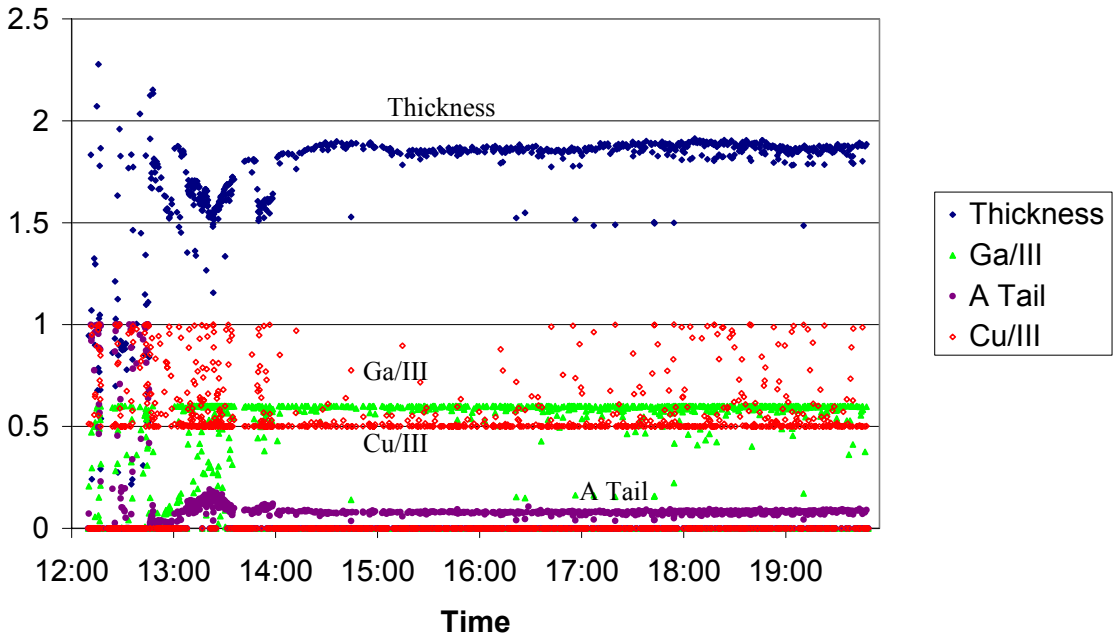

Figure 43. The results of real-time numerical solution for all possible parameters for an entire CIGS deposition. The vertical scale is in arbitrary units.

Convergence to reasonable solutions is a significant issue with reflectance from the complex CIGS thin films. Actual numerical solutions in real-time require a very good understanding of the optical/electronic properties of the films at the outset. In general, data analysis provides film thickness and Ga/(In+Ga) ratio information with reasonable accuracy (Figure 43). However, solutions for other parameters, such as Cu/(In+Ga) ratio exhibit higher variability. Another parameter, indicative of the density of optically active absorbing tail states ("A Tail") yields reasonable values, but additional experience is required to validate a correlation. In general, more robust data analysis occurs as more parameters become fixed values. Thus,

the numerical solutions of the reflectometry data will become more robust/reasonable as the process control and optical property characterization improves.

5.4. Automatic Run Data Upload Sputter Deposition Chambers

As each Mo or ITO deposition cycle progresses, selected critical process variables are monitored and logged in real time. A standalone custom data acquisition application communicates with the central process control computer on each chamber, extracting instantaneous process variable values at regular time intervals and saves the results locally as a standard text file. Data generated in this manner is subsequently utilized by the process engineer to review actual conditions present during each deposition cycle, comparing these to expected nominal values, noting any discrepancies and checking for unexpected behavior. Before the process data can be reviewed, the raw logged data must first be processed into a useful format (e.g., in the form of tables, graphs, etc.).

Historically, logged run data for the ITO and Mo sputtering processes was recorded as multiple text files: at least one distinct saved file for each of the pump down, web bake out and deposition phases of a typical process cycle. These files were manually combined, where necessary, and pasted into a pre-formatted Excel spreadsheet template for review and analysis. Processing the raw data in this way was very time-consuming and prone to error. A more robust, less time-consuming approach was developed through specific modifications to the data acquisition application and the incorporation of custom Visual Basic code within the Excel template used for review. This data management methodology included:

Data Acquisition

1) Monitoring up to 256 discrete process variables
2) Appending new logged data to existing files, allowing the entire history of a given deposition run to be captured in a single file, minimizing data loss.

Excel Template

1) Automatically importing (single-file) raw data through the use of Excel's built-in database (ODBC) drivers
2) Retrieving other pertinent production data (e.g., operator comments, incident records, etc.) from a proprietary internal database
3) Providing, through additional logic functions, for the discrimination of each phase of the process cycle, producing the appropriate graphical feedback, calculations for review.

Process data for a given deposition run is displayed for the process engineer/management automatically through a graphical user interface. Implementation of the new data management procedure has reduced the average time required to generate process review reports by 53%, enabling personnel to concentrate on the actual review of each run or on other important tasks.

5.5. XRF Inspection Table Constant Tension Control

Due to limitations in the original mechanical design of the cross-web uniformity "Inspection Table" that limited throughput and potentially damaged the coatings, it became necessary to develop controls based on in-situ load cell tension measurements and control algorithms implemented in the Galil motor controller. Due to the limitations of the Opto display software it was also necessary that the control algorithms and operator interface be implemented in Visual Basic and integrated with the control platform to provide a more powerful and robust tool. Implementation in Visual Basic enables additional features to be integrated to improve the usability and flexibility of the unit. Features include:

- Independent pay-out and take-up mandrel 'jog' mode
- Complete 'reverse mode' operation that allows all the normal web drive functionality to operate in reverse

- Cross web scan increments set to one half inch providing for a total of 25 unique cross web scan positions.
- Automated script operation that allows the operator to write a script containing down web and cross web scan information and save the script as a text file. The text file can then be loaded into the machine interface and executed as an automated command file. This feature provides the operator with an enormous degree of flexibility with regard to programming unique cross web profiles for different down web locations.
- Manual cross web scan selection that allows the unit to perform a cross web scan independently of a script that may be running. This again increases the operators' flexibility when using the equipment because the operator may stop the web at any interesting down web location and perform a cross web scan. Any automated script that may be running at the time the web was stopped is automatically resumed at the completion of the cross web scan.
- Cross web scan abort.

The new constant tension control software is now the exclusive control software on the system and is being used full-time in production. Implementation of the load cell and associated controller has increased throughput by 70%. In addition to web tension control, physical placement of the web with respect to the XRF system was implemented to minimize detection error associated with variable alignment. To automate this alignment function, a vacuum plate was mounted on the table beneath the XRF head to provide sufficient force to pull the web flat against the table and thereby maintain a constant geometry between the x-ray source and the web. An existing digital output from the Opto controller was redefined in the control code to switch the vacuum plate on and off in synchronization with the measurement activities.

6. In-situ Diagnostic Tool Development and Implementation

Sensor development is at the core of the process control efforts. In-situ sensors can be used to provide direct feedback control or be used as part of fault tolerance. To achieve the next level of cost reductions and increase product quality, yield and performance, intelligent outer loop control, based on in-situ process, flux, and film property diagnostics, was implemented for the Mo, CIGS, CdS and ITO deposition processes. Furthermore, since GSE processes require hours of continuous operation, sensor robustness and fault detection/tolerant control are mandatory. As part of the PV Manufacturing R&D effort, several specific control parameters of all the PV production deposition systems were identified where benefits could be realized with in-situ diagnostics. Once specific concepts were identified, importance and feasibility criteria were applied to narrow the scope of effort to provide maximum results with the given resources. In the CIGS deposition systems, for example, thermocouples provide information about source temperatures and physics-based models provide guidance about expected effusion flux and anticipated film properties. In general, effusion source temperature and flux measurements enable more direct and simple process control but are less closely tied to desired film properties, whereas in-situ measurements of film properties provide information directly but require more sophisticated process control. After considering all of the different factors, several sensor development activities were performed during this program, including:

- RGA, OES, and QCMs to provide flux and chamber health monitoring for the Mo and ITO sputtering systems
- Pyrometry to improve source and substrate temperature monitoring
- Emissometry to measure film temperature, roughness, and emissivity
- Se flux monitoring
- Metal flux monitoring
- NaF flux monitoring
- Alternative input current/voltage measurement methodologies to monitor system health and provide process control
- Film sheet resistance monitoring
- Reflectometry to provide characteristics of the various coatings
- Visible imaging for CdS film thickness.

While other sensors are either already being used in the vacuum deposition systems or may be implemented at some point in the future, these sensor development activities were down selected as being the most germane to this PV Manufacturing R&D effort. A brief overview of representative development and integration efforts is provided below. In general, the RGA and OES are only applicable to sputter processing and the visible imaging is only applicable to the CdS process. Furthermore, with the exception of the in-situ resistive probe, the Se flux monitor and the remainder of the sensors were only investigated for use with CIGS processing.

6.1. Molybdenum

For the Cr-Mo system, initial in-situ diagnostics were needed to measure background vapor contamination, oxygen/water levels, substrate temperature during bake out, thickness, conductivity and morphology. An in-situ thickness sensor similar to that used for CIGS deposition could provide composition and thickness information but at this point is not deemed warranted. Thickness measurements performed in the CIGS processing provides post Mo deposition thickness information that is closely monitored to ensure Mo thickness uniformity. Primarily, the main sensor development activities included:

- Deposition environment monitoring through OES and RGA development,
- Flux/film thickness monitoring with QCMs, and
- Investigation of scatterometry to determine suitability of roughness.

The main sensor development activity focused on deposition environment monitoring through OES and RGA measurements, and flux/film thickness monitoring with QCMs. An RGA system and an OES system were procured and integrated with production deposition systems for testing. QCMs were also procured to provide deposition rate measurements. Initial analysis of in-situ OES/RGA measurements during Mo deposition (Figure 44) indicated that the RGA system detected hydrogen in the deposition chamber. Changes in hydrogen pressure correlated with changes in web speed but not with Ar pressure or other chamber related parameters. In addition, corresponding oxygen changes by the RGA were not observed. As opposed to water coming in with the Ar, these measurements are consistent with adsorbed water on the stainless steel web coming off in the deposition zone and being ionized; the oxygen reacting with the Cr or Mo during deposition. Further comparison of in-situ OES/RGA measurements indicates that Mo flux may be changing significantly with no correlation to Ar pressure, chamber pressure, web speed changes, or power (Figure 44 and Figure 45). Thus, OES could provide improved Mo deposition control. In either case the data indicated that OES provided equivalent or better flux information compared to the QCM and better information regarding deposition health monitoring compared to the RGA. The data indicated the need for active real-time health monitoring of the Mo deposition systems and was instrumental in adjusting Mo deposition procedures where an initial heating step was added prior to Mo deposition to ensure that excess water from the web did not adversely affect the back contact performance.

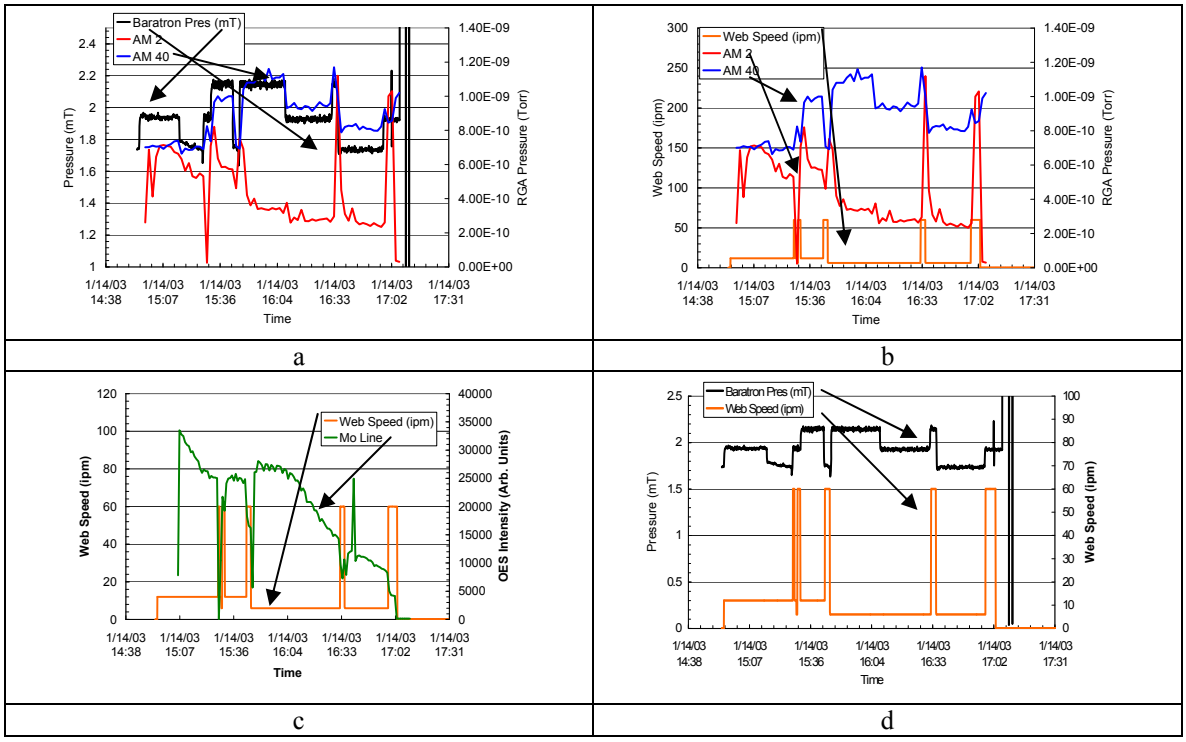

Figure 44. Comparison of in-situ OES and RGA measurements during Mo deposition. a) Comparison of Ar and H_2 RGA measurements with chamber pressure indicates that the RGA measured Ar pressure is correlated with overall chamber pressure, but the H_2 pressure is not. b) Comparison of RGA Ar and H_2 pressure with web speed indicates that some of the spikes observed in the H_2 pressure may be related to water desorption from the web. c) Comparison of web speed with OES measured Mo flux indicates that an increase in web speed creates a significant drop in Mo flux within the deposition zone. d) The data indicate that a change in web speed did not have a significant effect on chamber pressure, but unfortunately, web speed was changed at the same time as Ar inlet flow.

6.2. CIGS

The complex CIGS system uses thermocouples and in-situ thickness sensors to provide film property information for process control. However, the control of several process parameters were improved with the implementation of additional diagnostic tools. Several potential process parameters were identified including Se flux (uniformity and element specific flux), actual pool temperatures of the effusion sources, improved robustness of the boat temperature, and NaF flux. Sensors investigated to provide process control information included:

- Optical measurement of film properties,
- Alternate source temperature measurements and control strategies,
- Metal flux monitoring/control,
- Improved Se flux monitoring/control, and
- NaF flux monitoring and control.

Detailed information for recent/representative in-situ sensor development activities for this PV Manufacturing R&D program are provided below.

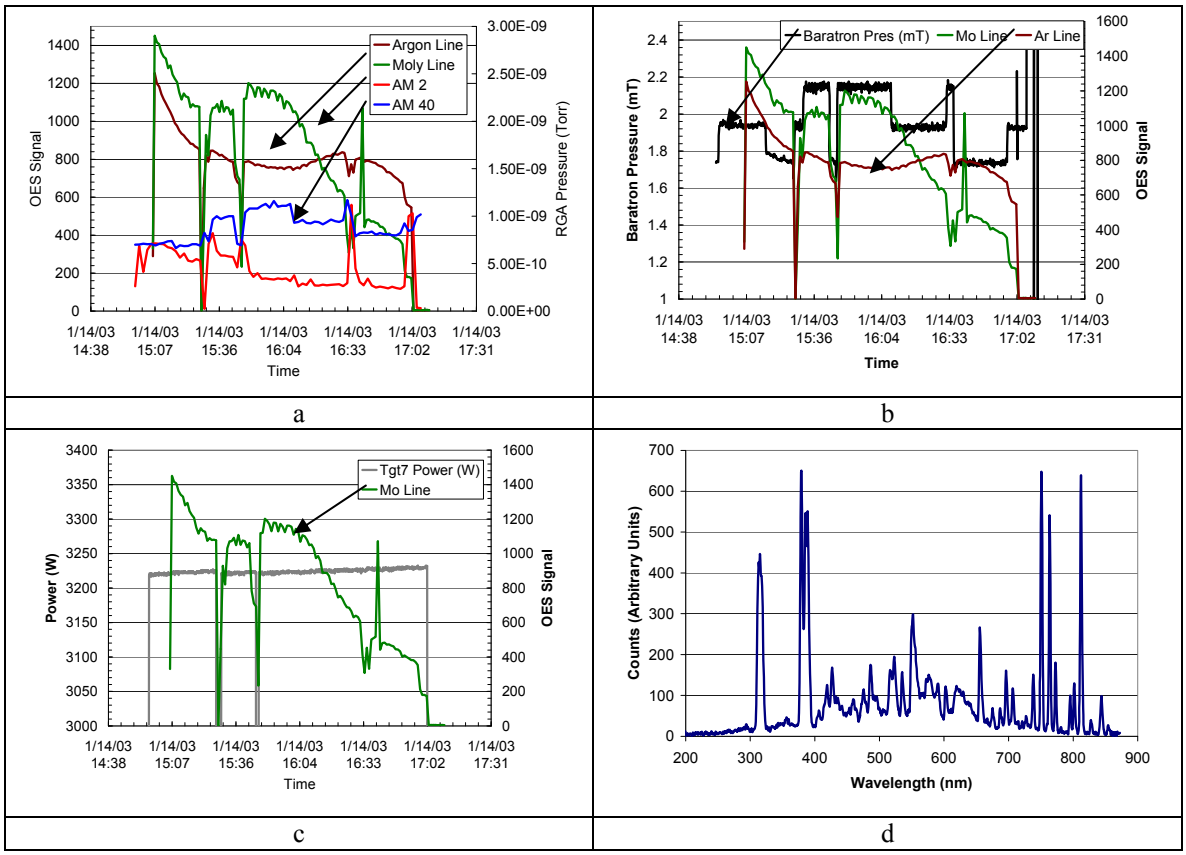

Figure 45. Analysis of in-situ OES measurements during Mo deposition. a) Comparison of Ar and H_2 RGA with Ar and Mo OES measurements indicate that Mo flux has limited correlation with Ar flux and virtually no correlation with RGA measure Ar or H_2 pressure. b) Comparison of OES Ar and Mo flux has virtually no correlation with chamber pressure. c) No correlation of Mo flux with input power is observed. d) Representative in-situ OES data obtained in the Mo deposition zone. All these data indicate that OES has the potential to provide information for Mo sputtering process control and chamber health monitoring that cannot be obtained from RGA or other sensors outside the deposition zone.

6.2.1. Process Parameter/Source Sensors

Alternate Source Delivery Closed Loop Control

While pyrometers provide direct measurement of pool temperatures, the intrinsically harsh environment inside a CIGS manufacturing system provides extreme challenges for any sensor implementation. Indirect monitoring of the provided electrical contributions to the sources has been demonstrated to provide equivalent or improved control capabilities compared to thermocouple based control. This strategy enables accurate and robust control of the pool temperature and thus effusion flux without the need for expensive in-situ sensors that fail due to a myriad of physically induced mechanisms.

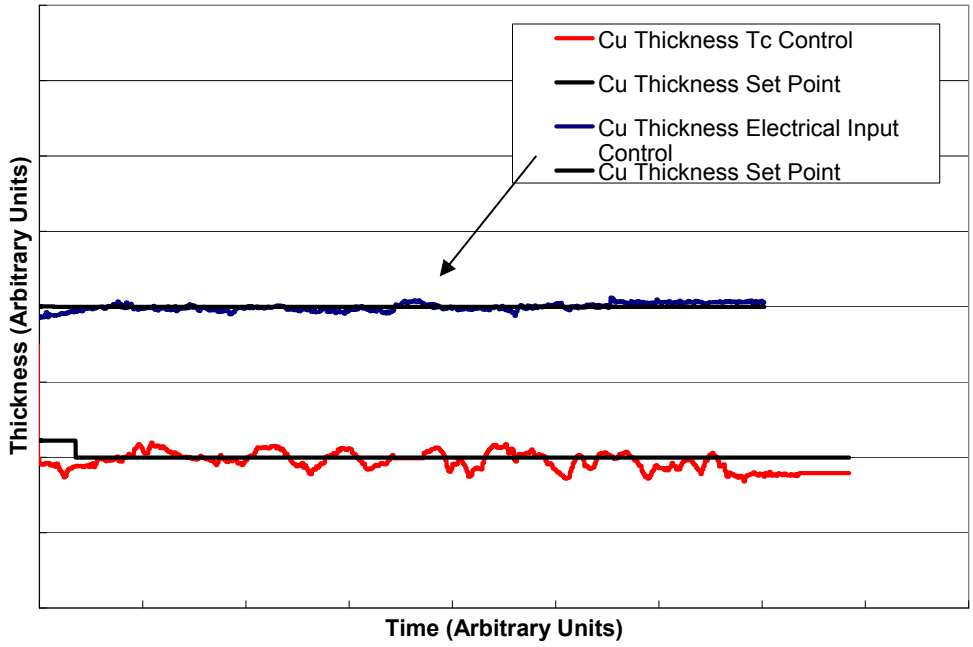

Figure 46. Representative data comparing measured Cu thickness as a function of time for process control strategies based on thermocouple measurements and monitoring of electrical input to the sources.

As in the semiconductor industry, input power quality was determined to be critical for both the deposition sources and sensors. Besides monitoring input power, additional sensors were integrated with the evaporation and sputter deposition systems to provide system monitoring and control information. In addition, monitoring electrical contributions to the sources provides equivalent control capabilities when compared to thermocouple based control. Figure 46 compares Cu thickness variability for the two different control sensors. In this particular case, the control based on electrical input monitoring provided as good or better thickness control compared to control based on source thermocouple measurements. At the very least, this control methodology offers a fault recovery strategy if a source thermocouple fails during processing, eliminating the costly continued deposition of CIGS films with no control or the termination of the processing if the thermocouple fault is detected. However, this alternate source delivery control strategy offers potential in significant cost reductions and increased reliability if expensive thermocouples with short mean time between failures can be entirely eliminated from the deposition process control strategy.

6.2.2. CIGS Flux Sensors

Atomic Absorption Spectroscopy Flux Monitors

One of the difficult issues for physical vapor deposition (PVD) manufacture of multi-component thin films is the measurement and control of the deposition rate for different constituents. In-situ measurements of flux are directly related to film thickness and do not have any significant time response limitations, thus providing real-time information of dynamic and unexpected process fluctuations. Conventional quartz crystal monitors are viable in the deposition of single element films but are insensitive to flux composition and are therefore not well suited to the control of multiple effusion sources of varying elements. Ideally, a single in-line flux and chemical identification sensor is desired for the multi-element vapor phase deposition process. This sensor must be able to remotely determine the vapor composition, flux, and flux velocity in real-time and perhaps the composition of the deposited film. Presently, no commercially available or developmental sensor exists that can meet all of these specifications. However, an atomic absorption spectrometry (AAS) system provides element-specific optical measurement and control of the deposition flux. The system relies on AAS principles to measure the vapor phase density of the element of

interest. Experiments were performed to demonstrate that AAS sensors provide effusion rates of copper, gallium and indium by monitoring the absorption in the characteristic spectrum of each species at a representative location in the chamber. The sensors were set up to monitor the absorption in a narrow path across the deposition region. Results of these experiments indicated that the AAS system provided accurate and reproducible real-time control the metal effusions in CIGS manufacturing.

The AAS system allows optical and element-specific measurement and control of deposition flux. Furthermore, since multiple sources of In and Ga are sufficiently separated during processing, AAS measurements can provide independent measurements of the flux and thus film thickness from the individual sources. The system relies on atomic absorption spectroscopy principles to measure the vapor phase density of the element of interest. AAS functions by measuring the attenuation of a beam of light having an element-specific characteristic wavelength. While AAS has been used as a viable wet chemistry measurement for some time, use of AAS for real-time, element-specific, measurement and control of vapor phase deposition has been limited.

The main limitations of the AAS system involve the intensity of the source and detected light and the single element specificity of an individual instrument. These limitations could be overcome with the use of lasers. However, the present cost of a tunable laser or the cost of a custom designed laser diode material with the appropriate wavelength is prohibitive for use in an AAS sensor. Furthermore, commercially available diode lasers with the exact wavelength needed for each element do not exist.

Thermal expansion issues of optical hardware at the temperatures used in CIGS processing and adequate protection of optics coating significantly limited the use of AAS systems for CIGS process control. While the AAS system did compensate for an ~10% degradation in signals due to window coating, additional modifications to the base unit where needed to allow for lower signal degradation while maintaining accurate measurements. A shutter was used to allow for in-situ calibrations while flux is present. In addition several revolutionary new hardware optics configurations were designed and tested to resolve all the major issues related to performing AAS measurements in a CIGS deposition system.

Closed Loop AAS Process Control for CIGS - Figure 47 shows data for Cu during CIGS deposition and compares the controlled AAS flux to the corresponding boat temperatures and measured film thickness. For both In and Cu AAS provided control of the measured metal fluxes. However, In was controlled to a better extent than Cu. Flux measurement resolutions is better than the temperature resolution, indicating that we should be able to control the metal fluxes better with AAS. The control of the In flux is an example of AAS having better sensitivity and thus potentially better control than source temperature. This is seen by the fact that changes in the In source temperature were significantly smaller than the controlled flux measured by AAS.

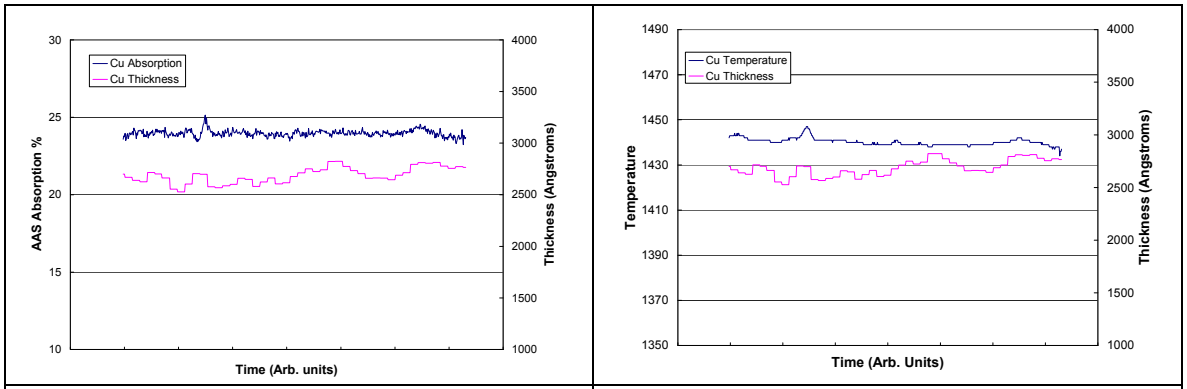

a b

Figure 47. Measured Cu Source (a) Flux and (b) Temperature During CIGS Processing.

NaF QCM

While thermocouples for NaF sources provide some control, flux monitoring was desirable to substantially improve control. Since NaF is deposited in a portion of the deposition chamber that is physically separated from other deposition processes, a QCM was procured and installed. Initial tests of the sensor provided very promising results for improved process control. Representative data is shown in Figure 48. Outer loop control algorithms based on QCM measurements were designed and implemented to provide set points for the primary thermocouple inner-loop control. The data for Na indicate that while the QCM sensor is operational, this control methodology provided improved deposited Na film thickness uniformity along the web. However, as seen in Figure 48, the signal to noise of the QCM degrades significantly during production as NaF deposits on the QCM active component. This renders the sensor unusable. Thus, fault detection algorithms were developed to identify when the QCM is no longer functional, and the system is converted to thermocouple only control. This results in thickness control that is significantly less accurate than with the QCM but enables continued operation.

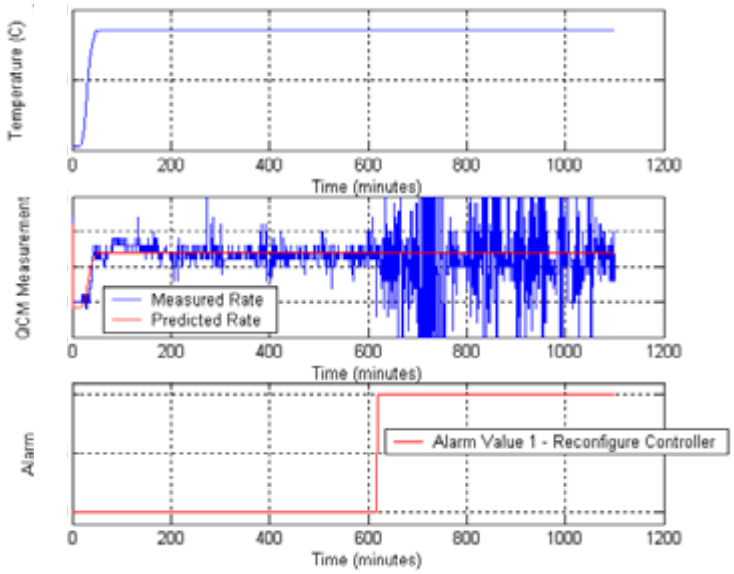

Figure 48. Representative in-situ real-time NaF flux data obtained with a QCM sensor to provide improved process control.

Se Flux

Temperature measurements of the Se source have proven to be inadequate for accurate control. Incorporation of In in the deposited film is highly dependent upon the Se availability and Cu and Ga flux plumes are affected by the relatively high Se fluxes. Unfortunately, a Se specific flux monitor is not available at this time. AAS cannot be used since Se is typically a multi-atomic molecule in the manufacturing process. Other light based absorption methods may be possible but will need significant development time since no commercial system is available. In the interim, a Se non-specific flux measurement was tested and implemented for feedback process control of the Se flux for CIGS deposition. This sensor system provides reasonable Se flux control for CIGS manufacturing. Figure 49 presents representative data from the Se-flux sensor, the Se source temperature and the resulting Se film thickness.

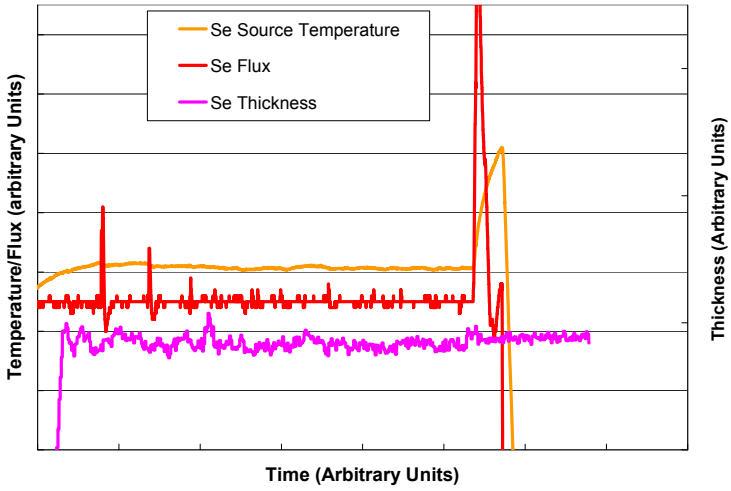

Figure 49. Comparison of Se flux and temperature measurements used for control. The flux control is clearly more sensitive and has less thermal lag than Se source temperature measurements. When flux measurement control is used for all Se sources, the uniformity of Se thickness is improved.

Na-Specific Sensor Development

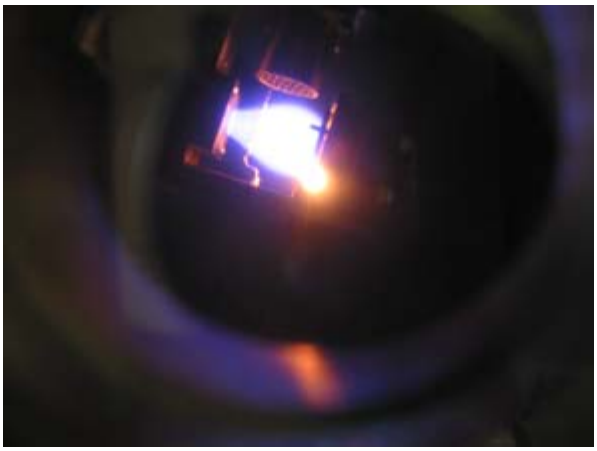

Figure 50. Image of an EIES device in operation, providing a strong visible emission in the vacuum environment.

Na as an impurity in the CIGS layer has been demonstrated to have a significant beneficial effect on device performance. However, Na must be added extrinsically, since none is available from the stainless steel or polyimide substrates in use, unlike the case with soda-lime glass substrates. Na content must be critically controlled since too little reduces device performance and too much may adversely affect adhesion between the CIGS and the Mo layers. Presently, a non-specific flux sensor is used to control Na deposition. However, since this detector is sensitive to and cannot distinguish between other elements in the deposition zone, including Se, accuracy can be adversely affected if other species become present in significant quantities. An undesirable outcome is that the Na monitor may provide unreliable signals for the rate of the Na deposition. Thus an effort was initiated to develop and implement a sensor that measures the sodium flux rate specifically and is unaffected by other elements present such as Se.

Electron impact emission spectroscopy (EIES) was chosen since light created by the electrons interacting with the vapor fluxes (Figure 50) provide unambiguous spectral identification and rate information for different elements in a deposition plume. After significant sensor design and testing activities were performed to resolve major implementation issues, tests in a roll coating chamber indicated an excellent correlation between Na flux and the measured signals from the Na specific sensor (Figure 51).

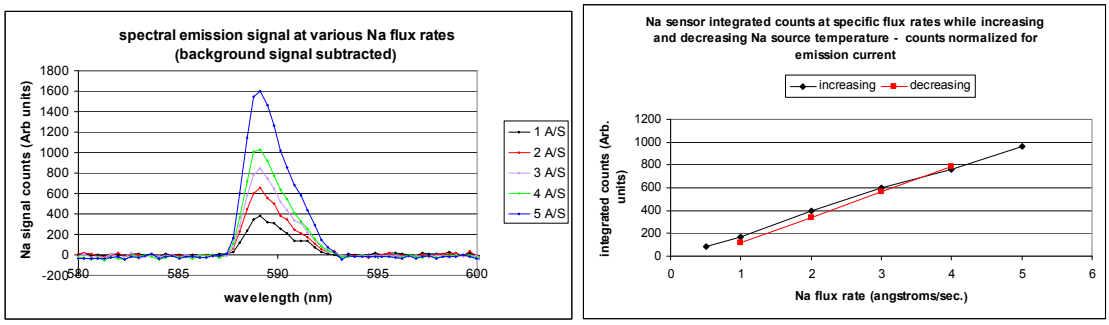

Figure 51. EIES measurements (left) for different sodium flux rates demonstrates a linear well correlated relationship (right) with flux measurements from an in-situ QCM.

Additional tests were performed and demonstrated that the sensor provided repeatable and stable flux measurements (Figure 52) during Na deposition during CIGS processing. However, effects on EIES signals and thus inferred flux rates was observed during tests where Se was systematically included during the Na deposition (Figure 52). Comparisons between the measured Na signal with and without Se for a given Na source temperature indicated some inherent variability that seemed to be more prevalent at lower Se flux. The key issue here is that Se has may interfere with either the Na flux or the EIES signal. However, perhaps Se flux can be monitored as well with EIES and subtracted from the Na measurement, should this prove to be a significant issue. The results from this testing indicate that improved control from an EIES based measurement should provide Na specific measurements that will improve control, especially when unanticipated Se fluctuations occur.

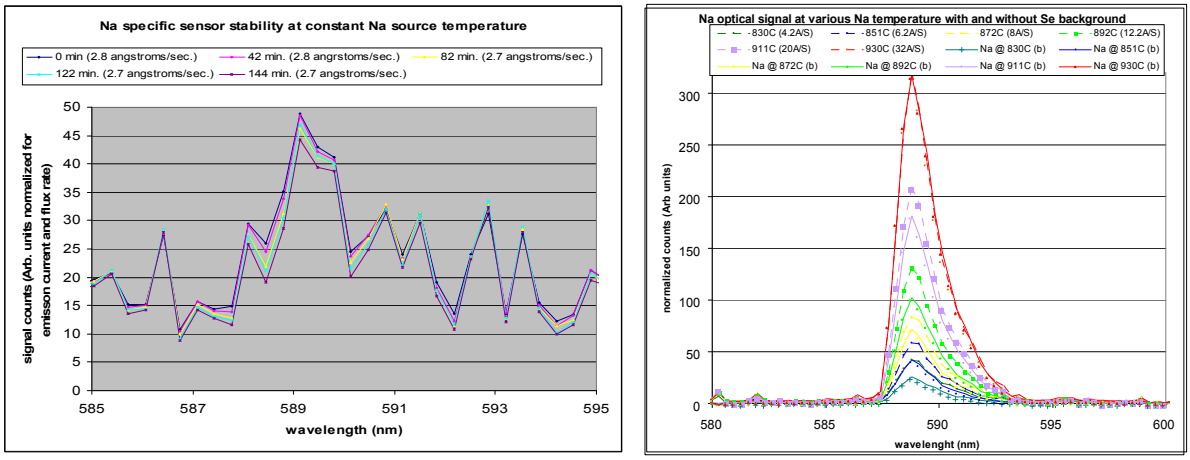

Figure 52. Tests (left) with the Na source held at constant temperature indicated relatively good stability over the period of hours. Slight variations in the Na spectra correlated well with QCM measurements possibly demonstrating that flux control based on EIES are QCM improved control. EIES spectra (right) obtained in the presence of a selenium background flux compared to the signal obtained at the same Na source temperature with no selenium present demonstrates slight but significant variations that may indicate interference from Se, especially at lower Na pressures.

6.2.3. CIGS Film Properties

Useful properties to be monitored for process control include surface roughness, emissivity after the Cu deposition, thickness and optical properties at all stages, and film temperature during deposition. The main issues with performing film property measurements close to sources during deposition includes high temperatures (possibly > 1000°C), coating of optical surfaces, and corrosion of materials due to the Se environment. Initially, the use of reflectometry and a commercially available emissometer that also measures surface roughness and temperature was investigated as complementary sensors. Also, pyrometry was investigated to provide actual film temperature measurements.

Reflectometer

Film properties and temperature can be obtained from optically-based measurement systems like reflectometry and pyrometry. Thus, reflectometry hardware was installed and tested in roll-to-roll production processing systems. Representative results shown in Figure 53 indicate that the reflectometry measurements provide useful information for process control/monitoring about the different deposited layers. As discussed above in the control platform section, the main issue is developing appropriate real-time interpretation algorithms to accurately determine optical properties and quantifiable structural information from the measured signals. In addition, wrinkles in the web induce sufficient misalignment to substantially change the reflectometry measurement; this requires real-time identification of these events and discontinued use of reflectometry measurements until the wrinkle has passed.

6.3. ITO Deposition Systems

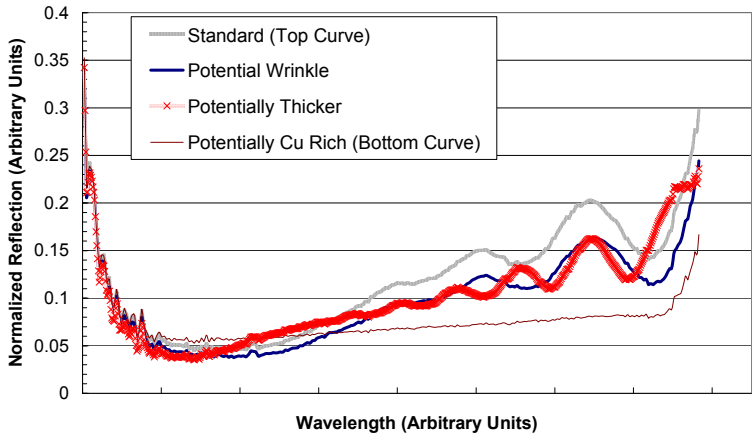

Figure 53. Reflectometry measurements indicate that some film property information can be obtained and may be quantifiable. However, the measurement is susceptible to misalignment due to substrate wrinkles and coating of optical surfaces.

For the ZnO/ITO process, OES was identified to provide appropriate flux composition control that includes water/oxygen concentration. However, the main issue is optical transparency quality and providing sufficient process control based on in-situ film diagnostics. Resistivity provides conductivity (sheet) measurements, but, there is only a limited correlation between conductivity and transmissivity. Reflectometry or ellipsometry may provide appropriate process control information. However, implementation to measure a transparent film deposited on the optically challenging CIGS/CdS films is very difficult. Perhaps a subtraction methodology based on reflectometry or ellipsometry could be devised. Furthermore, since substrate temperature is used as part of the processing, perhaps IR-thermometry/emissivity could provide valuable process control information. In addition, an in-situ light induced voltage/current measurement could provide valuable process control and quality control information about the entire multilayer stack. Ultimately, ITO optical transmission and electrical (sheet) conductivity are the most important properties that must be optimized for maximum module performance. Unfortunately, process parameters that improve transmission typically adversely affect conductivity, and vice versa. Thus, maximum module performance is highly dependent upon finely tuned control of the ITO film properties. However, optical characterization of the ITO film is very difficult and resistivity measurements cannot provide useful information about optical transmission quality. ITN/GSE evaluated the use of in-situ conductivity, optical reflectance (differential), and light induced voltage/current measurements to develop a monitoring strategy that provided the required information for optimized process control of the ITO film depositions.

Reflectometry - Tests were performed to determine the applicability of using differential reflectometry for process control of ITO film properties. Representative data are shown in Figure 54. The initial differential reflectometry tests indicated that this technique had sufficient sensitivity to provide in-situ real-time ITO film quality information for process control. The normalized difference data shown in Figure 54b, indicated that both optical properties (absorption) and thickness may be deduced from the data. However, position and orientation repeatability before and after the ITO deposition is absolutely critical. Therefore, discussions with NREL about their unique reflectometer that is less position and orientation sensitive were held in order to determine if the instrument could provide the appropriate differential reflection measurements, the results were useful for process control, and the instrument hardware could be adapted for in-situ measurements inside a vacuum deposition system. While, the instrument may be able to meet all these performance specifications, integration into a vacuum deposition system was determined to be very difficult and thus the effort was deferred until determined absolutely necessary based on future ITO process evaluations. Ultimately, this effort was deemed outside the present program activity and thus deferred to future efforts if necessary.

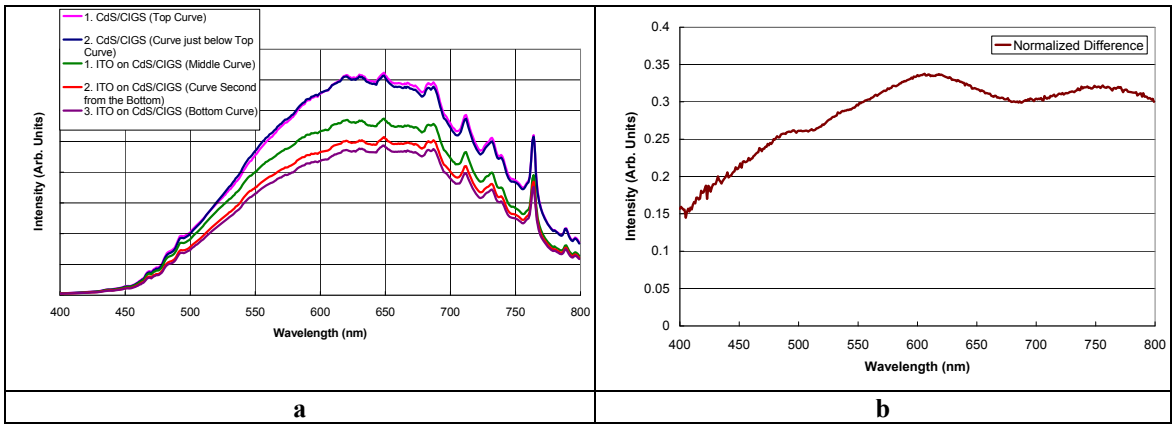

Figure 54. Representatiev reflectometry data with and without ITO films on CIGS/CdS substrate layers. a) Reflection spectra from CdS/CIGS films and ITO/CdS/CIGS films. b) Normalized difference of reflectance data with and without ITO. The oscillations as a function of wavelength may be related to ITO thickness.

RGA - Extended-pressure RGA monitoring was installed on production ITO deposition chambers. RGA provides monitoring of the reactive and/or residual gas partial pressures over the entire run for system health and control. Figure 56 shows representative data of peak intensities of several molecules from an RGA sensor on an ITO deposition system. General agreement between RGA and simultaneous OES process data was good (semi-quantitatively) for those chemical species quantifiable by both techniques.

OES - OES provides direct measurement of the ionic composition of the sputtering plasma which can be used for health monitoring and process control. Probe optics and optical fibers were fixtured to sample across the widths of the production deposition systems targets for optimum signal collection. Spectra are obtained at set intevals throughout the course of each deposition cycle. Software logs the spectra and intensities of specific peaks are analyzed to provide real-time data for process control. As an example, analysis of ZnO emission data (Figure 55) from production runs indicated that the surface stoichiometry of the ZnO targets were changing using standard sputter conditions. Thus, the processing conditions were adjusted to prevent target degradation.

In another example, ITO sheet resistance increased with time during the production deposition run (Figure 58). RGA and OES (Figure 57) measurements correlated this observation with both steadily increasing O_2 partial pressure and steadily decreasing H_2O background. These results identified a potential source for the observed resistance increase and a potential for process control. Subsequent testing verified the findings and corrective process adjustments were implemented that resolved issue and controlled the ITO film resistance.

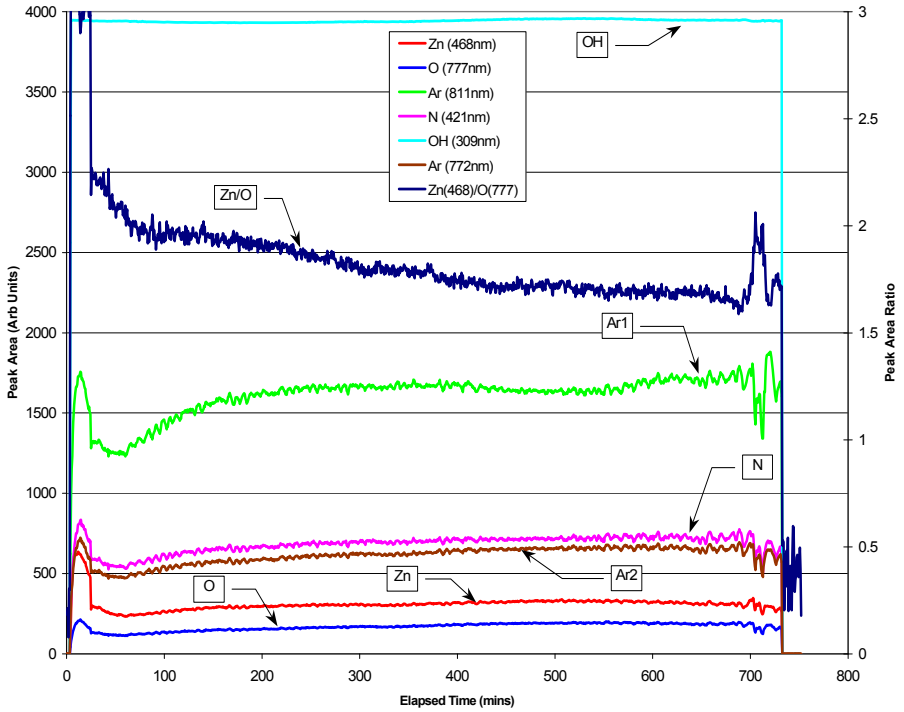

Figure 55. Representative OES data from ZnO production deposition.

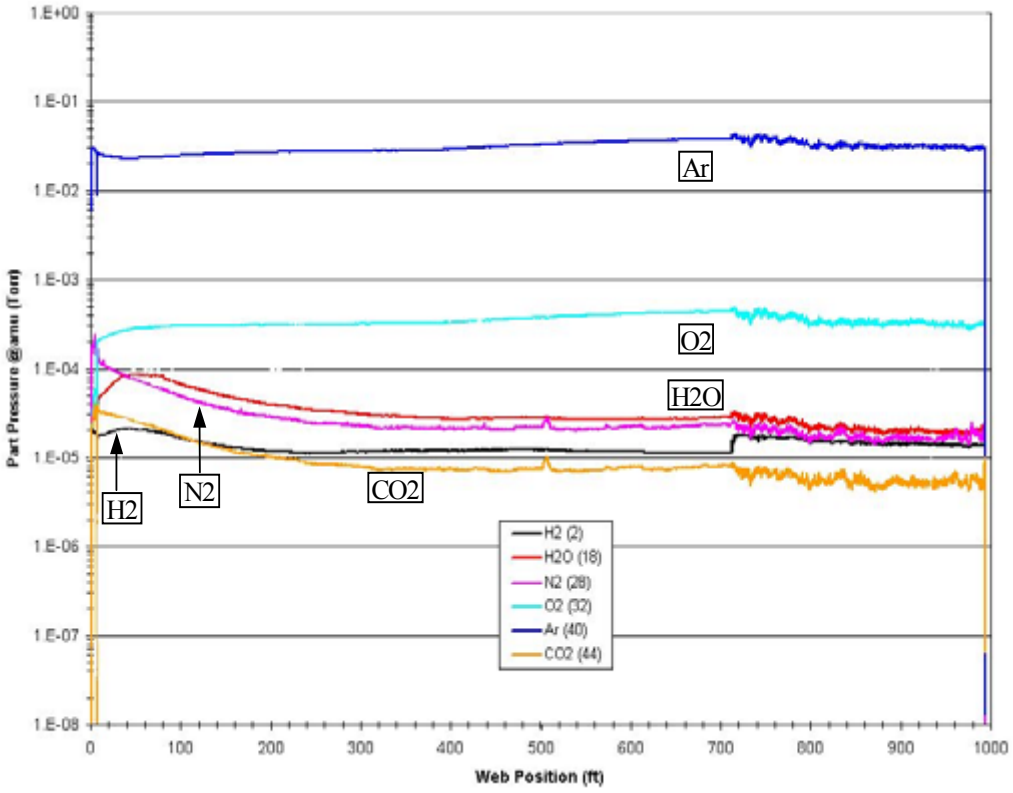

Figure 56. Representative RGA data from ITO production deposition. The series represent peak intensities during the production run.

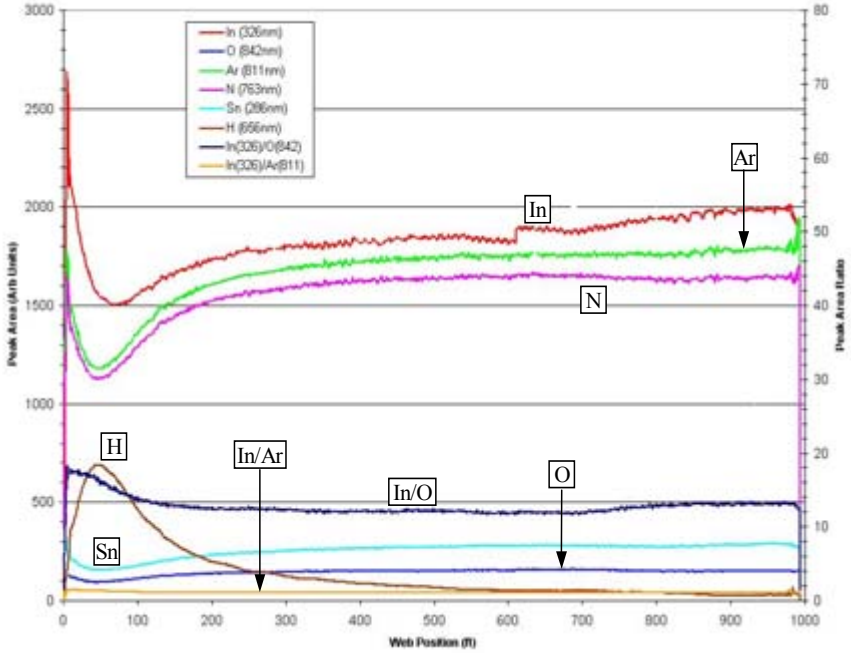

Figure 57. Representative OES data from ITO production deposition.

6.3.1. In-situ Film Resistance Probe

An in-situ probe was developed to monitor change in sheet resistance of deposited ITO. This is important since significant increases in sheet resistance detrimentally affect cell performance. Representative data are presented in Figure 58 demonstrating that the sheet resistance varies significantly over the course of a production run. Also plotted in Figure 58, are ex-situ sheet resistance measurements, which correlate well with the in-situ data. The data indicate that the in-situ resistance measurement is acceptable for real-time process control.

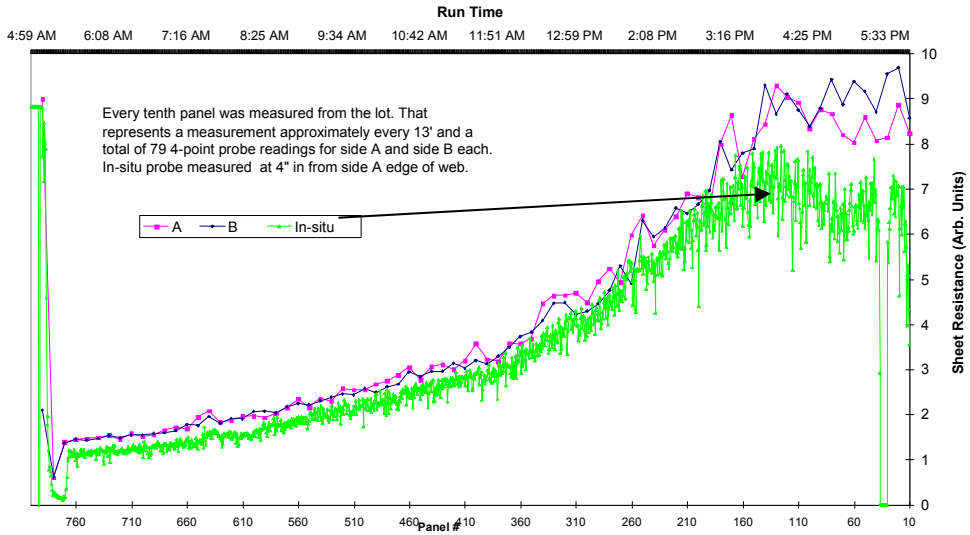

Figure 58. Representative data from in-situ resistance measurements. Ex-situ measurements (dark and light blue) are comparable to the in-situ (green) measurements.

Once the reliability and the non-harmful impact upon the surface of the coated material of the in-situ sheet resistance probe was demonstrated, activities were performed to determine appropriate process parameters and control strategies that can be used to maintain desired sheet resistance. As part of this activity, systematic experiments were performed where process gas flows and mixtures were modified. This required the installation of additional mass flow controllers and their associated hardware and software modifications. Critical to these evaluation efforts is use of actual CIGS production systems/materials and measurements of both ITO and overall cell performance properties. For example, while a series of tests adjusting process parameters demonstrated improvement in ITO sheet resistance (), subsequent cell performance analysis indicated detrimental affects to overall cell performance. If a larger cell configuration is used then this specific process modification may be of benefit, as the larger cell area will profit more from a lower sheet resistance than the current cell configuration. The resultant data and the additional insight into process characteristics has provided insight into other candidate modifications that may provide both ITO and cell performance improvements.

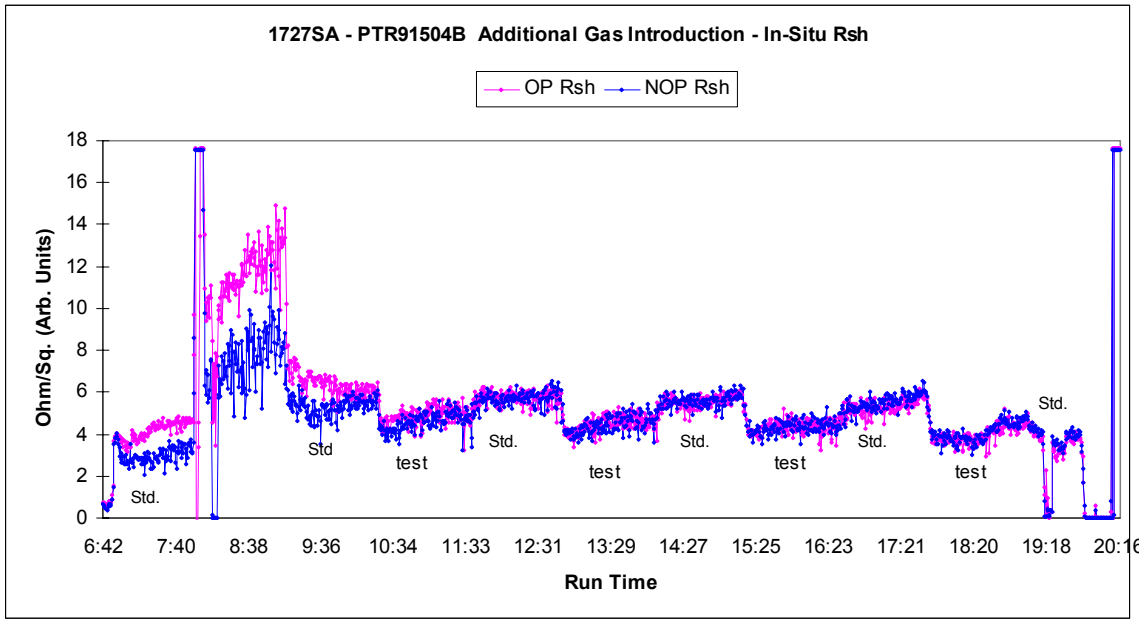

Figure 59. Changes in sheet resistance throughout the course of tests where specific additional gas specie were systematically adjusted to affect ITO sheet resistance changes.

6.4. CdS

The CdS deposition system requires thickness and uniformity measurements for process control. In-situ evaluation of the buried CIGS/CdS interface could substantially improve performance and enhance process control. Reflectometry and visible imaging were investigated as potential film property measurements. In addition, digital imaging and reflectometry systems were procured to provide film thickness and uniformity information. Electronic sensors were also procured and implemented to provide input stream measurements for improved process control. An initial evaluation of the anticipated response from reflectometry on CdS/CIGS films was performed using measured CdS and CIGS optical properties. It was determined that the dependence on optical properties and probably surface roughness will require that a systematic study be performed to determine the range of variation observed for "standard" CIGS and CdS films. However, since detailed evaluations (including the spectroscopic ellipsometry measurements) indicated that this level of process control was not needed at this time, implementation of reflectometry for in-situ measurements was determined to not be necessary.

Visible Imaging – CdS thickness-to-color correlation provided an indirect in-situ product performance feedback. Representative data in Figure 60 illustrate this correlation for five clearly distinguishable CdS coating colors on production material. In conjunction with digital image analysis algorithms, 100% of the CdS coated CIGS can be analyzed to determine if CdS coating thickness is within the lower and upper

specification limits. These limits have been determined via statistical design of experiment studies. The visible imaging is used as a quality control monitor and could be used for process control if the need arises.

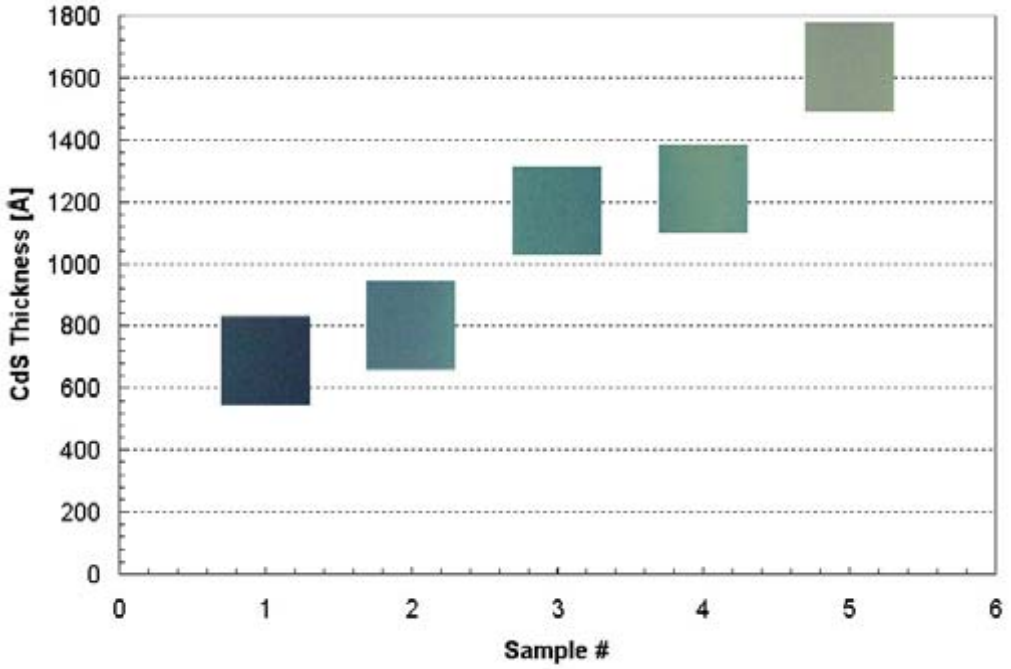

Figure 60. CdS film thickness as determined by cross-section FE-SEM at 60,000 magnification as a function of CdS color on CIGS

7. Autonomous and Robust Manufacturing Equipment Based on Diagnostic and Process Control development/Models

As part of the overall program objectives, studies were performed to identify and, where appropriate, implement additional capabilities of model-based diagnosis and control in the CIGS PV production environment. For example, the physics-based models of the different components and overall processing chambers were used to identify potential improvements in systems designs. As discussed above, this was very successfully used to design, construct and implement new metal sources for the CIGS deposition process. These new sources substantially eliminated the single largest control issue that lead to process upsets at the outset of the program. In addition, these models demonstrated how enhanced Se control was achieved through improved process chamber designs. Additional development activities were also performed associated with improved component/system design and the potential for "feed forward" capabilities leading to improved process control and process optimization.

7.1. Process control/optimization

As discussed throughout this document, all the infrastructure for model-based control, fault tolerance, and process/component improvement have been implemented into the production deposition environment. While not specifically articulated, this also includes feed-forward capabilities for quality control and even process control. Presently, process/sensor data is collected and distributed in real time for operator and management review. The collected data is archived in a proprietary database and can be accessed at any point in the thin-film manufacturing process. Thus the architecture is available for feed-forward control

where measured film/process properties from previous processes can be used to adjust/optimize subsequent processes. For example, process upsets in Mo deposition have adverse affects on the control for CIGS processing. Implementation could enable autonomous correction of the CIGS sensing/processing based on Mo process data to ensure that CIGS material is deposited within specified limits. Furthermore, the process/sensor information from the CIGS deposition, can be applied to CdS adjustments/optimization. Typically, thinner CdS material is desired since light absorption will diminish overall device performance. However, this must be balanced with a need to provide good insulating properties on a rough surface that often has pinholes. Thus, based on optical surface quality measurements, the CdS thickness can be adjusted to optimize PV device performance on a real-time basis.

For any of the feed forward control, an exact web position throughout all processing steps is critical. Thus, web tracking capabilities were evaluated that involved printing unique identification codes at designated positions on the web using ink-jet printing and reading a 2-dimensional matrix code to provide exact position/cell tracking. The test results indicated good code readability despite the rampant optical reflections from the shiny surface. Full integration of this capability into production manufacturing will enable both product tracking and feed forward control, if required.

7.2. Component/system design improvement

In addition to metal source design and development, component development activity included Se source optimization. Furthermore, system design/optimization activities included improved intrinsic ZnO, side-to-side uniformity, and development of an inter-process testing system.

7.2.1. Se Sources

Se consumption during CIGS deposition must be consistent and well-controlled. The standard Se source design has exhibited flux instability (Figure 61) during CIGS deposition. This flux instability can occur at random times where erratic behavior occurs and/or sometimes the flux develops a regular, rhythmic oscillation pattern as the Se source charge is depleted. PID optimization and power limits can be used to mitigate the oscillations but require operator intervention. Thus, the Se sources were redesigned with significantly enhance volumes and changes in heater configurations to improve both issues associated with flux instability. These redesigned sources used understandings from the physics based models developed for this program and engineering expertise to develop and construct sources with new features/geometries. Subsequent evaluations and source design iterations have resulted in substantially improved Se flux control (Figure 61), with the virtual elimination of the regular rhythmic oscillations. Additional testing of new source designs is ongoing. Full evaluation requires good performance with no flux instabilities for a large number of runs to determine if the source design changes improved the overall performance of the new Se sources.

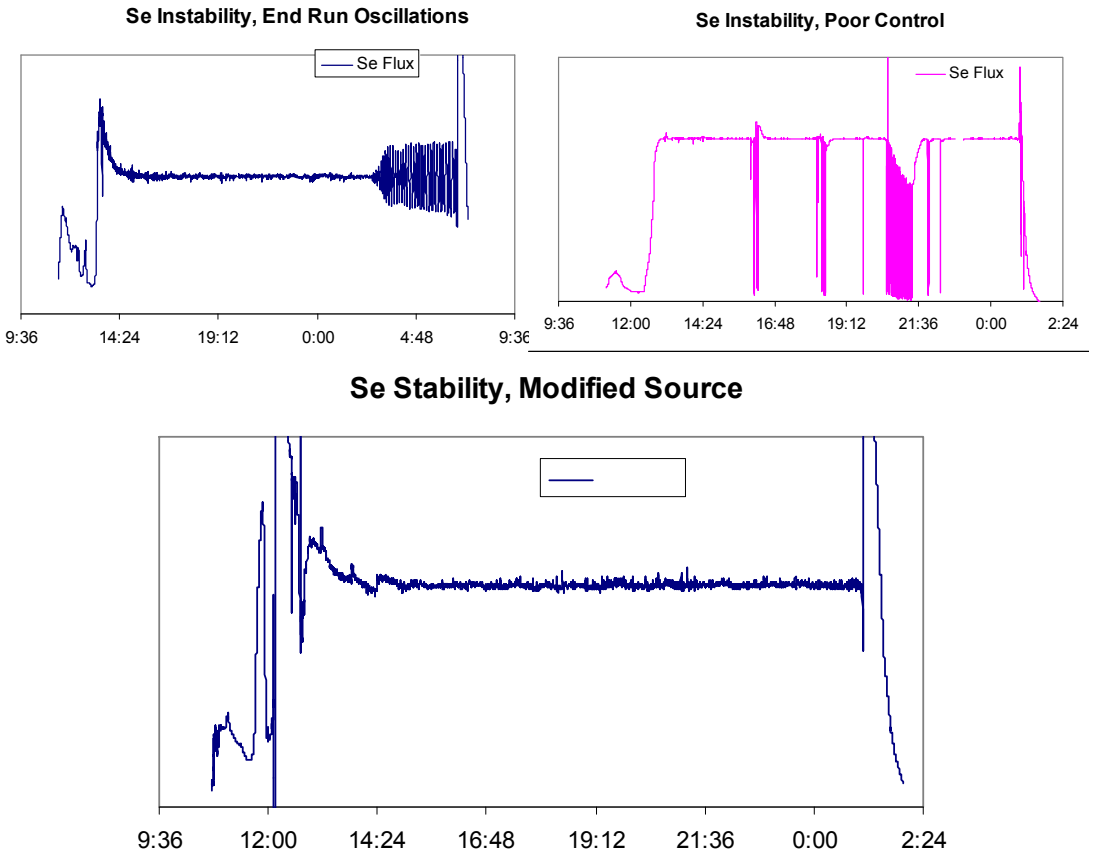

Figure 61. Top: examples of Se flux instability from old sources. Bottom: example of stable Se flux from redesigned source.

7.2.2. CIGS Composition Uniformity Optimization

Cross web non uniformity due to metals flux profile has had a significant impact on CIGS cell production yields/efficiencies. Post CIGS deposition webs are scanned for composition at several locations across the web with an XRF spectrometer. Figure 62 illustrates the type of cross web thickness profiles for various CIGS metals typically achieved in production prior to systematic model based improvements were implemented. The CIGS cross web thickness profile for each metal proved to be dependant on a few specific dimensional details of components in the individual source assemblies. Variability in the source component fabrication process resulted in significant variability. However, the effect of the fabrication variance on the flux uniformity was also found to depend on the specific operating parameters of the source. Since each metal constituent of the CIGS film is associated with specific operating parameters (source temperature, flux rate), the cross web thickness profile of a single source varied depending on the metal and chamber geometries within the CIGS deposition sequence. For characterization purposes a curve peak ratio (CPR, the ratio of the thickness maximum between 0" and the web center to the thickness maximum in the range from web center to 12") was developed to indicate the symmetry of the distribution. The ideal CPR is one, indicating a perfectly symmetric profile.

It is desirable to align unique cross web profiles for each metal / heater combination so that the overlapping profiles of Cu, In and Ga were similar even when the CPR wasn't approaching 1. Thus, the similarity in the overlapping profiles could still produce a compositionally "in-spec" film across the web, although the total CIGS thickness would vary. Thus, by controlling the thickness profile for individual sources, and aligning that distribution with similar distributions for other metals / sources in the same CIGS chamber, composition uniformity across the web, and consequently yield and average device efficiency could be improved.

To determine the functional dependence of the thickness profile on specific critical source dimensions, 12 position cross web XRF scan data were collected from over 100 CIGS production lots. The data were analyzed statistically to develop a method to predict the cross web thickness profile of a heater based on several critical dimensions and its operating parameters. The understanding has also enabled development of methods to intentionally modify critical dimensions in existing source parts to control the cross web thickness profile. Studies were conducted to show that source parts could be modified in one critical dimension after fabrication to adjust their individual profiles to attain a symmetric distribution (CPR = 1.0).

Modeling efforts between indicated that the three different metals, copper, indium and gallium, required three different models. However, the form of the models was quite similar and typically required similar adjustments to the critical dimension for the involved source parts to attain a symmetric distribution. Source parts are typically produced in "batches", with heaters in each batch having a characteristically similar deposition profile. As a result, source parts in a given batch were modified using the model calculations, resulting in cross web thickness profiles being greatly improved (Figure 63).

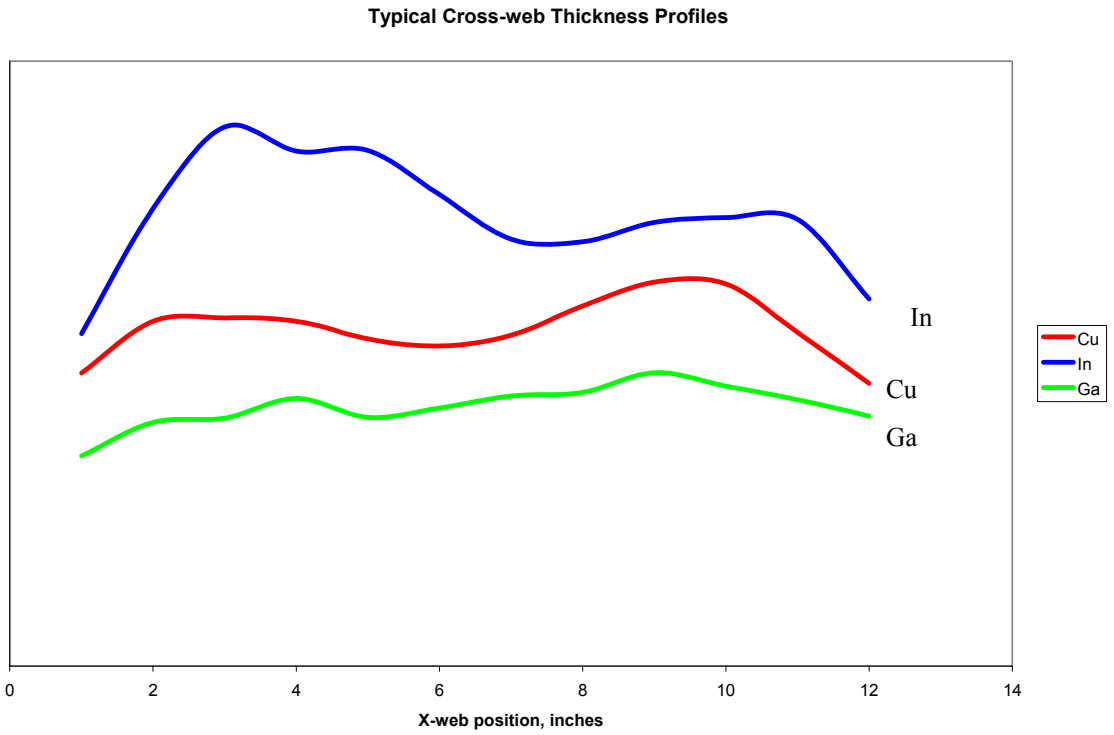

Figure 62. Representative XRF measurements of Cu, In, and Ga thicknesses across a stainless steel web.

Thus, a viable method to improve cross web CIGS uniformity was successfully developed. By simply measuring critical source components at given locations and using the results in a mathematical model, the required dimensional modification were determined, restoring symmetry to the source deposition profiles. Efforts continue to develop practical means for further improvements in cross web uniformity. Ultimately the most desirable profile is one that is flat in addition to being symmetric (Figure 64).

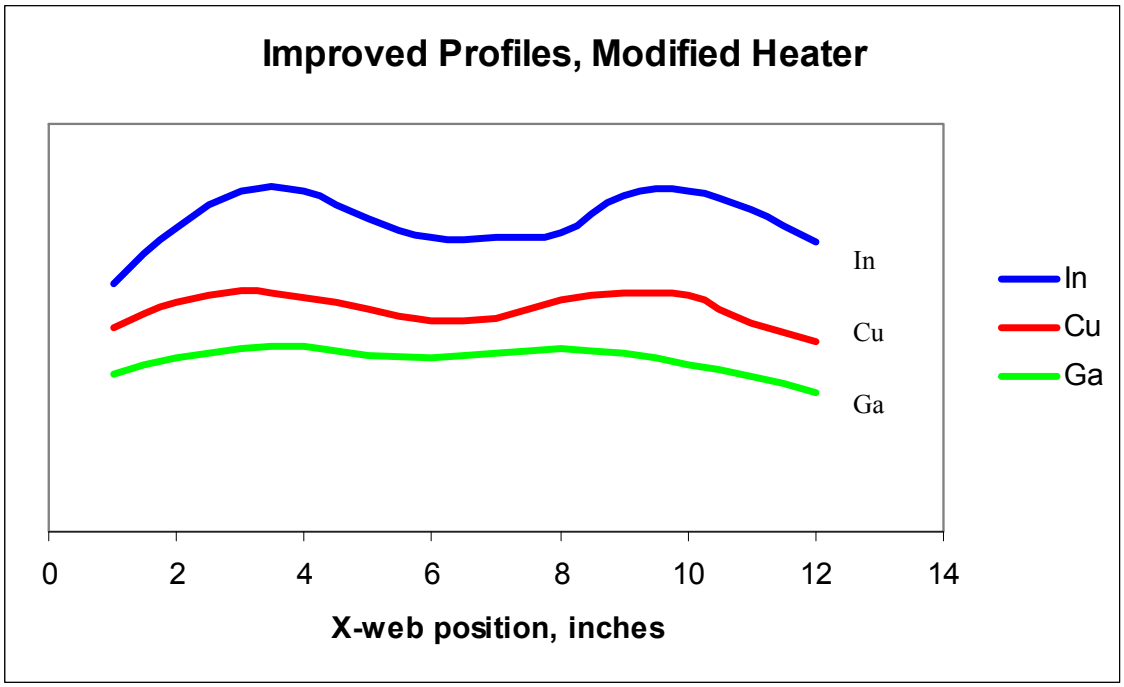

Figure 63. Representative XRF measurements of Cu, In, and Ga thicknesses across a stainless steel web where the source components were modified based on model predictions to improve symmetry.

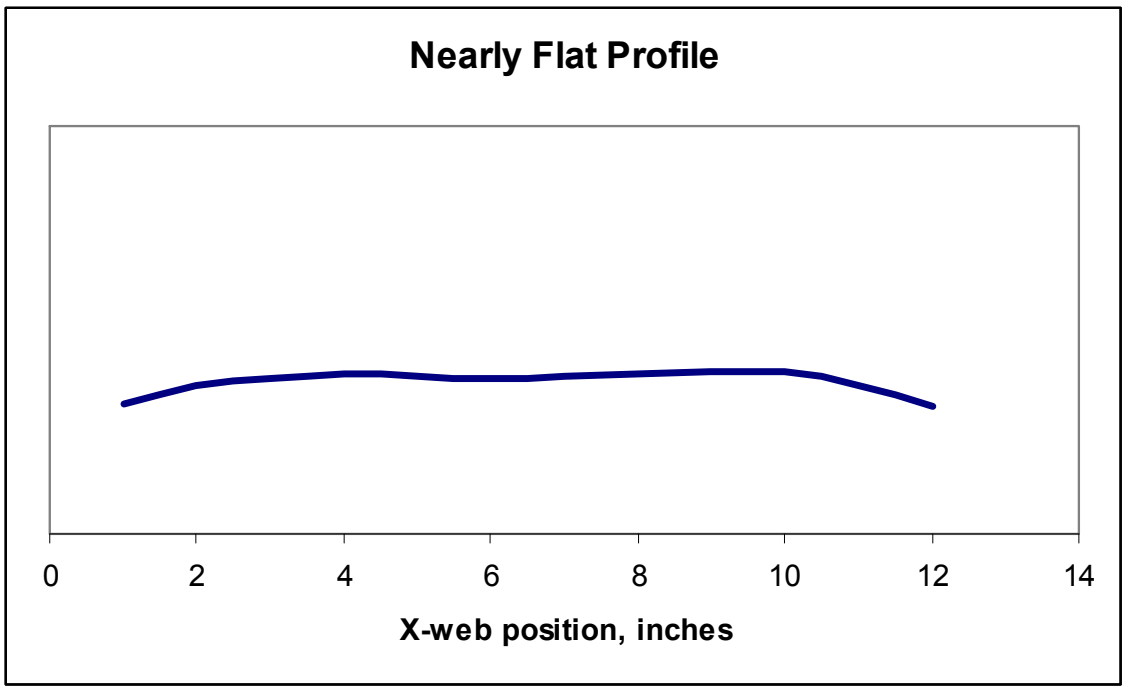

Figure 64. Representative XRF measurements of a metal thickness across a stainless steel web where the source components were modified based on model predictions to improve uniformity.

7.2.3. Na-Mediated CIGS-Substrate Adhesion Testing

Adhesion between the CIGS layer and substrate is a critical factor for product durability and reliability. Poor adhesion leads to early product failure, as well as lower yields from material losses during handling in module assembly. Adhesion of the CIGS on the substrate depends on several factors including the level of extrinsic Na added for CIGS performance enhancement. In addition to improved Na deposition control, post deposition analysis through highly quantifiable adhesion measurements is desired. Initially a technique was developed to monitor the film for adhesion failures during the CDS process, where the pictures already being taken to monitor for film thickness were passed through an additional algorithm to find areas with poor adhesion. The images, as shown in Figure 65, are passed through automated image handling routines and patched together to form a web map that is analyzed to find areas of a particular color which represent adhesion failures. This technique has flagged 14 webs (of 228 webs, since introduction of the method) as containing poorly adhering material, with only one false positive result. The single false positive resulted when an area that was of a peculiar composition induced a response in the discrimination algorithm normally associated with poor adhesion.

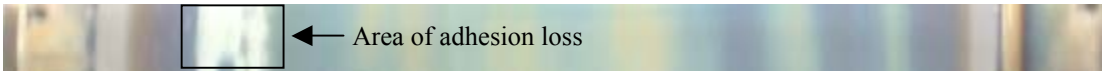

Figure 65. Representative image of web, showing area of NaF related adhesion loss. Images such as this one are recorded every 3-10 feet of web and when combined form a map of adhesion failure.

To augment the image analysis technique, a quantitative methodology was developed based on systematic application of pressure through a conductive tip. While several methods for adhesion testing was evaluated, including ultrasonic reflection analysis, ultrasonic acceleration to failure, impact deformation, stud pull, tape pull, friction acoustic, variable radius fold and a variety of scratch testing, systematic evaluation, trials, and concept reviews developed a technique and apparatus (Figure 66) that reliably measures the adhesion of the CIGS film at the Mo interface. As shown in Figure 67, the use of a probe tip drug across the CIGS film with increasing pressure eventually breaks through the film. The pressure at which break through occurs provides a quantitative measure of adhesion that can be reproducibly determined.

Specifically, an electrical signal, the natural photovoltage of the finished device stack, is produced and monitored due to incident light on the CIGS sample under test. The photovoltage is picked up between the tip of the stylus moving on the CIGS/CdS/TCO sample surface and the underlying back contact of the sample. As the stylus force increases, eventually disrupting the CIGS layer, the photovoltage drops precipitously to low values associated with the loss of CIGS and direct contact between the stylus tip and the underlying back contact. The downward force and electrical signal are monitored in real time as the stylus moves along the film. Figure 67 shows SEM micrographs of the deformation caused by the use of a relatively sharp probe tip drug across the CIGS film with increasing pressure that eventually breaks through the film making contact with the substrate. The pressure and distance at which breakthroughs occur provides a quantitative measure of adhesion that can be reproducibly determined. Thus, unlike “tape pull” tests or other less quantitative adhesion measurements such as the image analysis above, the scratch tester provides a quantifiable measure of adhesion with a high degree of spatial resolution that can be correlated with manufacturing conditions to determine optimum processing. However, there are many factors that affect the reproducibility of the method, including stylus shape, material and orientation, and heterogeneity of the film.

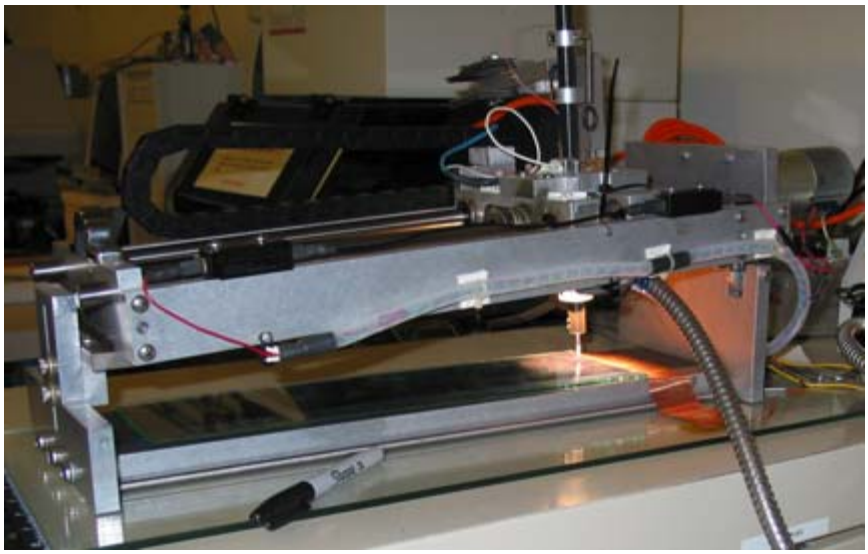

Figure 66. Scratch testing apparatus. The stylus is resting on the glass plate. Note the angle of the stylus track relative to the plate providing a significantly greater force at the end of the travel (on the left hand side of the picture).

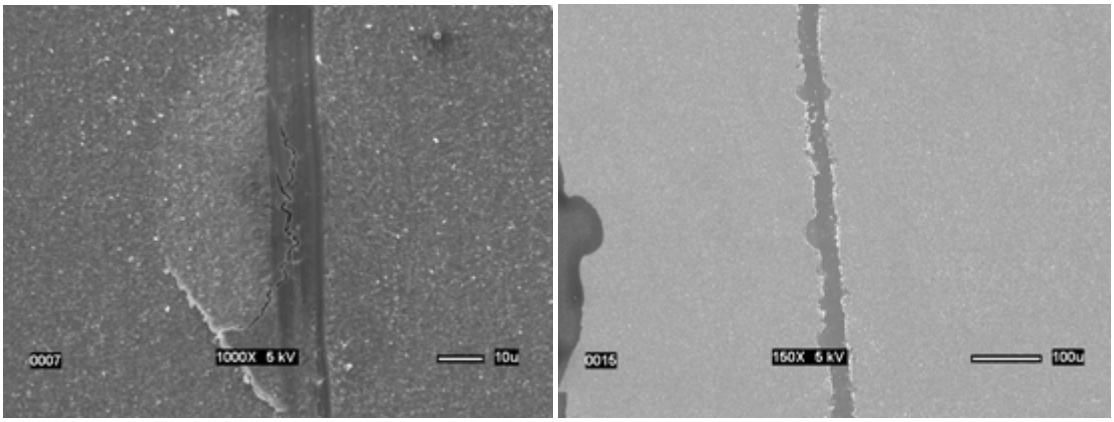

Figure 67. Representative SEM images of scratches testing the adhesion of the CIGS film to the Mo contact layer. Left: a scratch on the CIGS film surface just prior to breaking through and creating a scratch that physically removes the CIGS film from the Mo (right). While damage is induced as increasing pressure is applied to a probe tip, adhesion can be quantified when the scratch tip actually breaks through the CIGS film to the Mo film below.

Example results comparing a tape peel test and the scratch test are shown in Figure 68 and Figure 69. In this comparison, a sample with good adhesion is designated with "A" and a sample with poor adhesion is designated "B". The tape test uses 3M Scotch tape 810 applied to the film and pulled off. The tape is then placed on paper and the image digitized for analysis. An image analysis algorithm calculates the percent of material removed by the tape. More material on the tape represents worse adhesion. For the scratch test the electrical signal from the scratch is divided into break areas and float areas. Example electrical signals are shown in Figure 69. The break areas are where the stylus breaks through the CIGS and makes electrical contact with the back contact. The float areas are where the stylus rides on top of the CIGS. To compare the signal directly with the tape pull test the break areas are represented as a percent of the total scratch length. Representative data from nine samples with a variety of adhesion strengths are shown in Figure 70. The results from tape, scratch and also a visual assessment of the adhesion quality were used. All data is shown in percent to allow direct comparison of the techniques. Very good correlation is observed between all three techniques. In six of the nine samples the reproducibility of the scratches was better than the tape

pulls. In addition to the increased reproducibility of the technique, a larger range of samples can be assessed, samples that would give either 0 or 100% removed on the tape test can be put into the extended range of the scratch tester. With the current force range samples that showed no material removed with the standard tape test had up to 10% breakthrough with the scratch test. Additionally, the force range of the scratch test can be extended from the current range as manufacturing improvements demand.

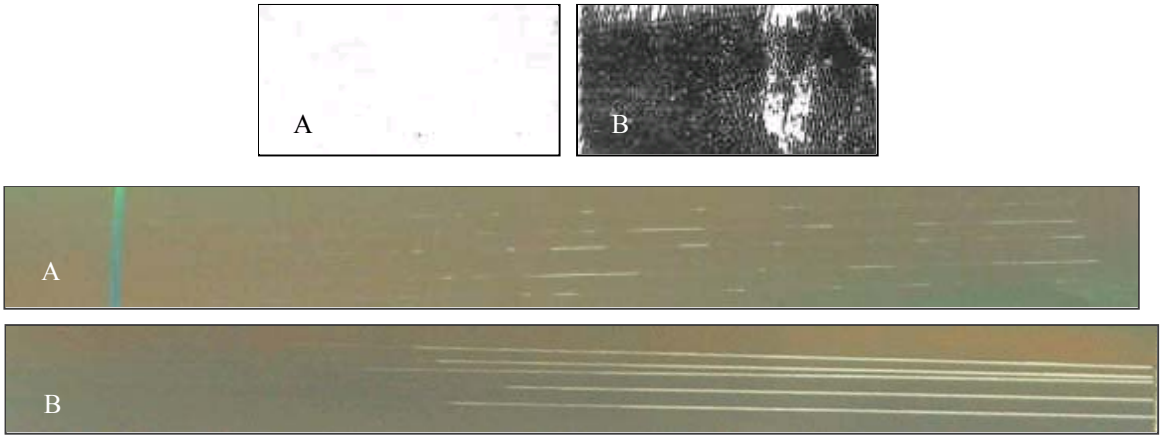

Figure 68. Example of Tape pull results (top) and scratch test results (bottom). Samples designated with an "A" were deemed to have "good" adhesion and with a "B" were deemed to have poor adhesion. Increasing force was applied from left to right on the scratch test images.

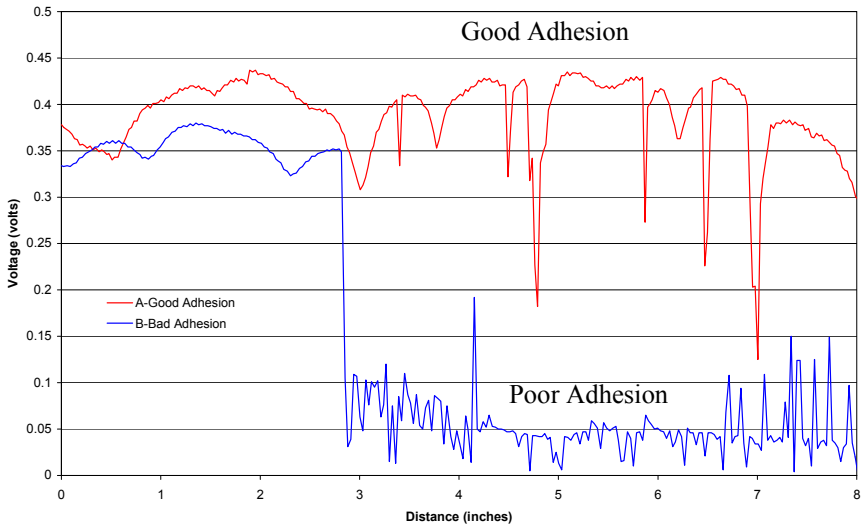

Figure 69. Electrical signal from two representative tests; one with good adhesion and one with poor adhesion. A. Good adhesion characterized by several very minor film breaks. The breaks (drops in voltage) just before the 5 inch mark and at 7 inches are the most prominent breakthroughs. B. Poor adhesion characterized by complete breakthrough before 3 inches.

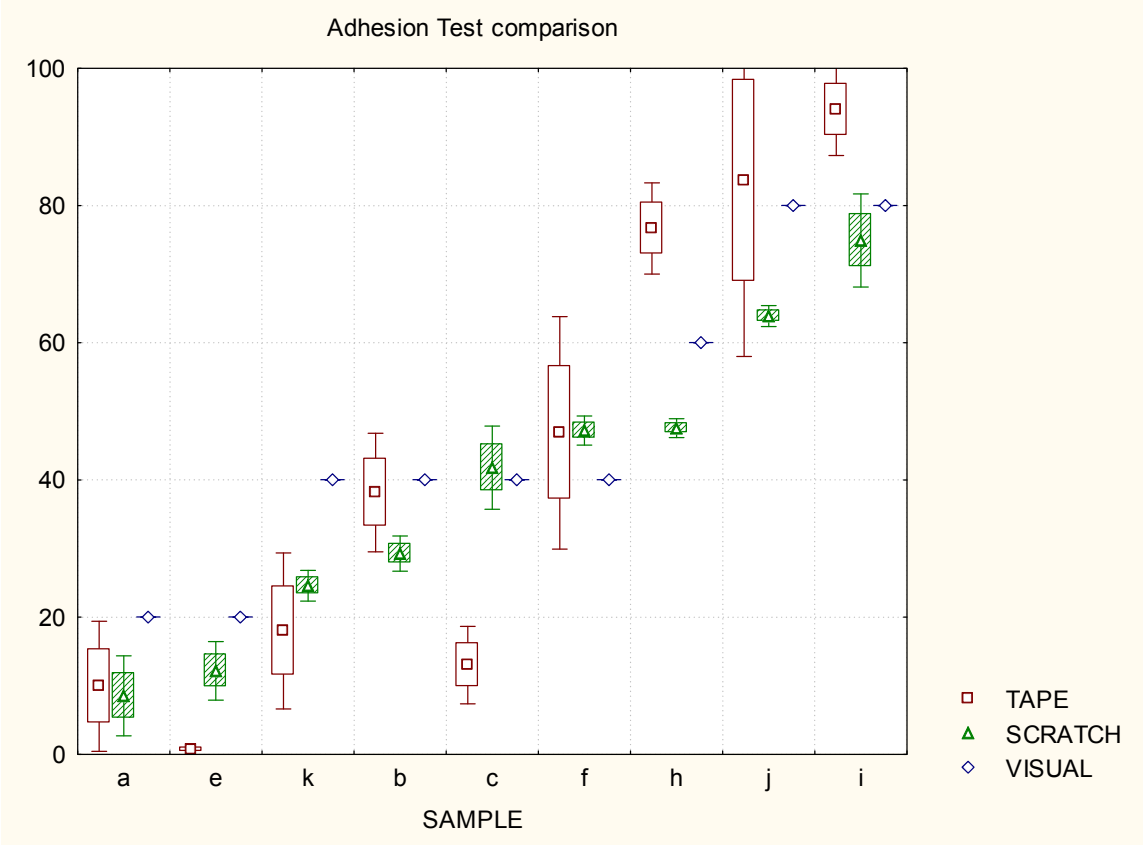

Figure 70. Graph comparing results from 3 different adhesion tests: Tape Pull, Scratch Test, and Visual assessment of a sample group of data. 3 analyses of the Tape Pull and Scratch Data, error bars are 1 sigma. Each sample designated by a different letter, represents either a panel or location on a panel. Larger values on the Y axis represent worse adhesion i.e. greater percent of CIGS removed from the substrate.

8. CONCLUSION

ITN and GSE with the assistance of NREL's PV Manufacturing R&D program are continuing to advance flexible CIGS production technology through a multidisciplinary approach focused on substantial improvements in thin-film deposition processing. During the program, progress was made in several areas, including:

- The design and implementation of trajectory oriented physics-based control models on production deposition systems to provide improved dynamic control, systems design, and fault tolerance. Comprehensive physics-based deposition system models were completed to enable overall system design evaluations and high fidelity process control. These models were used to develop improved metal deposition sources, start-up control and process related issues. In addition, model reduction strategies were developed to provide algorithms for real-time feedback control.
- Fault tolerance strategies were evaluated, identified and implemented for production deposition systems. These activities included detection of faulty sensors (e.g. Se, Na, sputter targets, thermocouples, etc.), fault mitigation through autorestart (e.g. Se, Na, sputter targets, etc.), and fault recovery by automatically switching to alternative control/processing strategies that enable continued processing, thus eliminating the time and high costs associated with run termination.

- Development and implementation of additional robust in-situ sensors to provide real-time process and product information for feedback and feed-forward control. Development activities included source, flux and thin-film property sensors to provide the most appropriate information for the best control possible.
- Improved component and systems designs that resulted in enhanced processing and product performance.

These activities resulted in outstanding improvements in CIGS cell performance (>13% large area cells, >10% average) and yields (>90%), while substantially reducing fault events due to component/system breakage. These gains have primarily been due to improved process parameters identified through systematic evaluation that was enabled by the improved control provided by the PV Manufacturing R&D program activities. The performance, throughput and cost reduction improvements have substantially enhanced the viability of flexible CIGS PV manufacturing. This unique product enables new PV markets that will expand the use of PV in the commercial energy production sector and is cost competitive when all attributes are considered.

ACKNOWLEDGEMENTS

The authors gratefully acknowledge and thank UniSource Energy Corporation and the Department of Energy's National Renewable Energy Laboratory, Photovoltaic Manufacturing R&D Technology Program, Subcontract Number ZDO-2-30628-07, for their support. We would also like to thank all the people who have contributed to the success of the program including Lin Simpson, Nick Gomez, Bharat Joshi, Greg Kleen, Garth Jensen and Kevin Williams at ITN Energy Systems, Inc.; Scott Wiedeman, Jeff Britt, Jane VanAlsburg-Westerman, Marcus Beck, Jim Taylor, John Muha, Eric Sheehan, Bob Huntington, Sarah Lundberg, Doug Mason, and Omran Musbah at Global Solar Energy, Inc.; Tyrone Vincent, J.P. Delplanque, Robert Key, Jeff Hanna, and Matt Hilt at the Colorado School of Mines; and Erten Eser, Robert Birkmire, William Shafarman, and Steve Hegedus at the Institute of Energy Conversion, University of Delaware, DE.

REFERENCES

[i] Hanna, Jeffrey, "Finite-Element Modeling of Thermal Behavior found in High-Rate Metal Vapor Effusion Sources and a Multiphase Flow Model of Particle Formation and Growth in the Metal Vapors," Colorado School of Mines

[ii] R. J. Kee, F. M. Rupley, J. A. Miller, "Chemkin-II: A fortran chemical kinetics package for the analysis of gas-phase chemical kinetics," Report SAND89-8009/UC-401, Sandia National Laboratory (March 1991)

[iii] DS2V software by G.A. Bird (G.A. Bird, *Molecular Gas Dynamics and the Direct Simulation of Gas Flows,* (Clarendon, Oxford, 1994)

[iv] Hilt, Matthew J., "Validation and Reduction of Models for High Rate Metal Vapor Effusion Sources," Colorado School of Mines

[v] Kodas, Toivo T. and Hampden-Smith, M., Aerosol Processing of Materials, Chapters. 4 and 5, "Particle Growth, Evaporation, and Nucleation" and "Collision and Coalescence," pp. 75-128.

REPORT DOCUMENTATION PAGE

Form Approved
OMB No. 0704-0188

PLEASE DO NOT RETURN YOUR FORM TO THE ABOVE ORGANIZATION.

1. REPORT DATE *(DD-MM-YYYY)*	2. REPORT TYPE	3. DATES COVERED *(From - To)*
October 2005	Subcontract Report	13 May 2002–30 May 2005

4. TITLE AND SUBTITLE
Trajectory Oriented and Fault Tolerant Based Intelligent Process Control for Flexible CIGS PV Module Manufacturing; Final Technical Report, 13 May 2002–30 May 2005

5a. CONTRACT NUMBER
DE-AC36-99-GO10337

5b. GRANT NUMBER

5c. PROGRAM ELEMENT NUMBER

6. AUTHOR(S)
L. Simpson, J. Britt, R. Birkmire, and T. Vincent

5d. PROJECT NUMBER
NREL/SR-520-38681

5e. TASK NUMBER
PVB56101

5f. WORK UNIT NUMBER

7. PERFORMING ORGANIZATION NAME(S) AND ADDRESS(ES)
ITN Energy Systems, Inc.
8130 Shaffer Parkway
Littleton, CO 80227

8. PERFORMING ORGANIZATION REPORT NUMBER
ZDO-2-30628-07

9. SPONSORING/MONITORING AGENCY NAME(S) AND ADDRESS(ES)
National Renewable Energy Laboratory
1617 Cole Blvd.
Golden, CO 80401-3393

10. SPONSOR/MONITOR'S ACRONYM(S)
NREL

11. SPONSORING/MONITORING AGENCY REPORT NUMBER
NREL/SR-520-38681

12. DISTRIBUTION AVAILABILITY STATEMENT
National Technical Information Service
U.S. Department of Commerce
5285 Port Royal Road
Springfield, VA 22161

13. SUPPLEMENTARY NOTES
NREL Technical Monitor: R.L. Mitchell

14. ABSTRACT *(Maximum **200 Words**)*

ITN Energy Systems, Inc., and Global Solar Energy, Inc., assisted by NREL's PV Manufacturing R&D program, have continued to advance CIGS production technology by developing trajectory-oriented predictive/control models, fault-tolerance control, control platform development, in-situ sensors, and process improvements. Modeling activities included developing physics-based and empirical models for CIGS and sputter-deposition processing, implementing model-based control, and applying predictive models to the construction of new evaporation sources and for control. Model-based control is enabled by implementing reduced or empirical models into a control platform. Reliability improvement activities include implementing preventive maintenance schedules; detecting failed sensors/equipment and reconfiguring to continue processing; and systematic development of fault prevention and reconfiguration strategies for the full range of CIGS PV production deposition processes. In-situ sensor development activities have resulted in improved control and indicated the potential for enhanced process status monitoring and control of the deposition processes. Substantial process improvements have been made, including significant improvement in CIGS uniformity, thickness control, efficiency, yield, and throughput. In large measure, these gains have been driven by process optimization, which in turn have been enabled by control and reliability improvements due to this PV Manufacturing R&D program.

15. SUBJECT TERMS
PV; trajectory-oriented; fault-tolerant; intelligent process control; manufacturing; module; solar cell; reliability; CIGS;

16. SECURITY CLASSIFICATION OF:			17. LIMITATION OF ABSTRACT	18. NUMBER OF PAGES	19a. NAME OF RESPONSIBLE PERSON
a. REPORT	b. ABSTRACT	c. THIS PAGE			
Unclassified	Unclassified	Unclassified	UL		19b. TELEPONE NUMBER (*Include area code)*